Stony Brook University

Quantum Field Theory in Coordinate Space

A Dissertation Presented

by

Ahmet Ozan Erdoğan

to

The Graduate School

in Partial Fulfillment of the

Requirements

for the Degree of

Doctor of Philosophy

in

Physics and Astronomy

Stony Brook University

August 2014

Stony Brook University

The Graduate School

Ahmet Ozan Erdoğan

We, the dissertation committee for the above candidate for the

Doctor of Philosophy degree, hereby recommend

acceptance of this dissertation.

George Sterman – Dissertation Advisor
Distinguished Professor, C.N. Yang Institute for Theoretical Physics,
Department of Physics and Astronomy

Peter van Nieuwenhuizen – Chairperson of Defense
Distinguished Professor, C.N. Yang Institute for Theoretical Physics,
Department of Physics and Astronomy

Alfred Goldhaber – Committee Member
Professor, C. N. Yang Institute for Theoretical Physics,
Department of Physics and Astronomy

Harold Metcalf – Committee Member
Distinguished Teaching Professor, Department of Physics and Astronomy

William Kilgore – Outside Member
Associate Physicist, Department of Physics,
Brookhaven National Laboratory

This dissertation is accepted by the Graduate School.

Charles Taber
Dean of the Graduate School

Abstract of the Dissertation

Quantum Field Theory in Coordinate Space

by

Ahmet Ozan Erdoğan

Doctor of Philosophy

in

Physics and Astronomy

Stony Brook University

2014

In order to provide a new coordinate-space perspective applicable to scattering amplitudes, in the first part of this dissertation, the structure of singularities in perturbative massless gauge theories is investigated in coordinate space. The pinch singularities in coordinate-space integrals occur at configurations of vertices which have a direct interpretation in terms of physical scattering of particles in real space-time in the same way as for the loop momenta in the case of momentum-space singularities. In the analysis of vertex functions in coordinate space, the well-known factorization into hard, soft, and jet functions is found. By power-counting arguments, it is found that coordinate-space integrals of vertex functions have logarithmic divergences at worst. The hard-collinear and soft-collinear approximations that allow the application of gauge theory Ward identities in the formal proof of factorization in coordinate space are introduced.

In the second part, the perturbative cusp and closed polygons of Wilson lines for massless gauge theories are analyzed in coordinate space, and expressed as exponentials of two-dimensional integrals. These integrals have geometric interpretations, which link renormalization scales with invariant distances. A direct perturbative prescription for the logarithm of the cusp and related cross sections

treated in eikonal approximation is provided by web diagrams. The sources of their ultraviolet poles in coordinate space associated with their nonlocal collinear divergences are identified by the power-counting technique explained in the first part. In the study of the coordinate-space matrix elements that correspond to scattering amplitudes involving partons and Wilson lines in coordinate space, a series of subtractions is developed to eliminate their divergences and to show their factorization in coordinate space. The ultraviolet finiteness of the web integrand is shown by relating the web expansion to the application of this additive regularization procedure to the massless cusp. Generalizations for multieikonal and partonic amplitudes are discussed, and the factorization of these coordinate-space amplitudes into hard, jet and soft functions is verified.

To my parents

Table of Contents

List of Figures

Acknowledgements

First and foremost, I would like to express my deep appreciation and gratitude to my advisor, George Sterman, for his patience, his invaluable insights and advices, and for his constant support. I feel priviliged to have worked with him, and I am indebted to him for all of his teachings in science and research.

I am grateful to Peter van Nieuwenhuizen for all the physics knowledge I learned from him in his excellent courses at Stony Brook and for his endorsement of my graduate research career at the YITP.

I would like to express my gratitude to Alfred Goldhaber for the time he spent working with me at the initial stages of my graduate studies, and for his kindness and support all the time.

Furthermore, I would like to thank Roderich Engelmann for his support and 'partnership' during the summer of 2008, and also Kenneth Lanzetta, Robert McCarthy, Harold Metcalf, and Peter Stephens for their support and appreciation of my work as a teaching assistant. I also would like to acknowledge the stimulating courses thaught by Barry McCoy and Konstantin Likharev. Thanks also go to my fellow cohorts with whom I enjoyed having exchanges, specially to Marcos Crichigno, Pedro Liendo, and Dharmesh Jain, for their help at various times.

I would like to thank my uncle Efraim Avşar who has inspired me to study science since my childhood for all of his support and encouragement. I am also grateful to the family of 'Reisins' for creating a family environment for me while I was far away from home during my studies. I would like to express my gratitude and appreciation for my friends who made it possible to enjoy life and endure difficulties during graduate school, Güneş Demet Şentürk, Defne Över and Ceyhun Ekşin, and for my girlfriend, Billur Avlar, who has given me joy and encouragment.

Of course, my deepest gratitute is due to my dear parents, Nursel and İsmail Erdoğan, who have sacrificed everything for us, for me and my sister, Başak. I could not have accomplished anything, if it were not for them. My "little" sister deserves credit for supporting me at difficult times, as well as distracting me at good times.

Lastly, I would like to acknowledge financial support from the Department of Physics and Astronomy at Stony Brook University, C.N. Yang Institute for Theoretical Physics, and National Science Foundation, grants No. PHY-0969739 and No. PHY-1316617.

Chapter 1

Prologue

The desire to understand nature, the physical reality that surrounds us, may be the most human characteristic, and has taken place throughout the history of human thought. With the development of the scientific method, our growing knowledge and understanding of natural phenomena has led us not only to gain insight into the underlying structure of the physical reality but also to explore the first principles. By an interplay between experiment and theory, we discovered elementary particles and their interactions that are the basic constituents of matter and forces in nature.

Our knowledge of the microscopic world from the experimental results is formulated in terms of quantum field theory (QFT), which is a theoretical framework where the principles of quantum mechanics and special relativity are combined consistently. There is no other part of human knowledge that has been tested and confirmed to the degree of accuracy and precision as the principles and results of QFT in the history of mankind. In these theories, the fundamental objects are the fields, while the particles are bundles of energy, or quanta, of various fields. A field is a physical quantity that has a value for each point in space and time, and can be thought of as some stress in space.

QFTs that are invariant under a continuous group of local transformations are called gauge theories. The representations and interactions of the fields are governed by the gauge symmetry group. All of the four fundamental forces in nature, the electromagnetic, weak, strong, and gravitational interactions are described by a gauge theory, where each force between the fields and the particles is mediated by a gauge field. The quantum field theories for all fundamental interactions are based on the principle of (gauge) symmetry, however, their unification in one framework is still lacking.

The most studied QFT known as the 'Standard Model' describes the electromagnetic, weak, and strong interactions of all elementary particles as known today, while gravity remains unaddressed. Despite its many successes, because

of its incompatibility with general relativity, its deficiency in explaining phenomena, such as dark matter and dark energy among others, and its dependence on many parameters that are simply arbitrary, the 'Standard Model' is far from being a complete theory of nature. In a modern perspective, both 'Standard Model' and general relativity are considered as *effective field theories* that are low-energy descriptions of a more fundamental theory emergent at a higher energy scale.

The most promising candidate for a unified theory to date is string theory, where the extended, one-dimensional objects called strings are the fundamental objects, and may provide substructure for fields and even space-time. Nevertheless, string theory is closely connected to quantum field theory. String theories use the language and methods of ordinary field theories, and can be formulated as field theories. Any gauge theory is related to a string theory in a certain limit of the rank of the gauge group, while low-energy limits of string theories yield gauge theories. Therefore, presumably, the 'fundamental theory' of nature, whatever its structure may be, will be founded on quantum field theory.

Objects in quantum field theories can be expressed in two equivalent representations, in coordinate space or in momentum space. Although the idea of fields is intrinsically connected to space-time, the states and other field theory objects are conventionally expressed in terms of energies and momenta rather than space-time coordinates. The calculations of scattering amplitudes, which quantify the information from the theory that is to be compared with the experimental results to test the theory and its predictions at a certain degree of precision, are mostly carried out in the momentum-space representation. The calculational techniques and the methods of QFTs are much less developed in coordinate space. This thesis is based on graduate research that aimed for a new, coordinate-space perspective applicable to amplitudes for massless gauge theories.

The problem of the strong-coupling dynamics of gauge theories is still a challenging one to solve in general, even though some progress has been made in supersymmetric and conformal theories through the gauge/gravity duality. The methods for solving the dynamics of QFTs are well known at weak coupling, that is for small values of the 'coupling constant', which is a multiplicative factor associated with each interaction. In this regime, perturbation theory can be applied to get explicit knowledge from the theory to check against observables in terms of amplitudes. Perturbation theory consists of a systematic expansion in the coupling constant(s), where the interactions are treated as small perturbations to the free theory. Perturbative expansion of the path integral involves calculation of Feynman integrals that contain ultra-

violet and infrared divergences in general. Such divergences are required to be isolated and removed so that a finite result can be obtained from the theory.

In the study of this thesis, the analyses are mainly done in the framework of massless nonabelian gauge theories like Quantum Chromodynamics (QCD), the theory of strong interactions, but the results and applications are quite more general. We will review some basic properties of QCD briefly below.

1.1 Preliminary review of QCD

Quantum Chromodynamics (QCD) is the gauge theory of strong interactions with an unbroken SU(3) gauge symmetry group. Its name comes from the existence of three kinds of charge referred to as "color". In QCD, gluons mediate the strong interaction between the quarks inside the nucleus. The gluon fields A_a^μ transform under the adjoint representation of the color gauge group, where the color index a of the gauge field runs up to the dimension of the group, $a = 1, \ldots, N^2 - 1$ for SU(N). The quark fields ψ_i, however, transform under the fundamental representation of the color group with $i = 1, \ldots, N$. The self-interactions of gluons due to the nonabelian nature of the color group increase the complexity of QCD tremendously compared to Quantum Electrodynamics (QED). We will now briefly review basic concepts in field theory to mention important characteristics of QCD here, while for pedagogical discussions and details we refer to Refs. [1–7].

1.1.1 Foundations of QCD

QCD was accepted as the theory of strong interactions only after the SLAC experiments that started in the 1960s and after theoretical developments in nonabelian gauge theories by the early 1970s. Before that, even though nonabelian gauge theories were introduced long ago [8], the focus for strong interactions was on other ideas like the analyticity properties of the S-Matrix, current algebra, and string theory rather than a field theory description.

The situation changed when the deeply inelastic scattering (DIS) experiments at SLAC showed pointlike substructure in hadrons. Their data revealed a striking property of the 'structure functions' called *scaling*, that these functions become independent of momentum transfer for its large values due to predominant wide-angle scattering from pointlike structures within the nucleons [9, 10]. The parton model was developed to explain these results [11, 12], while the quark model emerged out of hadron spectroscopy [13–15], and required a new quantum number, "color", for the constituent quarks [16, 17]. A relation for the structure functions derived in the parton model provided

evidence that the partons detected in DIS are the quarks of hadron spectroscopy [18].

Meanwhile, there have been important theoretical developments that established the successes of current algebra in field theory. The current commutation rules were shown to be replaced by divergence equations [19], which can be derived from a theory with gauge invariance [20]. The proofs of unitarity and renormalizability of nonabelian gauge theories [21–23] cleared up any theoretical concerns before the extension of the global SU(3) model of quarks to a local nonabelian gauge theory [24]. The final crucial step was the discovery that 'asymptotic freedom' was satisfied by QCD [25], which provided natural explanation of the success of the parton model for DIS. Finally, QCD was identified as the theory of strong interactions.

1.1.2 Renormalization and the running of the coupling

QCD has a "running" coupling meaning that the value of the coupling constant changes with the energy (or distance) scale so that the theory is not conformal, it inherits a scale $\Lambda_{\rm QCD}$ that leads to confinement of quarks inside the nucleus.

Perturbative gauge theories suffer from ultraviolet divergences leading to infinite results in theoretical calculations. However, we can still obtain sensible results for physical observables by the process of *renormalization*, in which such infinities are rendered into unobservable, 'bare' quantities. The perturbation series is made finite by expressing the theory in terms of 'renormalized' quantities that depend on a scale, usually taken as the scale of the experimental measurements, instead of the 'bare' quantities. The proof that this idea works in the case of nonabelian gauge theories, that is the proof of renormalizability for such theories, was shown by Refs. [22, 23].

After renormalization, the parameters of the theory depend on the renormalization scale explicitly, for instance, the coupling is no longer a constant but a function of this scale. However, physical quantities can be computed equally from either 'bare' or 'renormalized' quantities. The fact that physical observables cannot depend on the renormalization scale leads to a *renormalization group equation* [26–29],

$$\frac{d}{d\mu}\sigma \;=\; 0\;, \tag{1.1.1}$$

where σ represents a physical observable, which may be a cross section or an S-Matrix element. For simplicity, let us assume σ is an "infrared safe" cross section, that is, it does not depend on quark masses in the short-distance limit. We can then rewrite Eq. (1.1.1) expressing σ in terms of the renormalized

coupling g_R, the renormalization scale μ, and a set of measured quantities Q_i, and applying the chain rule,

$$\left(\frac{\partial}{\partial\mu} + \beta(g_R(\mu))\frac{\partial}{\partial g_R}\right)\Big|_{g_R} \sigma(g_R(\mu), \mu, Q_i) \;=\; 0 \;, \tag{1.1.2}$$

where the renormalized coupling is held fixed. The function β defined by

$$\beta(\, g_R(\mu)\,) \;=\; \frac{\partial}{\partial\mu} g_R(\mu) \;, \tag{1.1.3}$$

encodes the running of the coupling and can, in principle, be calculated from the coupling renormalization constant $Z_g \equiv g_0/g_R$, with g_0 the bare coupling, to any order in the coupling in perturbation theory. For conformal field theories, the beta function vanishes, and the coupling is literally a constant. In QCD, the first term in the expansion of the beta function in the strong coupling g_s is given by

$$\begin{aligned} \beta_{\rm QCD}(g_s) &= -g_s\left(b_0\frac{\alpha_s}{4\pi} + b_1(\frac{\alpha_s}{4\pi})^2 + \cdots\right) \\ &= -\frac{g_s^3}{16\pi^2}\left(\frac{11}{3}N - \frac{4}{3}n_f T_f\right) \;+\; \mathcal{O}(g_s^4) \;, \end{aligned} \tag{1.1.4}$$

with $N = 3$, $n_f = 6$, and $T_f = 1/2$. The dependence of the strong coupling in QCD, or equivalently of "alpha-strong", on the renormalization scale μ is then found from the solution of Eq. (1.1.3),

$$\alpha_s(\mu^2) \equiv \frac{g_s^2(\mu)}{4\pi} = \frac{16\pi^2}{b_0\,\ln(\mu^2/\Lambda^2_{\rm QCD})} \;, \tag{1.1.5}$$

where b_0 is the coefficient of the first term in the expansion of $\beta_{\rm QCD}$ given above, while $\Lambda_{\rm QCD}$ is the 'QCD scale' where the perturbation theory breaks down, and the nonperturbative, confining domain of QCD starts.

1.1.3 Asymptotic freedom

An important characteristic of QCD is that the coupling decreases as the distance scale over which it is measured decreases [25]. It eventually vanishes at very short distances (or at very high energies), thus this characteristic is called 'asymptotic freedom'. We can observe this feature of QCD in Eq. (1.1.5), $\alpha_s(\mu^2)$ vanishes in the limit $\mu^2 \to \infty$. This property allows us to make accurate calculations within the perturbation theory at high energies, that is at short

distances.

QCD is effectively a *massless* gauge theory, although the quark masses can be generated dynamically by spontaneous breaking of chiral symmetry [30]. Because of the confinement, however, the masses of the quarks are not directly observable, but they also vanish as the renormalization scale increases in an asymptotically free theory, which allows us to define "infrared safe" cross sections to determine the coupling independent of the masses from the experiments.

1.1.4 Factorization

A consequence of these properties is *factorization*, the systematic separation of short- and long-distance dynamics, which leads to great predictive power and phenomenological success of QCD. The factorization theorems were proven by a diagrammatic analysis in momentum space [31]. For a general process involving a large momentum transfer, Q, a relevant cross section can be factorized in the general form,

$$Q^2\,\sigma_{\rm phys}(Q,m) \;=\; C_{\rm SD}(Q/\mu,\alpha_s(\mu)) \;\otimes\; f_{\rm LD}(\mu,m) \;+\; \mathcal{O}(1/Q^p)\;, \qquad (1.1.6)$$

where m represents infrared scales, and μ is the factorization scale separating the short-distance dynamics in $C_{\rm SD}$ from the long-distance dynamics in $f_{\rm LD}$ that is a product of universal parton distributions. Here, $\otimes$ represents a convolution between these two functions, usually in terms of parton momentum fractions, which is accurate up to power corrections as indicated. The parton distributions in $f_{\rm LD}$ are based on experimental data, while the information in $C_{\rm SD}$ can be calculated very accurately in perturbation theory. As examples of the processes involving hadrons where factorization holds in this sense, we can list deeply inelastic scattering, e^+e^- annihilation, and Drell-Yan processes.

The factorization in cross sections for these processes originate from the structure of singularities in perturbative gauge theories with massless fields in Minkowski space. The underlying Ward identities of the gauge theory ensure that the singularities of diagrams for the relevant amplitudes factorize after summing over all diagrams contributing at any given order in perturbation theory. The subject of this thesis is the analysis of these singularities and their factorization in coordinate space.

1.2 Outline

The contents of this thesis consists of research published in Refs. [32–34]. The main subject of these articles is the study of matrix elements corresponding to scattering amplitudes, their divergences and factorization properties analyzed directly in coordinate space.

We will start with the analysis of the singularities in perturbative massless gauge theories in coordinate space [32]. We will first review pinch singularities, and the conditions for them to occur in coordinate-space integrals. The pinch singularities in coordinate-space integrals occur at configurations of vertices which have a direct interpretation in terms of physical scattering of particles in real space-time in the same way as for the loop momenta in the case of momentum-space singularities.

In the analysis of vertex functions related to partonic scattering, we will find that their coordinate-space integrals have logarithmic divergences at worst by power-counting arguments, and determine the conditions for existence of these logarithmic divergences and their structure in coordinate space. A fundamental consequence of the structure of these 'leading singularities' is the well-known factorization into soft, hard, and jet functions. We will define the 'hard-collinear' and 'soft-collinear' approximations that allow us to apply the gauge theory Ward identities in the formal proof of factorization in coordinate space. We also extend the results to the vacuum expectation values of products of path-ordered exponentials for our following discussion.

In Chapter 3, we will analyze the perturbative cusp and closed polygons of Wilson lines for massless gauge theories in coordinate space, and express them as exponentials of two-dimensional integrals [33]. A direct perturbative prescription for the logarithm of the cusp and related cross sections treated in eikonal approximation is provided by web diagrams. We will give to the integrals of web diagrams geometric interpretations, which link renormalization scales with invariant distances. We will note that the forms of the web integrands for the cusp and closed polygonal loops agree with the expressions given for conformal theories via the gauge/gravity duality. The surface interpretation relies on the cancellation of subdivergences in webs, which we will show by analyzing the nested and overlapping regions in coordinate space in the following chapter.

In Chapter 4, we will consider the coordinate-space matrix elements that correspond to scattering amplitudes involving partons and Wilson lines in coordinate space [34]. In coordinate space, both collinear and short-distance limits produce ultraviolet divergences, as shown in Chapter 2. We develop a series of subtractions that organize these divergences, and allow their factorization, by analogy to the treatment of infrared logarithms in momentum space.

Using the subtraction terms that impose the coordinate-space 'hard-collinear' and 'soft-collinear' approximations specifically for each leading region from which an ultraviolet divergence can arise, we will rederive the factorization in coordinate space. As an explicit application of our construction, we will show the ultraviolet finiteness of the web integrand by relating this additive regularization procedure in terms of nonlocal ultraviolet subtractions to the exponentiation properties of the massless cusp. We also discuss generalizations to amplitudes with multiple Wilson lines and external fields in configurations related to scattering, and verify the factorization of these coordinate-space amplitudes into hard, jet and soft functions.

Finally, we will comment on the scope of our results, and discuss their possible extensions, and generalizations in the epilogue.

Chapter 2

Analysis of Singularities in Coordinate Space

The contents of this chapter is published in Ref. [32].

2.1 Introduction

The structure of singularities in perturbative gauge theories has long been a subject of study for theoretical interest and for phenomenological applications [35, 36]. There is a vast literature on the subject, and most modern analyses are carried out in momentum space to calculate scattering amplitudes [37–40]. Calculations involving Wilson lines, however, are often simpler in coordinate space [41,42] and coordinate-space integrals were used for Wilson lines in the application of dual conformal invariance [43,44]. It is therefore natural to consider using them for amplitudes as well. The purpose of this study is to provide a new, coordinate-space analysis of singularities in perturbation theory applicable to amplitudes for massless gauge theories.

It is well known that the momentum-space singularities of Feynman integrals in a generic quantum field theory occur at configurations of internal loop momenta that have a direct interpretation in terms of physical scattering of on-shell particles in real space-time [45, 46]. In this study, we will analyze the origin and structure of these singularities directly in coordinate space.

Massless gauge theories suffer from infrared (IR) divergences, which characterize the long-distance contributions to perturbative predictions, in addition to ultraviolet (UV) divergences, which can be removed by local counterterms. An analysis of infrared divergences in gauge theories from the point of pinch singularities of Feynman integrals over loop momenta was given by Ref. [47]. Following [48], which dealt with scalar theories, we will show that

the coordinate-space singularities of massless gauge theories have the same interpretation in terms of physical scattering of particles with conserved momenta. In contrast to momentum space examples, however, we will see that collinear singularities are of ultraviolet nature in coordinate space, and require $D < 4$ in dimensional regularization. This analysis can be applied to a variety of field theory objects derived from Green functions, including form factors and vertex functions, Wilson lines, as well as cut diagrams for cross sections.

In a detailed analysis of vertex functions in coordinate space, we will find the factorization into hard, soft, and jet functions familiar from momentum space analysis [7, 31]. In coordinate space, the soft function is finite when the external points are kept at finite distances from each other. Therefore, ultraviolet regularization is needed only for the jets and the hard function. Adapting the power counting technique developed for momentum space in [47], the residues of the lightcone poles of vertex functions in coordinate space will be shown to have logarithmic divergences at worst.

This chapter is organized as follows. In section 2.2, a brief, general review of pinch singularities will be followed by a derivation of conditions for singularities in coordinate-space integrals together with their physical interpretations. We will also comment on the case with massive lines in Appendix A.1. In section 2.3, we will analyze the structure of singularities of vertex functions in coordinate space, solving the conditions for pinch singularities, first explicitly at lowest loop order and then extending the solutions to arbitrary order in perturbation theory. In section 2.4, we will adapt the power counting technique developed in [47] to the coordinate-space vertex functions, and show that divergences are at worst logarithmic relative to their lowest-order results at higher orders in perturbation theory. In the last section, we will discuss the approximations that can be made in the integrand to obtain the leading singularity. We will describe the "hard-collinear" and then the "soft-collinear" approximations, which will lead to factorization of jets from the hard and soft functions. Lastly, we will show that the fermionic vertex function can be approximated by a Wilson line calculation, by imposing the conditions for a pinch singularity inside the integrands.

2.2 Analysis of singularities

This section treats the coordinate-space singularities of Feynman diagrams in gauge theories. The discussion is in many ways similar to the momentum-space analysis of Refs. [5, 35, 49]. The results of this section will be employed to identify the natural subregions of the corresponding diagrams in order to study their behavior in coordinate space.

We start our analysis with an arbitrary Feynman integral with massless lines in coordinate space. We work in $D = 4-2\varepsilon$ dimensions using dimensional regularization. For gauge theories, we employ Feynman gauge. The integrands in scalar and gauge theories are similar, except that in the latter case, gauge field vertices have derivatives that act on attached lines. These derivatives change the powers of denominators and produce numerator factors, which may enhance or suppress the integrals.

In coordinate space, we can represent graphical integrals schematically as

$$I(\{x_i^\mu\}) = \prod_{\text{vertices } k} \int d^D y_k \prod_{\text{lines } j} \frac{1}{[-(\sum_{k'} \eta_{jk'} X_{k'})^2 + i\epsilon]^{p_j}} \times F(x_i, y_k, D) \ , \tag{2.2.1}$$

where the positions of internal vertices y_k^μ are integrated over all space-time for fixed external points x_i^μ. For each line, the sum over $\{X_{k'}\} = \{y_k, x_i\}$ includes all vertices, internal and external, where η_{jk} is an "incidence matrix", which takes values $+1$ and -1 when the line j ends or begins at vertex k, respectively, and is zero otherwise. The orientation of a line is at this point arbitrary, but we will see that at singularities it is determined by the time-ordering of the vertices it connects. Before the action of derivatives, the power of the denominator of line j is $p_j = 2 - \varepsilon$ for fermion lines, and $p_j = 1 - \varepsilon$ for scalar and gauge field lines; however, if a derivative acts on a line, the power of its denominator is increased by 1. This expression holds for scalar and gauge theories, for which we sum over terms with different numbers of derivatives, and the functions $F(x_i, y_k, D)$ include remaining constants, group theory factors, and numerator factors, which do not affect the locations of the singularities but will matter in power counting. They are simply numerical constants for scalar theories. For theories with spin, they also carry the spin-dependence, which we have suppressed here. The integrand in (2.2.1) becomes singular when a line moves to the lightcone.

After combining the propagators of each line with Feynman parametrization, the integral will be of the form,

$$\begin{aligned} I(\{x_i^\mu\}) = \prod_{\text{lines } j} \int_0^1 d\alpha_j \, \alpha_j^{p_j - 1} \, \delta(1 - \sum_j \alpha_j) \\ \times \prod_{\text{vertices } k} \int d^D y_k \, D(\alpha_j, x_i, y_k)^{-N(\varepsilon)} \, \bar{F}(x_i, y_k, D) \ , \end{aligned} \tag{2.2.2}$$

where we have absorbed the prefactors of the parametrization into $\bar{F}(x_i, y_k, D)$,

and where the common denominator is given by

$$D(\alpha_j, x_i, y_k) = \sum_j \alpha_j \left[-z_j^2(x_i, y_k) + i\epsilon \right] \ . \tag{2.2.3}$$

Here, α_j is the Feynman parameter of the jth line, and z_j^μ denotes the argument of its propagator, which is the coordinate difference between the vertices it connects. The overall power of the denominator is $N(\varepsilon) = \sum_j p_j(\varepsilon)$, in particular, $N(\varepsilon) = N(1-\varepsilon)$ for a diagram with N scalar lines only. For gauge theories, for a diagram with N_g gauge field lines, N_f massless fermion lines, and V_{3g} three-vector vertices it is given by $N(\varepsilon) = N_f(2-\varepsilon) + N_g(1-\varepsilon) + V_{3g}$.

The zeros of the denominator $D(\alpha_j, x_i, y_k)$ in Eq. (2.2.3) determine the positions of the poles of the integrand in (2.2.2). These poles may produce branch points of $I(\{x_i^\mu\})$, depending on whether or not they may be avoided by contour deformation in the complex (α, y)-space. We recall here the summary given in Ref. [35]. In general, the singularities of a function $f(z)$ defined by a single integral,

$$f(z) \ = \ \int_{\mathcal{C}} dw \, \frac{1}{g(z,w)} \ , \tag{2.2.4}$$

arise if and only if the poles $\tilde{w}(z)$ of the integrand, which are zeros of $g(z,w)$, cannot be avoided by contour deformation. This follows from a theorem proven by Hadamard [50], and happens either when one of the poles migrates to one of the end-points of the contour, an *end-point singularity* or when two or more isolated poles coalesce at a point trapping the contour between them, resulting in a *pinch singularity*.

These conditions for the existence of singularities can be generalized as necessary conditions for functions of several (external) variables that are defined by multiple integrals,

$$f(\{z_i\}) \ = \ \int_{\mathcal{H}} \prod_j dw_j \, \frac{1}{g(\{z_i\}, \{w_j\})} \ , \tag{2.2.5}$$

such as $I(\{x_i^\mu\})$ in our case. Here, the hypercontour $\mathcal{H}$ denotes the multi-dimensional region of integration. The set of points $S = \{\tilde{w}(\tilde{z})\}$ on which $g(\{z_i\}, \{w_j\}) = 0$ defines surfaces in the complex (z, w)-space. If $g(\{z_i\}, \{w_j\})$ factors as $g = g_1(\{z_i\}, \{w_j\}) \times \cdots \times g_r(\{z_i\}, \{w_j\})$, then there are r such singular surfaces, which may or may not intersect with each other. As in the case of an integral over a single variable, the singularities occur when an intersection of these singular surfaces with the hypercontour $\mathcal{H}$ cannot be avoided. Summarizing the arguments presented in Ref. [35], this again happens either when a singular surface S overlaps with the boundary of $\mathcal{H}$ (*end-point*

singularity) or when the hypercontour $\mathcal{H}$ is trapped between two or more singular surfaces or between two different parts of the same singular surface (*pinch singularity*). At an end-point, $\mathcal{H}$ cannot be moved in the directions normal to its boundary, while at a pinch it cannot be moved away from singular regions in the direction of the normals to two (or more) singular surfaces, which are in opposite directions. In both cases, the vanishing of the gradient of $g(\{z_i\},\{w_j\})$ on S is the necessary condition,

$$\frac{\partial}{\partial w_j}\, g(\{z_i\},\{w_j\})\Big|_{g=0} \;=\; 0\ . \tag{2.2.6}$$

In the following, we use the terminology of Ref. [5], and call the variables that parametrize directions out of the singular surface S *normal*, and those that lie in the surface *intrinsic*. The larger the volume of normal space, the less singular the integral. Refs. [5, 35, 49] present pedagogical discussions of these concepts.

This reasoning enables us to derive a powerful set of necessary conditions for singularities of integrals like $I(\{x_i^\mu\})$ in Eq. (2.2.1) using the representation in Eq. (2.2.2), where a singular surface S in (α, y)-space is defined by the set of points $S = \{\tilde{\alpha}, \tilde{y}\}$ on which $D(\alpha_j, x_i, y_k)$ vanishes. The singularities of (2.2.2) can come only from the end-point $\alpha_j = 0$ of the α_j-integral, because $D(\alpha_j, x_i, y_k)$ is linear in the α_j. Note that $\alpha_j = 1$ is not a different end-point singularity, as it sets all α_i, $i \neq j$, to zero because of the delta function. On the other hand, there are no end-point singularities in y-integrals, since they are unbounded. However, in y-integrals the contour of integration can be trapped at a pinch singular point when the two solutions of the quadratic equation $D = 0$ are equal, *i.e.*,

$$\frac{\partial}{\partial y_k^\mu}\, D(\alpha_j, x_i, y_k)\Big|_{D(\tilde{\alpha},\tilde{y})=0} \;=\; 0\ . \tag{2.2.7}$$

The momentum space analogs of these conditions are summarized as the Landau equations [45] in the literature. They were also written in coordinate space for scalar theories in [48]. In coordinate space, they are given by Eq. (2.2.7) above,

$$\alpha_j \;=\; 0\ , \quad \text{or} \quad z_j^2 \;=\; 0\ , \tag{2.2.8}$$

and

$$\sum_{\text{lines } j \text{ at vertex } k} \eta_{kj}\, \alpha_j\, z_j^\mu \;=\; 0\ . \tag{2.2.9}$$

The conditions in the first line come from $D = 0$, while those in the second

line come from $(\partial/\partial y_k^\mu)D = 0$. The "or" in the first line is not necessarily exclusive. The condition $(\partial/\partial\alpha_j)D = 0$ for all j is equivalent to $D = 0$ since D is homogenous of degree one in the α_j.

A physical interpretation of the momentum space Landau equations was originally given by Coleman and Norton in [46]. The momentum space analog of Eq. (2.2.9) in terms of momenta k_i^μ of lines is,

$$\sum_{\text{lines } i \text{ in loop } l} \eta_{li}\, \alpha_i\, k_i^\mu \;=\; 0 \;. \tag{2.2.10}$$

Then, with the identification of $\alpha_i k_i^\mu \equiv \Delta x_i^\mu$ with a space-time vector for each on-shell line, these relations can be thought as describing on-shell particles propagating between the end- and starting points of line i, which are separated by interval Δx_i^μ. This way, α_i is interpreted as the ratio of the time of propagation to the energy of particle i; and thus the analog of Eq. (2.2.8) states that there is no propagation for an off-shell line.

Similarly, in coordinate space, after the rescaling $\Delta\bar{x}_j^\mu = \alpha_j z_j^\mu$, Eq. (2.2.9) directly gives the same physical picture of on-shell particles propagating in space-time. The interpretation with particles propagating forward in time fixes the orientation of lines by the time-ordering of vertices. Additionally, we may identify the product $\alpha_j z_j^\mu$ with a momentum vector,

$$p_j^\mu \;\equiv\; \alpha_j\, z_j^\mu \;. \tag{2.2.11}$$

Then Eq. (2.2.9) gives momentum conservation for the on-shell lines with momenta p_j^μ flowing in or out of vertex k. Moreover, with a further identification of α_j as the ratio of the energy of line j to the time component of z_j,

$$\alpha_j \;\equiv\; p_j^0/z_j^0 \;, \tag{2.2.12}$$

we obtain a relation between the energies and momenta of the propagating particles associated with the pinch singularities of Eq. (2.2.2),

$$p_j^\mu \;=\; E_j\, v_j^\mu \;, \quad \text{with } v_j^\mu = (1, \vec{z}/z_j^0) \;. \tag{2.2.13}$$

This is the relation between energy and momentum of free massless particles; the magnitude of their velocity is indeed $c = 1$ since $(z^0)^2 - |\vec{z}|^2 = 0$. Therefore, to each pinch singularity we can associate a physical picture in which massless particles propagate freely on the lightcone between vertices, while their momenta satisfy momentum conservation at each internal vertex as well [48].

In the physical picture above, only lines on the lightcone "carry" finite momenta. Lines not on the lightcone, that is lines connecting vertices at finite

distances, have $\alpha_j = 0$ which by Eq. (2.2.12) sets their $p_j^\mu = 0$. In momentum space, because the momenta of lines with $\alpha_j = 0$ do not show up in the momentum-space analog of (2.2.9), in a graphical representation, one can contract such off-shell lines to points. The resulting diagrams are called *reduced diagrams* that represent *lower-order* singularities of a Feynman diagram, while the diagram with all the lines on the mass-shell (*i.e.* no lines with $\alpha = 0$) is said to give the *leading* singularity [35, 51]. In contrast, in coordinate space, these "contracted" lines should be compared to "zero lines", with $z_j^\mu = 0$ that do not contribute to the sum in (2.2.9) either. They represent "short-distance" (UV) singularities, which occur when two connected vertices coincide at the same point, but are not *lower-order* singularities of the coordinate integral. These pinch singularities originate from the denominator of a single propagator, where the contour of integration, the real line, is pinched between two poles of the same propagator. Therefore, we will first identify such UV singularities of an arbitrary integral like (2.2.1), and then combine the rest of the denominators by Feynman parametrization to find other types of singularities from groups of lines in the remaining integrals using the Landau conditions (2.2.8) and (2.2.9). We should note that not all UV singularities give UV *divergences*. Divergences can be identified by the power counting procedure below.

As an example of the application of Eq. (2.2.7) to coordinate-space integrals, we shall now find the configurations of lines for pinches in the integration over the position of a single three-point vertex at a point y^μ. For simplicity, let us consider the following integral in a scalar theory

$$I(x_1, x_2, x_3) \;=\; \int d^D y \prod_{i=1}^{3} \frac{1}{[-(x_i - y)^2 + i\epsilon]^{1-\varepsilon}} \;. \tag{2.2.14}$$

Apart from the the UV singularities when $y^\mu = x_i^\mu$ for $i = 1, 2$ or 3, the conditions for a pinch between different lines in the y^μ integral are given by Eqs. (2.2.8) and (2.2.9) after Feynman parametrization,

$$\alpha_1 \, z_1^\mu + \alpha_2 \, z_2^\mu + \alpha_3 \, z_3^\mu \;=\; 0 \;, \tag{2.2.15}$$

with $z_i^\mu \equiv x_i^\mu - y^\mu$. For a pinch singularity, these vectors are either lightlike, $z_i^2 = 0$, or have $\alpha_i = 0$. Equation (2.2.15) cannot be satisfied if all three vectors have positive entries. Thus, at least one external point must have $x_i^+ < y^+$ and one must have $x_j^+ > y^+$, so that there is at least one incoming and one outgoing line. These considerations naturally provide a time ordering for vertices and a direction for lines at any singularity. Assuming all $\alpha_i \neq 0$ and that all lines are on the lightcone, $z_i^2 = 0$ and Eq. (2.2.15) imply that $z_j \cdot z_k = 0$ as well. That is, all of these lines are parallel. If any one of the

lines is off the lightcone with $\alpha_i = 0$, then the other two are on the lightcone and again parallel to each other by (2.2.15). These pinch singularities can be interpreted as a merging or splitting of three particles, which occurs at point y^μ, with the ratios of their momenta given by the ratios of the α_i. Note that these results hold for the three-point vertices of a gauge theory as well, and can be generalized to n-point vertices. The coordinate-space singularities of Green functions represent physical particle scattering and thus can be related naturally to physical scattering amplitudes.

2.3 Coordinate-space singularities at a vertex

We will now study how coordinate-space singularities in a vertex function in a massless gauge theory emerge from pinches in Feynman integrals in perturbation theory. For simplicity, the first example that we consider will be the correlation of two scalar fields with a color-singlet gauge current. We also discuss the correlation of fermions with the same kind of current. The results of Sec. 2.2 will be applied to identify the configurations that can lead to singularities of such vertex functions in coordinate space.

The scalar vertex function of interest is obtained from the vacuum expectation value of the time-ordered product of two charged scalar fields with an incoming color-singlet current,

$$\Gamma_S^\nu(x_1, x_2) \;=\; \langle 0 \,|T\left(\Phi(x_2)\, J^\nu(0)\, \Phi^*(x_1)\right)|\, 0\rangle \;. \tag{2.3.1}$$

Here, we have shifted the position of the current to the origin using the translation invariance of the vacuum state. $\Gamma_S^\nu(x_1, x_2)$ transforms as a vector under Lorentz transformations. Its functional form is well-known and is determined by the abelian Ward identity,

$$-\,i\,(\partial_1 + \partial_2)_\nu\; \Gamma_S^\nu(x_1, x_2) \;=\; \left[\delta^D(x_2) \,-\, \delta^D(x_1)\right]\; G_2((x_2 - x_1)^2)\;, \tag{2.3.2}$$

where G_2 is the scalar two-point function, which is only a function of the invariant distance between the external points. A general solution to this inhomogenous partial differential equation can be given by a particular solution that satisfies (2.3.2) plus the general solution to the homogenous equation,

$$(\partial_1 + \partial_2)_\mu \Gamma^\mu_{S,(H)}(x_1, x_2) = 0 \;. \tag{2.3.3}$$

A particular solution to the abelian Ward identity, which has the structure of

the lowest order result, is given by

$$\Gamma^{\nu}_{S,(I)}(x_1,x_2,\mu) \;=\; \left(\frac{x_2^{\nu}}{(-x_2^2+i\epsilon)^{1-\varepsilon}} - \frac{x_1^{\nu}}{(-x_1^2+i\epsilon)^{1-\varepsilon}}\right)\frac{\Sigma_S\big(\mu^2(x_2-x_1)^2\big)}{x_1^2\,x_2^2}\;, \tag{2.3.4}$$

where the form factor $\Sigma_S(\mu^2(x_2-x_1)^2)$ is a dimensionless function, with μ^2 the renormalization scale, and is related to the renormalized scalar two-point function by

$$i\,G_2(x^2,\mu^2) \;=\; \frac{\Sigma_S(\mu^2x^2)}{(-x^2+i\epsilon)^{1-\varepsilon}}\;. \tag{2.3.5}$$

Note that at zeroth order one obtains $\Sigma^{(0)}(x_1,x_2)=1$ from both equations above.

The general solution to the homogenous equation can be found easily in momentum space, since one then has an algebraic equation,

$$(p_1^{\mu}-p_2^{\mu})\tilde{\Gamma}^{\mu}_{S,(H)}(p_1,p_2)=0\;, \tag{2.3.6}$$

whose solution involves polynomials of momenta times one independent function[1]. Here, momentum p_1 flows into the vertex and p_2 out. The general solution in momentum representation is given by

$$\tilde{\Gamma}^{\mu}_{S,(H)}(p_1,p_2) = \Big[(p_2^2-p_1\cdot p_2)\,p_1^{\mu}+(p_1^2-p_1\cdot p_2)\,p_2^{\mu}\Big]\,\tilde{f}_H(p_1,p_2)\;. \tag{2.3.7}$$

After inverse Fourier transform with $p_1^{\mu}\to i\partial_1^{\mu}$ and $p_2^{\mu}\to -i\partial_2^{\mu}$, the part of the vertex that vanishes in the abelian Ward identity (2.3.2) is of the form,

$$\Gamma^{\mu}_{S,(H)}(x_1,x_2) \;=\; -i(\partial_1-\partial_2)_{\nu}[\partial_1^{\mu}\partial_2^{\nu}-\partial_1^{\nu}\partial_2^{\mu}]\,f_H(x_1,x_2)\;, \tag{2.3.8}$$

where f_H is a function of mass dimension two. In conventional terms, the inhomogenous solution gives the 'longitudinal' part of the vertex while the homogenous solution is the 'transverse' part. Note that any f_H that is a function of only $(x_1\pm x_2)^2$ vanishes under the derivatives in Eq. (2.3.8). Thus, f_H must depend on x_i^2 separately to contribute to the scalar vertex. This will allow lightcone singularities to factorize from the rest of the vertex.

The fermionic counterpart of Eq. (2.3.1) is,

$$(\Gamma_F)^{\nu}_{ba}\,(x_1,x_2) \;=\; \big\langle 0\,\big|T\left(\psi_b(x_2)\,J^{\nu}(0)\,\bar{\psi}_a(x_1)\right)\big|\,0\big\rangle\;, \tag{2.3.9}$$

[1]Starting from $(p_1-p_2)_{\mu}(A\,p_1^{\mu}+B\,p_2^{\mu}) = 0$, the homogenous equation is solved for $\frac{A}{B}=\frac{p_2^2-p_1\cdot p_2}{p_1^2-p_1\cdot p_2}$. The Ward identity reduces the number of independent functions by one.

whose tensor and Dirac structure is determined by the invariance under the global symmetries of the theory while its functional form is similarly constrained by the Ward identity for fermion fields. Chiral invariance for a massless theory requires this vertex to have odd number of gamma matrices. Skipping the details given for scalars above, a particular solution for the 'longitudinal' part of the fermionic vertex function is given by

$$\left(\Gamma_{F,(I)}\right)^{\nu}_{ba}(x_1,x_2,\mu) \;=\; \frac{(\not{x}_2\,\gamma^\nu\,\not{x}_1)_{ba}}{(-x_2^2+i\epsilon)^{2-\varepsilon}\,(-x_1^2+i\epsilon)^{2-\varepsilon}}\,\Sigma_F\big(\mu^2(x_2-x_1)^2\big)\;, \tag{2.3.10}$$

where $\Sigma_F(x^2)$ is related to the renormalized fermion two-point function $S_F(x^2)$ by

$$i\,S_F(x^2,\mu^2) \;=\; \not{x}\,\frac{\Sigma_F(\mu^2x^2)}{(-x^2+i\epsilon)^{2-\varepsilon}}\;. \tag{2.3.11}$$

The 'transverse' part of the fermionic vertex function that vanishes in the abelian Ward identity can be written in the form,

$$\begin{aligned}\Gamma^{\mu}_{F,(H)}(x_1,x_2) \;=\;& \gamma^\mu\left[(\Box_1+2\partial_1\cdot\partial_2+\Box_2)f_1(x_1,x_2)+(\Box_1-\Box_2)f_2(x_1,x_2)\right]\\ &-(\not{\partial}_1+\not{\partial}_2)\,(\partial_1+\partial_2)^\mu\,f_1(x_1,x_2)\\ &-(\not{\partial}_1+\not{\partial}_2)\,(\partial_1-\partial_2)^\mu\,f_2(x_1,x_2)\\ &+(\not{\partial}_1-\not{\partial}_2)\,(\partial_1+\partial_2)_\nu\left(\partial_2^\nu\,\partial_1^\mu-\partial_1^\nu\,\partial_2^\mu\right)f_3(x_1,x_2)\\ &+\gamma_5\,\epsilon^{\mu\nu\rho\sigma}\,\gamma_\nu\,(\partial_1-\partial_2)_\rho\,(\partial_1+\partial_2)_\sigma\,f_4(x_1,x_2)\;.\end{aligned} \tag{2.3.12}$$

Here, all form factors $f_i(x_1,x_2)$ have mass dimension four except $f_3(x_1,x_2)$, which has dimension two. The tensor decomposition of this vertex and the list of form factors in momentum space can be found in Ref. [52]. Again, these form factors can have arbitrary dependence on x_i^2, which allows factorization of lightcone singularities.

We are interested in singularities that are related to scattering processes, thus the limit $x_1 \to x_2$ will not be considered in the discussion below as it gives effectively a two-point function. We also assume here that x_1^μ and x_2^μ are fixed, nonzero vectors that are not lightlike separated ($x_1\cdot x_2 \neq 0$). Given these external data, the only power singularities of the coordinate-space vertex functions will be in x_i^2, which correspond to single-particle poles of the external propagators in momentum space. Furthermore, both $\Sigma_S(x_1,x_2)$ in (2.3.4) and $\Sigma_F(x_1,x_2)$ in (2.3.10) remain finite when both $x_i^2=0$ with $x_1\cdot x_2\neq 0$. Thus, the leading divergence of the scalar vertex can come from $f_H(x_1,x_2)$ in (2.3.8) while the leading divergence of the fermionic vertex comes along again from the 'transverse' part of the vertex.

Let us now illustrate how the lightcone singularities of the vertex functions

given above emerge at one loop in perturbation theory. The integrand of the one-loop diagram in Fig. 2.1, the first nontrivial contribution to the scalar vertex function, is of the form,

$$\begin{aligned}\Gamma_S^{(1)\,\mu}(x_1,x_2) \;&=\; C_S^{(1)} \int d^D y_1\, d^D y_2\, g^{\alpha\beta}\, \frac{1}{[-(y_2-y_1)^2+i\epsilon]^{1-\varepsilon}} \\ &\times \left(\frac{1}{[-(x_2-y_2)^2+i\epsilon]^{1-\varepsilon}} \overleftrightarrow{\partial}_{y_2^\alpha} \left[\frac{1}{[-(y_2-z)^2+i\epsilon]^{1-\varepsilon}} \overleftrightarrow{\partial}_{z^\mu} \right.\right. \\ &\left.\left. \frac{1}{[-(z-y_1)^2+i\epsilon]^{1-\varepsilon}} \right]_{z=0} \overleftrightarrow{\partial}_{y_1^\beta} \frac{1}{[-(y_1-x_1)^2+i\epsilon]^{1-\varepsilon}} \right) \,,\end{aligned} \tag{2.3.13}$$

with $C_S^{(1)}$ a numerical constant. Compare this expression to that of the one-loop diagram for the fermionic vertex function,

$$\begin{aligned}\Gamma_F^{(1)\,\mu}(x_1,x_2) \;&= C_F^{(1)} \int d^D y_1\, d^D y_2\, \frac{1}{[-(y_2-y_1)^2+i\epsilon]^{1-\varepsilon}} \\ &\times \left(\not{\partial}_{x_2} \frac{1}{[-(x_2-y_2)^2+i\epsilon]^{1-\varepsilon}} \right) \gamma^\alpha \left(\not{\partial}_{y_2} \frac{1}{[-y_2^2+i\epsilon]^{1-\varepsilon}} \right) \gamma^\mu \\ &\times \left(\not{\partial}_{y_1} \frac{1}{[-y_1^2+i\epsilon]^{1-\varepsilon}} \right) \gamma_\alpha \left(\not{\partial}_{x_1} \frac{1}{[-(y_1-x_1)^2+i\epsilon]^{1-\varepsilon}} \right) \,.\end{aligned} \tag{2.3.14}$$

Clearly, both have the same pole structure, more precisely, the positions of the poles are the same, although term-by-term their degrees may or may not be different. Using Feynman parametrization, either before or after the action of the derivatives on the lines, both integrals can be put into the form of Eq. (2.2.2) with the same common denominator but, of course, with different numerator factors and different powers of the resulting denominator in the integrands.

The pinch singularities of (2.3.13) and (2.3.14) can originate from the two poles of a single denominator or from poles from different denominators. For the latter case, we will combine the denominators by Feynman parametrization, and use Eq. (2.2.7), the coordinate-space analog of Landau equations. In general, at a pinch singularity, one encounters combinations of these two cases simultaneously. After Feynman parametrization the common denominator for either diagram is given by

$$\begin{aligned}D^{(1)}\big(x_1,x_2,y_1,y_2;\{\alpha\}\big) \;&=\; -\,\alpha_1\,(y_1-x_1)^2 - \alpha_2\,y_1^2 - \alpha_3\,y_2^2 \\ &\quad -\,\alpha_4\,(x_2-y_2)^2 - \alpha_5\,(y_2-y_1)^2 + i\epsilon \;.\end{aligned} \tag{2.3.15}$$

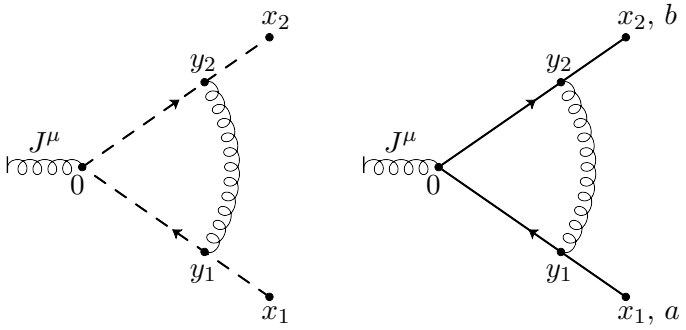

Figure 2.1: One-loop diagrams for the vertex functions in Eq. (2.3.1) and Eq. (2.3.9).

Using Eq. (2.2.7), we get the Landau conditions for pinches in the integration over the positions of internal vertices y_1 and y_2,

$$\alpha_1\,(y_1 - x_1)^\mu + \alpha_2\,y_1^\mu - \alpha_5\,(y_2 - y_1)^\mu \;=\; 0\;, \tag{2.3.16}$$

$$-\alpha_4\,(x_2 - y_2)^\mu + \alpha_3\,y_2^\mu + \alpha_5\,(y_2 - y_1)^\mu \;=\; 0\;, \tag{2.3.17}$$

when $D^{(1)}$ vanishes at a singularity.

We shall list the singularities of (2.3.13) or (2.3.14) starting with pinches without any zero lines. Eqs. (2.3.16) and (2.3.17) make up an underdetermined system of two vector equations, since the α_j also are unknowns. We will not list all solutions to these equations but only those that give the leading power singularities of the vertex functions, which are physically relevant. By leading power singularities of the vertex functions we mean the terms in

$$\hat{\Gamma}^\mu_{S,F}(x_1, x_2) \;=\; x_1^2\,x_2^2\,\Gamma^\mu_{S,F}(x_1, x_2) \tag{2.3.18}$$

that do not vanish when $x_1^2 = x_2^2 = 0$. The simplest solution is when only $\alpha_5 = 0$ while others are nonzero, where one gets

$$y_1^\mu \;=\; \frac{\alpha_1}{\alpha_1 + \alpha_2}\,x_1^\mu\;, \tag{2.3.19}$$

$$y_2^\mu \;=\; \frac{\alpha_4}{\alpha_3 + \alpha_4}\,x_2^\mu\;, \tag{2.3.20}$$

such that y_1^μ becomes 'parallel' to x_1^μ while y_2^μ is parallel to x_2^μ. The neccessary condition for a singularity, $D^{(1)} = 0$, is then satisfied only if $x_1^2 = x_2^2 = 0$. This solution can be interpreted as a "soft" gauge particle, say a gluon, propagating over a finite (invariant) distance between y_1 and y_2, such that the directions of the external particles have not changed after the emission or absorbtion of

the gluon. In momentum space, lines with negligible momenta are called soft, while in coordinate space soft lines are those which connect two points at a finite (invariant) distance. In this case, the scalar/fermion lines are on the lightcone for a pinch.

If α_5 were not equal to zero, the general solution to Eqs. (2.3.16) and (2.3.17) is such that y_1^μ, and similarly y_2^μ, are given as linear combinations of x_1^μ and x_2^μ. Assuming no other α_j vanishes either, $D^{(1)} = 0$ requires then not only $x_i^2 = 0$ but also $x_1^\mu \cdot x_2^\mu = 0$. These solutions, however, imply that x_1 and x_2 are lightlike separated. Likewise, when only $\alpha_2 = 0$ or $\alpha_3 = 0$, the condition $D^{(1)} = 0$ is only satisfied with x_1 and x_2 lightlike separated. On the other hand, if $\alpha_1 = 0$ the solution to Eq. (2.3.16) is such that $y_1^\mu \propto y_2^\mu$ and by Eq. (2.3.17) both y_1 and y_2 are then parallel to x_2 with $D^{(1)} = 0$ being satisfied for $x_2^2 = 0$. However, now the external line $(x_1 - y_1)^2$ can not be on the lightcone, so that this solution does not correspond to a leading power singularity of the vertex. Similarly, when $\alpha_4 = 0$, y_1 and y_2 will be parallel to x_1, and $D^{(1)} = 0$ is satisfied for $x_1^2 = 0$, so that the external line $(x_2 - y_2)^2$ can not be on the lightcone either. The solutions with two or more α_j vanishing are either ruled out because of the reasons given above or because they are equivalent to singularities from zero lines with $z_j^\mu(y_i) = 0$, which we now consider below.

Let us first consider the UV-type singularity of the internal line connecting the vertex at y_1 to the origin, $y_1^\mu = 0$, and look at the conditions for pinches in the remaining integral over y_2^μ. Eq. (2.3.17) is now satisfied for

$$y_2^\mu = \frac{\alpha_4}{\alpha_3 + \alpha_4 + \alpha_5} x_2^\mu \,. \tag{2.3.21}$$

Similarly, when $y_2^\mu = 0$, Eq. (2.3.16) gives

$$y_1^\mu = \frac{\alpha_1}{\alpha_1 + \alpha_2 + \alpha_5} x_1^\mu \,. \tag{2.3.22}$$

These solutions satisfy the condition $D^{(1)} = 0$ if $x_2^2 = 0$ and $x_1^2 = 0$, separately. According to the physical interpretation of pinch singularities given in the previous section, these solutions give "collinear" gauge particles that propagate on the lightcone parallel to one of the external scalars/fermions. We will refer to such lighlike lines with finite energies and momenta in the physical interpretation as jet lines.

Next, consider the case when both internal vertices move to the origin, $y_1^\mu = y_2^\mu = 0$, which makes three lines become zero lines simultaneously. Again, the vanishing of $D^{(1)}$ for a singularity requires $x_1^2 = x_2^2 = 0$ with all lines on the lightcone, otherwise $\alpha_1 = \alpha_4 = 0$. This solution represents an ultraviolet

(short-distance) divergence, and we call it a "hard" solution by analogy to hard scattering.

Among the remaining cases with zero vectors, first consider $y_2^\mu = x_2^\mu$ and $y_1^\mu = x_1^\mu$. The solution to Eq. (2.3.16) for the former, and to Eq. (2.3.17) for the latter, is such that y_1^μ, and similarly y_2^μ, is given as a linear combination of x_1^μ and x_2^μ, so that $D^{(1)} = 0$ is not satisfied for these (unless $\alpha_5 = 0$) because $x_1^\mu \cdot x_2^\mu \neq 0$. For $y_1^\mu = y_2^\mu = y^\mu$, both of the external lines can not be on the lightcone simultaneously. Among the cases when two propagators have zero arguments at the same time, $y_1^\mu = x_1^\mu$ together with $y_2^\mu = 0$, and $y_1^\mu = 0$ together with $y_2^\mu = x_2^\mu$ are limiting cases of collinear solutions in (2.3.22) and (2.3.21), respectively; while any other combination is ruled out because they require $x_i^2 = 0$ and $x_1 \cdot x_2 = 0$. The only possible solution with three zero lines is the hard solution we found, and there can not be any other with more zero lines, because $x_1^\mu \neq x_2^\mu \neq 0$. We have finished the list of solutions to Landau conditions for the leading power singularities of the vertex functions at one loop.

From the solutions to Landau conditions at one loop, one can draw the conclusion that the divergences of the vertex functions in coordinate space come from configurations where, whether the gluons are soft or collinear, the external particles move along *rigid, classical* trajectories along the directions of external points that are located on the lightcone. For the singular configurations at higher orders, we will not need to solve the Landau equations explicitly. Instead, we will make use of the physical interpretation of the necessary conditions for a pinch singularity given in the previous section, and confirmed above for the one-loop case.

In the case of the pinch singularities of the vertex function, to identify an arbitrary pinch surface, we can use the necessary condition (2.2.9) that the lightlike lines of the corresponding diagram must describe a physical process, where the two external lines start from the same point, say the origin, moving in different directions, toward x_1^μ and x_2^μ. For the sake of the argument, suppose the external particles are fermions. Any gauge field lines that connect them by vertices at finite distances have to be soft, because they cannot be parallel to both. They may still have a hard interaction at the origin reflecting a short-distance singularity. The integrals over the positions of the fermion-gluon vertices will be pinched either when the gluon and the fermion lines get mutually collinear, or when the two collinear fermions are connected by the emission of a soft gluon as described in the example given at the end of Sec. 2.2. Likewise, the integrations over the positions of vertices, to which these collinear gluons are connected, will be pinched if the other lines connected to these vertices also become parallel to them, such that all collinear lines make up a

"jet" moving in the direction of the external fermions. The Landau conditions allow these collinear gluons to emit soft gluon lines that can connect to the other jet as well. Therefore, the two jets can have hard interactions at very short distances, and they can only interact by the exchange of soft partons at long distances at later times. Eventually, the fermion lines end at the external points x_i^μ, which have to be on the lightcone, $x_i^2 = 0$, in order that $D^{(n)} = 0$ is satisfied.

To sum up, the pinch singularities of the integrals for vertex functions in coordinate space come from configurations where the (time-ordered) vertices, at which either soft or collinear gluons are emitted or absorbed, are aligned along *straight* lines going through the 'origin' and the external points. These two lines also determine the classical trajectories of the external particles in the Coleman-Norton interpretation. The behaviour of the integrals for arbitrary diagrams at higher orders near the corresponding pinch surfaces will be covered by general power counting arguments in the next section.

2.4 Power counting

In this section, we will apply a power counting technique similar to the one developed for momentum space integrals in Ref. [47] to study the behaviour of the divergences of vertex functions in coordinate space. We have studied in the previous section the pinch singularities in the integrals when the external points are on the lightcone. As the external propagators are not truncated, even the zeroth order results are very singular in coordinate space when the external points are on the lightcone; for instance, the fermionic vertex diverges as $1/(x_1^2\, x_2^2)^2$. Therefore, we will now only consider the external points set on the lightcone, and look for the degree of divergence of vertex functions with respect to their lowest-order results. In a sense, we are looking for any possible divergences in the residues of the lightcone poles, by analogy to the residues of single-particle poles in external momenta of Green functions in momentum space for S-Matrix elements. We will show at the end of this section by power counting arguments that vertex functions in coordinate space have at worst logarithmic divergences with respect to their lowest order results at higher orders in perturbation theory.

Since $x^2 = 0$ does not imply $x^\mu = 0$ in Minkowski space, naïve dimensional counting does not neccessarily bound the true behaviour of the integrals. As we already mentioned in Sec. 2.2, the divergences of the integrals are related to both the volume of the space of normal variables and the singularities of the integrand. Therefore, we will do the power counting by combining the size of the volume element of normal variables with that of the integrand, which

depends on both normal and intrinsic variables. In order to estimate the size of the integrand, we will first approximate the integrals near the pinch surfaces by keeping in each factor (numerator or denominator) only the terms of lowest order in normal coordinates, as their scale goes to zero. Then the resultant integrand is a homogenous function of normal variables, and the powers of the normal variables in the homogenous integrals combined with the *normal volume element* will give us the bounds on the original integrals.

Suppose $z_1, \ldots, z_n$ and $w_1, \ldots, w_m$ denote the normal and intrinsic variables for a pinch surface S of an integral I. The z_i vanish on S with a scale λ, while w_j remain finite (as $\lambda \to 0$) on S. For our discussion for vertex functions, we can choose a single scale λ for properly chosen normal coordinates in our integrals to do the power counting, although we should stress that this does not need to be the case in general. The scale λ bounds the size of each normal variable, and measures the "distance" of the hypercontour $\mathcal{H}$ from the pinch surface S. The homogenous integral $\bar{I}$ near the pinch surface S will have the form[2]

$$\bar{I} \sim \int d\lambda^2 \int_{\mathcal{H}} \left(\prod_{i=1}^{n} dz_i \right) \delta(\lambda^2 - \sum_i |z_i|^2) \int \left(\prod_{j=1}^{m} dw_j \right) \bar{f}(z_i, w_j) \ , \quad (2.4.1)$$

where the homogenous integrand $\bar{f}(z_i, w_j)$ is obtained by keeping only terms lowest order in λ in each factor of the original integrand such that

$$f(z_i, w_j) \ = \ \lambda^{-d_H} \, \bar{f}(z'_i, w_j) \, (1 + \mathcal{O}(\lambda)) \ , \quad (2.4.2)$$

for each normal variable $z_i = \lambda \, z'_i$ with d_H the degree of homogeneity of $\bar{f}(z_i, w_j)$. More specifically, as we will do the analysis for integrals of the form of Eq. (2.2.1), d_H equals the sum of the lowest powers of λ in the denominator factors minus that in the numerator factors in $f(z_i, w_j)$. The idea is then to scale out λ from each factor in the homogenous integral, to count the overall power, and find the behaviour of the integral as $\lambda \to 0$,

$$\bar{I} \sim \int d\lambda \, \lambda^{\gamma - 1} \int_{\mathcal{H}} \prod_{i=1}^{n} dz'_i \ \delta(1 - \sum_i |z'_i|^2) \int \prod_{j=1}^{m} dw_j \, \bar{f}(z'_i, w_j) \ , \quad (2.4.3)$$

where the overall degree of divergence γ is given by

$$\gamma \ = \ n - d_H \ . \quad (2.4.4)$$

[2]This form with a delta fuction having the sum of the squares of the absolute values of the normal variables in its argument corresponds to bounding the normal space with an n-dimensional sphere with radius λ.

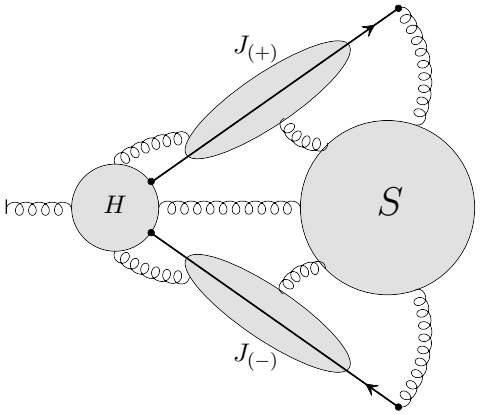

Figure 2.2: Illustration of the soft (S), hard (H), and jet ($J_{(\pm)}$) regions.

By overall degree of divergence, we mean the power of scale parameter λ in the overall integral when all normal variables have the same scale. For $\gamma = 0$, the divergences are logarithmic, while for $\gamma < 0$ there will be power divergences.

If some set of normal coordinates vanished faster than others on S, say as λ^2, that would only increase the power of λ in the volume element of the normal space, giving a nonleading contribution, unless there are new pinches in the homogenous integral after dropping terms that are higher order in the normal variables. These pinches, which could occur between poles that were separated by nonleading terms before they were dropped, could enhance the integrals in principle. However, we will argue that, for our choice of variables, only pinches of the hard-jet-soft type occur in the homogenous integrals. Notice also that, if every normal variable in a subregion vanishes faster than those of other regions, the power counting will still be the same for each subregion. Before two lines can produce a pinch singularity, they must approach the hypercontour to the same scale. Therefore, one can choose a single scale for all normal variables for the power counting for a particular vertex function near a pinch surface. We shall now apply this power counting technique for the fermionic vertex given by Eq. (2.3.9), which we will refer to as the vertex function in the following. As we shall see, power counting for the scalar vertex is essentially equivalent.

As we are dealing with lightlike lines, we will use lightcone coordinates, because the Landau equations for lightcone singularities can be solved more simply in these coordinates. By a combination of rotations and boosts, one can put one of the external points at $x_2^\mu = X_2\,\delta^{\mu+}$ and the other one at $x_1^\mu = X_1\,\delta^{\mu-}$ giving $x_1^2 = x_2^2 = 0$ with $x_1 \cdot x_2 \neq 0$. This will set our coordinate system.

For a particular pinch surface S, *i.e.* a particular solution to Landau equations, one has to identify the intrinsic and normal variables that parametrize

the surface and its normal space, respectively. For instance, let us take the solution with a soft gluon at one loop from Sec. 2.3. There, y_2^+ and y_1^- are the intrinsic variables that remain finite, while y_2^-, y_1^+, $y_{2,\perp}^2$, and $y_{1,\perp}^2$ are the normal variables that vanish on the pinch surface. Such lines connecting vertices at finite distances are part of the soft function. On the other hand, for the hard solution at one loop, all components of y_1^μ and y_2^μ were vanishing, and one has only normal variables for this solution. We will refer to the set of lines connecting a set of vertices all of whose coordinates vanish as the hard function. Lastly, in the one loop example, there were collinear lines. At one loop, for a line in the plus direction, y_2^+ is the intrinsic variable while the rest of the components are normal variables. The set of collinear gluons together with the external lines to which they are parallel define the jet function and its direction. Note that the limits of integration of y_2^+ here goes from zero up to X_2 on this pinch surface. For $y_2^+ > X_2$, the Landau equations can not be solved. Indeed, $y_2^+ > X_2$ does not correspond to a physical process where all lines move forward in time. In general, in a jet the limits of integration over the intrinsic variables for a given pinch surface are not unbounded, but are set according to the time-ordering of vertices along the jet direction.

In homogenous integrals, the denominators of the jet lines will be linear, and those of the hard lines quadratic in normal variables; while the soft lines are of zeroth order. The lines connecting the hard function with the jets are linear in normal variables, and we thus count them as part of the jets. Any line connecting the jets or the hard part to the soft function is zeroth order in normal variables, and hence they are counted in the soft function.

The only approximation in writing the homogenous integrand is dropping terms that are higher order in the normal variables. In fact, such terms occur only in lines connecting two different subdiagrams, namely, in lines connecting the jets to the hard and soft function or those connecting the hard and soft functions. In order for our power counting arguments to be valid, there must not be new pinches introduced in the homogenous integrals because of this approximation. In other words, the Landau conditions for the homogenous integral to be pinched must have the same solutions as those of the original integral (up to trivial shifts or rescalings in some of the variables). We mean by the same solutions, that the pinch singularities of both have the same physical picture. Note that soft lines are never pinched in coordinate space, and thus we only need to consider the pinches of the lines connecting a jet to the hard part in the original and homogenous integrals. To this end, one may consider, for instance, the following integral over two jet lines, which is a part of a jet function,

$$I = \int d^4y \, \frac{1}{-(x-y)^2 + i\epsilon} \, \frac{1}{-(y-z)^2 + i\epsilon} \, , \tag{2.4.5}$$

where x^μ, y^μ are jet vertices and z^μ is a hard vertex[3]. The Landau conditions for a pinch from these two lines after Feynman parametrization are given by

$$-\alpha_1 (x-y)^\mu \; + \; \alpha_2 (y-z)^\mu \; = \; 0 \; , \tag{2.4.6}$$

with $(x-y)^2 = (y-z)^2 = 0$. The only solution to these conditions is that all three vertices are aligned along the jet direction, say the plus direction, and are parallel to each other. The vertex z^μ is allowed to be hard by these conditions, *i.e.* z^+ can also vanish in Eq. (2.4.6) at the same rate as the other components. If one approximates the integral in (2.4.5) by a homogenous integrand with $(y-z)^2 \sim y^2 - 2y^+z^-$, the condition for a pinch in y^--integral is then the same as the condition (2.4.6) for the original integral with $z^+ = 0$. The integrals over the transverse components of y^μ can only be pinched at $y_\perp^2 = x_\perp^2 = 0$. These pinch singularities are present in both original and homogenous integrals. They show up as end-point singularities after the change of variables with $y^1, y^2 \to y_\perp^2, \phi$, which can always be carried out. In general, the pinches of the homogenous integral correspond to pinches of the original integral with some of the variables moved to their end-points.

This approximation can fail if z^+ becomes comparable to y^+ and x^+, or if y^+ diminishes like z^+, which are actually different solutions to the Landau conditions corresponding to different pinch surfaces. Nevertheless, we will see that the result of power counting will not differ in either case, whether the vertex z^μ is taken as part of the jet, or included in the hard part. In our analysis, we identify the normal variables of a pinch surface, group each vertex in a certain subdiagram depending on the size of the components of its position, and do the power counting for the divergence on that particular pinch surface. Generally speaking, the approximations in the homogenous integrals can change if two different regions overlap when some vertices escape to a different subdiagram. However, we will show that the changes in the powers of the factors of two subdiagrams due to removal of a vertex from one subdiagram and its inclusion to the other subdiagram cancel each other, leading to the same conclusion for the overall degree of divergence.

2.4.1 Power counting for a single jet

Before we do the power counting for the full vertex function in coordinate space, we begin with the power counting for a single jet, with the topology of a self-energy diagram, as depicted in Fig. 2.3. Let us take a "dressed" ultra-relativistic fermion moving in the plus direction, so that the plus coordinates

[3]Here, we have omitted the derivatives at each vertex in order to write a simple integrand to illustrate the idea.

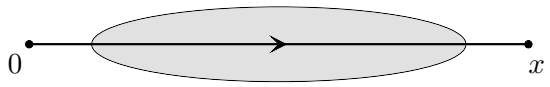

Figure 2.3: A single jet with the topology of a self-energy diagram.

of all vertices inside the jet are the intrinsic variables, while their minus coordinates and squares of transverse positions are the normal variables. With these choices, all normal variables appear linearly in jet line denominators. The condition that the vertices have to be on the lightcone for pinches leaves us with three variables for each vertex. The azimuthal symmetry around the jet axis allows us to choose the square of the transverse components as one normal variable. We will compute the contributions to the overall degree of divergence of the jet, γ_J, from the normal volume element, the denominators, and the numerators of the jet function as defined in Eq. (2.4.4) for a generic singular integral.

For every integration over the positions of the three- and four-point vertices inside the jet, one needs to add $+2$ to γ_J, that is, $+1$ for each normal variable (transverse square and minus component). In $D = 4-2\varepsilon$ dimensions, however, the power for transverse square components is $+(1-\varepsilon)$. In the homogenous jet function, the denominator of each gauge field line contributes a term $-(1-\varepsilon)$ while that of each fermion line contributes $-(2-\varepsilon)$ to γ_J, since the massless fermion propagator in coordinate space is given, as in Eq. (2.3.14), by

$$S_F(x) = \not\partial\, \Delta_F(x^2) = \frac{\Gamma(2-\varepsilon)}{2\,\pi^{2-\varepsilon}}\,\frac{\not x}{(-x^2+i\epsilon)^{2-\varepsilon}}\ . \tag{2.4.7}$$

We are interested in the degree of divergence with respect to the lowest order result, so we will multiply the diagrams of Fig. 2.3 by $[\not x/(-x^2+i\epsilon)^{2-\varepsilon}]^{-1}$. Equivalently, we add a term $+(2-\varepsilon)$ to γ_J to cancel the lightcone divergence of the lowest order diagram, which is simply the fermion propagator.

Now we consider the numerator suppressions. In order to get the leading divergences, in the numerators we will keep only the terms lowest order in normal coordinates, which therefore give the least suppression. To begin, we note that there is a factor contributing to the numerator from each fermion-gluon vertex at a point y_n^μ of the form,

$$\begin{aligned}(\not y_{n+1} - \not y_n)\,\gamma^\mu\,(\not y_n - \not y_{n-1}) \ =& \\ 2\,(y_{n+1}-y_n)^\mu\,(\not y_n - \not y_{n-1}) - \gamma^\mu\,(\not y_{n+1} - \not y_n)\,(\not y_n - \not y_{n-1})\ .&\end{aligned} \tag{2.4.8}$$

Here, the first term is unsuppressed as it is, although the vector with the index μ must form an invariant with some other vector. At the same time, terms proportional to γ^μ in Eq. (2.4.8) either vanish by $(\gamma^\mp)^2 = 0$ or vanish at least as the transverse coordinates of one of the vertices, which are at the order of $\lambda^{1/2}$. In the case of scalar, instead of gauge field lines, with Yukawa couplings to fermions, for each two-fermion-scalar vertex there would be a factor of $(\not{y}_{n+1} - \not{y}_n)\,(\not{y}_n - \not{y}_{n-1})$ in the numerator, giving the same power-counting suppression of at least $\lambda^{1/2}$.

In addition to numerator factors from fermion lines, there are factors from three-gluon vertex functions. A vertex at z_m^μ combines with gluon propagators to give terms that (dropping overall factors) can be written as

$$v_{3g}(z_m, \{y_i\}) \;=\; \epsilon_{ijk}\, g^{\mu_i \mu_j}\, \Delta(z_m - y_i)\, \Delta(z_m - y_j)\, \partial^{\mu_k}_{z_m} \Delta(z_m - y_k) \;, \qquad (2.4.9)$$

where the y_i are the positions of the other ends of the lines. Acting on the gluon lines, the derivatives bring vectors from their coordinate arguments to the numerator, while increasing the power of a denominator by one. These vectors also must form invariants in the numerator, either among themselves or with the Dirac matrices of the fermion-gluon vertices. Suppose we let z_i denote the position of the ith three-gluon-vertex, and y_j the position of the jth fermion-gluon vertex. The numerator is then a product of linear combinations of invariants of the form $\not{z}_i$, $\not{y}_j$, and $z_i \cdot z_{i'}$. Referring to Eq. (2.4.8), one could also get factors with $z_i \cdot y_j$. Each such invariant made out of two vectors is linear in normal variables. One can see then that each fermion-gluon vertex suppresses the numerator by $\lambda^{1/2}$ at least, while every pair of three-gluon vertices produce an invariant suppressing the numerator by λ, while if a three-gluon vertex is contracted with a Dirac matrix at a fermion-gluon vertex, it also suppresses the numerator by $\lambda^{1/2}$ at least. Hence, the contribution of the numerators to γ_J is given by

$$\gamma_{n_J} \;\geq\; \frac{1}{2}(V_3^f + V_3^g) \;=\; \frac{1}{2} V_3 \;, \qquad (2.4.10)$$

with V_3^f the number of fermion-gluon vertices and V_3^g the number of three-gluon vertices inside the jet. Adding all contributions, we obtain a lower bound for the overall degree of divergence of this fermion jet,

$$\gamma_J \;\geq\; 2(V_3 + V_4) + 2 - N_g - 2N_f - V_3^g + \frac{1}{2} V_3 + \mathcal{O}(\varepsilon) \;. \qquad (2.4.11)$$

Here, V_3 (V_4) is the total number of three-point (four-point) vertices, while N_g (N_f) is the number of gluon (fermion) lines in the jet. We can use the

graphical identity,

$$2N \;=\; E + \sum_{i=3,4} i\, V_i \;, \tag{2.4.12}$$

in Eq. (2.4.11), which relates the number of lines of a diagram to the numbers of its various kinds of vertices, where E is the number of external lines of the jet. A single jet has two external lines, $E = 2$, one connected to the external point x^μ and the other to the origin. Combining the number of lines $N = N_f + N_g$ and the number of three-point vertices $V_3 = V_3^f + V_3^g$, we can rearrange the terms in Eq. (2.4.11),

$$\gamma_J \;\geq\; \frac{3}{2} V_3 + 2V_4 - N + 2 + V_3^f - N_f \;, \tag{2.4.13}$$

which, using the graphical identity (2.4.12), can be reduced to

$$\gamma_J \;\geq\; 1 + V_3^f - N_f \;. \tag{2.4.14}$$

Here, we note that, because at each fermion-gluon vertex one fermion line enters and one exists, the number of fermion lines in the jet are equal to one plus the number of fermion-gluon vertices in the jet. Therefore, our power counting results in

$$\gamma_J \;\geq\; 0 \;. \tag{2.4.15}$$

Thus, a fermion jet in coordinate space with the topology of a self-energy diagram can have at worst logarithmic divergence. In contrast to the power counting in momentum space, we did not count the number of loops nor did need to use the Euler identity. Note that the power counting for a scalar jet gives the same result, because the derivatives at two-scalar-gluon vertices in a scalar jet correspond to the derivatives from fermion propagators in a fermion jet. Similarly, the two-scalar-two-gluon "seagull" couplings have no numerator factors, and are counted like the four-point gluon couplings.[4]

If we had kept the terms at $\mathcal{O}(\varepsilon)$ in the power counting of Eq. (2.4.11), we

[4]By the arguments given in the main text, the overall degree of divergence of a scalar jet is bounded from below by

$$\gamma_{SJ} \;\geq\; 2(V_3 + V_4 + V_4^{2g2s}) + 1 - N_s - N_g - V_3^g - V_3^{sg} + \frac{1}{2}(V_3^g + V_3^{sg}) + \mathcal{O}(\varepsilon) \;,$$

with N_s the number of scalar lines, V_4^{2g2s} the number of two-scalar-two-gluon vertices, and V_3^{sg} the number of two-scalar-gluon vertices. Each term on the right hand side cancels by Eq. (2.4.12) such that $\gamma_{SJ} \geq 0$ in this case as well.

would have derived a bound

$$\gamma_J \geq (\frac{1}{2}V_3 + V_4)\varepsilon \ , \tag{2.4.16}$$

which shows that these collinear singularities are regulated also by $\varepsilon > 0$ in coordinate space. No IR regularization is neccessary after UV renormalization when the external points are taken to the lightcone. However, in the Fourier transform of the vertex function for S-Matrix elements in momentum space, the divergences in $p^2 = 0$ will require IR regularization with $\varepsilon < 0$ when the external points are integrated to infinity.

The power counting above and the result (2.4.15) hold in the presence of self-energies inside the jet as well. For instance, cutting a gluon line in the jet and inserting a fermion loop does not change γ_J, because the changes due to extra fermion denominators are canceled by the terms for integrations over the positions of these two new vertices, while the denominator of the extra gluon cancels the contribution of fermion numerators to γ_J since $\not{y}(-\not{y}) = -y^2 \sim \mathcal{O}(\lambda)$ with y^μ the difference of the positions of the two vertices. In the case of inserting a gluon or a ghost loop, a similar cancellation occurs. The denominators of the two new lines in the loop each have a lower power by one compared to fermion lines, but there are now two derivatives at the new vertices raising those powers. A different power counting is needed for the case when such self-energies shrink to a point, that is $y^+ \to 0$ in the example above for a jet in the plus direction. When renormalization has been carried out, such UV-divergences are removed by local counter-terms.

2.4.2 Overall power counting for the vertex function

We are now ready to continue with the overall power counting for the vertex function including two jets, a soft subdiagram, and a hard subdiagram as in Fig. 2.2. We will do the analysis for the fermionic vertex function. As in the previous subsection, the counting is the same for the scalar vertex. It also straightforwardly extends to any amplitude for wide-angle scattering.

The homogenous soft function is independent of normal variables, and by dimensional counting it is finite for fixed external points. We introduce the notation $J^H_{(\pm)g}$ and $J^H_{(\pm)f}$ to denote the numbers of vector and fermion lines, respectively, that connect the hard subdiagram to the jets in the $\pm$ direction. In these terms, we also define

$$J^H_{g,f} = J^H_{(+)g,f} + J^H_{(-)g,f} \ , \tag{2.4.17}$$

$$J^H = J^H_g + J^H_f \ , \tag{2.4.18}$$

where J^H is the total number of lines attaching both jets to the hard subdiagram. Similarly, we define for the lines connecting the jets to the soft subdiagram,

$$S^J_{g,f} = S^J_{(+)g,f} + S^J_{(-)g,f} \ , \tag{2.4.19}$$

$$S^J = S^J_g + S^J_f \ , \tag{2.4.20}$$

and lastly for the lines connecting the soft and hard subdiagrams,

$$S^H = S^H_g + S^H_f \ . \tag{2.4.21}$$

Recall that all components of the vertices in the hard function vanish together, so that hard lines are quadratic in normal variables. Similar to Eq. (2.4.11) for a single jet, the overall degree of divergence for the vertex function relative to the lowest order diagram can be written as

$$\begin{aligned}\gamma_\Gamma \ \geq\ & 4(V_3^H + V_4^H) - 2N_g^H - 3N_f^H - V_{3g}^H \\ & + \sum_{i=+,-} \left[2(V_3^{J_{(i)}} + V_4^{J_{(i)}}) + 2 - N_g^{J_{(i)}} - 2N_f^{J_{(i)}} - V_{3g}^{J_{(i)}} + n^{J_{(i)}}\right] + \mathcal{O}(\varepsilon) \ ,\end{aligned} \tag{2.4.22}$$

where $n^{J_{(\pm)}}$ denotes the numerator contributions from the jet in the $\pm$ direction. The terms labeled H are contributions from the hard part, followed by contributions from the two jets. Note that there are no contributions from integrations over the positions of soft vertices here, because all of their components are intrinsic variables.

In the hard part, every three-gluon vertex produces a vector that must be proportional to a linear combination of the position vectors, z_i^μ of vertices in the hard subdiagram. These are all normal variables, and are hence order λ. These vectors may form invariants with a jet or a soft vertex suppressing the numerator by λ, or two of them may form an invariant at $\mathcal{O}(\lambda^2)$. Thus, each hard three-gluon vertex contributes $+1$ to scaling of the numerator while their derivatives increase the power of a gluon denominator that is quadratic in λ. In total, they contribute $-V_{3g}^H$ to γ_Γ.

The numerator contributions of jets are somewhat different compared to Eq. (2.4.11), because the vectors arising from the derivatives of three-gluon vertices inside the jets can now form invariants with vectors from three-gluon vertices in the hard or soft part, or from the opposite moving jet. At lowest order in normal variables, the invariants resulting from contracting a jet vertex with a soft vertex are zeroth order in normal variables, while those from a jet and a hard vertex are linear, which, however, we have already counted

in (2.4.22) among the contributions from the hard part. There can be at most J_g^H such vectors to form out-of-jet invariants, as many as the number of lines connecting jets to the hard part. The polarization of any of the S_g^J soft gluons connecting the jets to the soft function does not produce an invariant that contributes to $n^J = n^{J^{(+)}} + n^{J^{(-)}}$, and the fermion-gluon vertices in the jets where a soft fermion line attaches do not always give a suppression in the numerator. For the minimum numerator suppressions, we can thus subtract $J_g^H + S_g^J + S_f^J$ from the total number of three-point vertices in n^J,

$$n^J \;\geq\; \frac{1}{2}(V_3^J - J_g^H - S^J) \;, \tag{2.4.23}$$

where we use the notation of Eqs. (2.4.18) and (2.4.20).

We can again apply the graphical identity in (2.4.12) to the terms in Eq. (2.4.22) for the jets and the hard subdiagram separately. The E^H external lines of the hard function are either jet or soft lines,

$$E^H = S^H + J^H \;, \tag{2.4.24}$$

where we assume for this discussion that the minimum of the fermion lines connecting the jets to the hard part is two, $J_f^H \geq 2$, one from each jet. Pinch surfaces where only gluons attach the hard part to the jets in the reduced diagram are also possible, and may be treated similarly, with equivalent results. These external lines must be added to the number of hard lines, $N^H = N_g^H + N_f^H$, in the identity for the total number of lines connected to the hard part,

$$2N^H + E^H \;=\; 2V_2^H + 3V_3^H + 4V_4^H \;. \tag{2.4.25}$$

Here, we consider the vertex of the external current as a two-point-vertex, so that $V_2^H = 1$. The total number of jet lines are related to the number of vertices in both jets by

$$2N^J + S^J \;=\; 2 + J^H + 3V_3^J + 4V_4^J \;, \tag{2.4.26}$$

where the number of (soft) lines, S^J, connecting the jets to the soft part is added to the number of jet lines. Removing the contributions from the gluon lines and vertices they attach in Eq. (2.4.25), one can find a relation between the number of fermion vertices and the number of fermion lines in the hard subdiagram,

$$V_{3f}^H \;=\; N_f^H + \frac{1}{2}(S_f^H + J_f^H - 2), \tag{2.4.27}$$

while a similar relation can be found from (2.4.26) for jets

$$V_{3f}^J \;=\; N_f^J + \frac{1}{2}(S_f^J - J_f^H - 2)\;. \tag{2.4.28}$$

To derive a lower bound for γ_Γ in Eq. (2.4.22) it is convenient to begin by applying (2.4.25) to the 'H' terms of γ_Γ, and Eq. (2.4.26) to the jet terms. Then, we can readily use the relations of fermion lines to vertices, (2.4.27) and (2.4.28), for the hard subdiagram and for the jets, respectively, and the numerator inequality (2.4.23), to derive a lower bound for the overall degree of divergence of the vertex function,

$$\gamma_\Gamma \;\geq\; S_g^H + \frac{3}{2}S_f^H + \frac{1}{2}(S_f^J + J_f^H - 2)\;. \tag{2.4.29}$$

The condition for a (logarithmic) divergence is then that no line can connect the hard subdiagram directly to the soft subdiagram and that only a single fermion attach each jet to the hard subdiagram. This corresponds to similar results found for pinch surfaces in momentum space [7,47]. The soft and hard subdiagrams can only interact through jets. Moreover, when the lower bound is saturated, using the same relations above, the leftover terms in γ_Γ that are at the order of ε can be shown to be equal to

$$\gamma_\Gamma^{\mathcal{O}(\varepsilon)} = \Big(\frac{1}{2}V_3^J + V_3^H + V_4^J + 2V_4^H - \frac{1}{2}[S_g^J + J_g^H]\Big)\varepsilon\;. \tag{2.4.30}$$

For each line connecting the soft part to a jet there is a vertex in the jet, while for each line connecting a jet to the hard part there is a hard vertex. Thus, there will be enough vertices left over to make the coefficient of ε positive. Therefore, the logarithmic divergence of the vertex function is regulated by $\varepsilon > 0$ in coordinate space.

We shall now consider the changes in the power counting due to removal of a vertex from one subdiagram and its inclusion to the other subdiagram. This will happen at the boundary of integration in intrinsic variables. Suppose that one of the jet vertices connected to the hard part gets captured by the hard part and becomes part of it, or a vertex in the jet escapes to the soft part, as depicted in Fig. 2.4. In the first case, the line, which used to connect the hard part to one of the jets has become a hard line, while the other jet lines attached to that vertex now connect the hard part and the jet. Thus, if the vertex that gets captured is a three-gluon vertex, N_g^H, V_{3g}^H, and J^H each change by $+1$, while N_g^J and V_{3g}^J change by -1. Likewise, if a four-point vertex gets captured, N_g^H and V_4^H increase by $+1$ but J^H now increases by $+2$, while N_g^J and V_4^J change by -1. These changes, however, cancel exactly in Eq. (2.4.22)

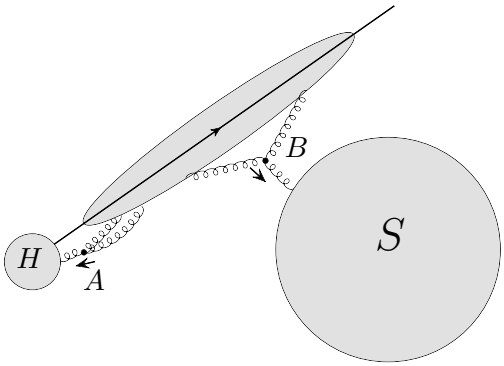

Figure 2.4: A jet vertex A gets captured by the hard part, while another vertex B escapes to the soft part. Power counting for this pinch surface gives the same result as when the vertices A and B were inside the jet. The other jet in the opposite direction is suppressed here.

using the bound for the jet numerator contributions n^J in Eqs. (2.4.23) for the most divergent configurations. Similarly, if a three-gluon vertex in the jet escapes to the soft part, it pulls two lines out of the jet making them soft, hence N_g^J and V_{3g}^J change by -2 and -1, respectively, while S^J increases by $+1$. For a four-point vertex that escapes the jet and joins the soft part, N_g^J and V_4^J decrease by -3 and -1, respectively, while S^J increases by $+2$. These changes also cancel in Eq. (2.4.22) for the most divergent configurations. Note also that when a hard vertex escapes to the soft part the leftover changes in Eq. (2.4.22) are equal to ΔS_H, the change in the number of lines connecting the hard and soft parts. Therefore, the leading behaviour does not change, even if two different subdiagrams do overlap, as was asserted at the beginning of this section.

To conclude, we have shown by power counting arguments that the vertex function in coordinate space can diverge at worst logarithmically times overall lowest-order behavior. This logarithmic divergence requires $D < 4$ in dimensional regularization.

2.5 Approximations and Factorization

A fundamental consequence of the structure of pinch surfaces is the factorization of soft gluons from jets and jet gluons from the hard part. This is shown in momentum space by the use of Ward identities [5, 31, 53]. In this section, we show how the same Ward identities, as they appear in coordinate space, result in the factorization of soft, jet and hard functions.

2.5.1 Hard-collinear approximation

Having identified the jet and hard regions that can give divergences in coordinate-space integrals in the previous section, we now construct a coordinate space *"hard-collinear"* approximation to the integral, which enables factorization of the jet and hard functions at the leading singularities. Recall that the only approximation made for writing a homogenous integrand to do the power counting for these two regions was dropping the terms higher order in normal variables in lines connecting the jets to the hard part. Thus, the approximation one needs is made on the propagators of these jet lines attached to the hard part. We shall explain this *"hard-collinear"* approximation with the example of the following integral,

$$I(y) \;=\; \int d^4z\, J^\nu(y)\, g_{\nu\rho}\, D^{\rho\mu}(y-z)\, H_\mu(z)\;, \tag{2.5.1}$$

where J^ν denotes a jet function with a direction β^ν, $D^{\rho\mu}(y-z)$ the propagator of the line that connects a jet vertex at y to a hard vertex at z, and $H_\mu(z)$ a hard function. We raise and lower the indices by the Minkowski metric. Here, we have suppressed the dependence on other vertices, which are also integrated over. The integral in (2.5.1) will have divergences when the jet moves in the plus or minus lightcone direction and all coordinates of the hard function vanish. In this limit, we can approximate this integral by picking out the large component of the jet, by replacing $g_{\nu\rho} \to \beta'_\nu \beta_\rho$ where $\beta^\mu = \delta^{\mu+}$ and $\beta'\nu = \delta^{\nu-}$,

$$I(y) \;\sim\; \int d^4z\, J^\nu(y)\, \beta'_\nu\, \beta_\rho\, \bar{D}^{\rho\mu}(y-z)\, H_\mu(z)\;. \tag{2.5.2}$$

In the gluon propagator, $\bar{D}$, we neglect the smaller terms coming from the hard vertex. Let us take the jet to be in the plus-direction, then the dependence on z^μ in the argument of the propagator will be largely through z^-, the component of the hard vertex in the opposite direction, because

$$(y-z)^2 = 2y^+(y^- - z^-) - y_\perp^2 + \mathcal{O}(\lambda^{3/2})\;, \tag{2.5.3}$$

for $y^+ \gg z^+$ and $y_\perp^2 \gg z_\perp^2$. We then write the propagator as

$$\begin{aligned}
\beta_\rho\, D^{\rho\mu}(y-z) \;&=\; D^{-+}(y-z)\beta^\mu\;, \\
\bar{D}^{-+}(y-z) \;&=\; \frac{\partial}{\partial z^-}\int_\infty^{z^-} d\sigma\, D^{-+}\big(2y^+(y^- - \sigma\,\beta'^-) - y_\perp^2\big)\;, \\
&\equiv\; \partial_{z^-}\mathscr{D}(y,z^-)\;.
\end{aligned} \tag{2.5.4}$$

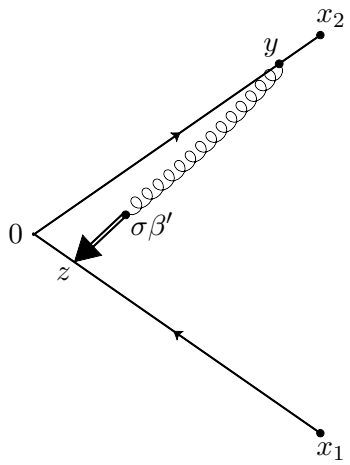

Figure 2.5: One-loop example for the *hard-collinear* approximation. The arrow represents the action of the derivative on the hard function $H(z)$, which is just a fermion propagator here.

For this representation, we should take $\varepsilon < 0$ in $\bar{D}^{-+}$. One can now integrate by parts in Eq. (2.5.2), so that $-\partial_{z^-}$ acts on the hard function $H_\mu(z)$,

$$I(y) \;\sim\; \int d^4z\, J^+(y)\, \mathscr{D}(y,z^-)\big(-\partial_{z^-} H^-(z)\big)\;. \tag{2.5.5}$$

There are no boundary terms as a result of integrating by parts, because in the hard function $H_\mu(z)$ there must be at least one propagator that vanishes at $z^- = \pm\infty$. Furthermore, we can add to the integrand the derivatives with respect to other components of z^μ such that we now have a full gradient ∂_z^μ acting on the hard function $H_\mu(z)$. Because the jet function and $\mathscr{D}(y,z^-)$ do not depend on z^+ and $z_\perp$, these added terms are total derivatives and vanish after the integration. The result of our approximation can then be expressed by

$$I(y) \;\sim\; \int d^4z\, \big(J^\nu(y)\,\beta'_\nu\big)\, \mathscr{D}(y,z)\big(-\partial^\mu H_\mu(z)\big)\;. \tag{2.5.6}$$

In other words, we have replaced the propagator of the gluon escaping from the jet to the hard part by $D^{\nu\mu}(y-z) \to \mathscr{D}(y,z)\beta'^\nu\partial_z^\mu$ with β'^ν being a vector in the opposite direction of the jet. The momentum-space analog of such a gluon is called "longitudinally" or "scalar polarized", and is associated with the scalar operator $\partial_\mu A^\mu(x)$ in coordinate space.

For the simplest example illustrated in Fig. 2.5, this approximation for the

vertex function at one loop results in

$$I^{(1)} \sim \int d^D z \frac{\not{x}_2 - \not{y}}{(-(x_2-y)^2+i\epsilon)^{2-\varepsilon}} \not{\beta}' \frac{\not{y}}{(-y^2+i\epsilon)^{2-\varepsilon}} \times \int_\infty^{z^-} d\sigma \frac{1}{(-2y^+(y^- - \sigma\,\beta') + y_\perp^2 + i\epsilon)^{1-\varepsilon}} \times \left(-\frac{\partial}{\partial z^\mu}\right) \left(\frac{-\not{z}}{(-z^2+i\epsilon)^{2-\varepsilon}} \gamma^\mu \frac{\not{z} - \not{x}_1}{(-(z-x_1)^2+i\epsilon)^{2-\varepsilon}} \right) , \tag{2.5.7}$$

where we have omitted the incoming current, integrations over jet vertices, and numerical factors. After acting with ∂_μ^z, there are two terms with a relative sign coming from the action of the derivative on either fermion propagator, canceling them in turn by the massless Dirac equation $\not{\partial} S_F(x) = -\delta^D(x)$,

$$I^{(1)} \sim \int d^D z \, \frac{\not{x}_2 - \not{y}}{(-(x_2-y)^2+i\epsilon)^{2-\varepsilon}} \not{\beta}' \frac{\not{y}}{(-y^2+i\epsilon)^{2-\varepsilon}} \times \int_\infty^{z^-} d\sigma \frac{1}{(-2y^+(y^- - \sigma\,\beta') + y_\perp^2 + i\epsilon)^{1-\varepsilon}} \times \left(\frac{-\not{z}}{(-z^2+i\epsilon)^{2-\varepsilon}} \, \delta^D(z-x_1) \, - \, \delta^D(z) \, \frac{\not{z} - \not{x}_1}{(-(z-x_1)^2+i\epsilon)^{2-\varepsilon}} \right) . \tag{2.5.8}$$

After integrating over z, the location of the attachment of the "scalar polarized" gluon, using the delta functions, the two terms differ only in the upper limits of the σ integrals, which can be combined so that the the remaining leading term is given by

$$I^{(1)} \;\sim\; -\frac{\not{x}_2 - \not{y}}{(-(x_2-y)^2+i\epsilon)^{2-\varepsilon}} \not{\beta}' \frac{\not{y}}{(-y^2+i\epsilon)^{2-\varepsilon}} \frac{-\not{x}_1}{(-x_1^2+i\epsilon)^{2-\varepsilon}} \times \left(\int_0^{x_1^-} d\sigma \frac{1}{(-2y^+(y^- - \sigma\,\beta') + y_\perp^2 + i\epsilon)^{1-\varepsilon}} \right) . \tag{2.5.9}$$

Therefore, after the *hard-collinear* approximation the "scalar polarized" gluon has been factored onto an eikonal line in the opposite direction from the jet of which it is a part such that the jet is now factorized from the rest of the diagram. Note that the integration over the eikonal line is a scaleless integral, which in the limit $x_1^- \to \infty$ will be defined by its ultraviolet pole only.

The *hard-collinear* approximation also allows us to apply the basic Ward identities of gauge theories directly to the leading singularity of the vertex function in order to factor the "scalar polarized" gluons from the hard function. This reasoning was used in the proofs of factorization in gauge theories in momentum space [31, 54, 55] and the same reasoning applies here. The Ward identity that we need is given by

$$\langle \text{out}|T\Big(\partial_{\mu_1} A^{\mu_1}(x_1)\cdots\partial_{\mu_n} A^{\mu_n}(x_n)\Big)|\text{in}\rangle \;=\; 0\;, \tag{2.5.10}$$

where $|\text{in}\rangle$ and $\langle\text{out}|$ are physical states involving particles of fermion and gauge fields with physical polarizations only. The gauge field $A^\mu(x)$ can be abelian or non-abelian, the above matrix element relation involving scalar polarized gauge fields holds at each order in perturbation theory after the sum over all contributing diagrams [22, 56].

At higher orders, the external lines of the hard function will be two physical fermion lines on the lightcone, one entering and the other exiting the hard function, and some number of "scalar polarized" gauge field lines with derivatives acting on the hard function. Consider the case with one such gluon line connected to the hard part as in Fig. 2.6. This diagram is equal to minus the diagram where the scalar-polarized gluon is acting on the fermion line in the same direction by the Ward identity (2.5.10), which gives a factored gluon onto an eikonal line as we showed above at lowest order. This summarizes the argument, which was also extended to arbitrary number of gluon lines, for the proof of factorization of jets (collinear singularities) from the hard function in momentum space, see the review of Ref. [31]. The same factorization can be shown in coordinate space after the *hard-collinear* approximation described above using the Ward identity (2.5.10), in the same way as in momentum space.

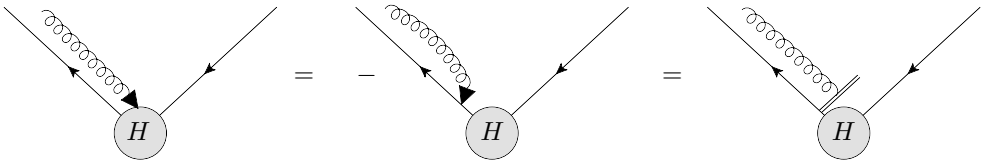

Figure 2.6: Factorization of one "scalar polarized" gluon from the hard subdiagram.

2.5.2 Soft-collinear approximation

One may also do a *"soft-collinear"* approximation for the lines that connect the jets to the soft function such that the collinear singularities of jets will be factored from the finite soft function. We will follow the same reasoning and repeat the same steps as we did for the "hard-collinear" approximation. To avoid repetition, we will skip those details of our arguments that were explained in the previous section. In analogy to the integral in (2.5.1), now consider

$$I(z) \;=\; \int d^4y\, S_\mu(z)\, D^{\mu\nu}(z-y)\, g_{\nu\rho}\, J^\rho(y)\;. \tag{2.5.11}$$

Here, $S_\mu(z)$ denotes the soft function, and J^ρ denotes a jet function with a direction β^ρ. $D^{\mu\nu}(z-y)$ is the propagator of the line that connects a soft vertex at z to a vertex in the jet at y, which are at a finite distance from each other. We suppress the dependence of either function on other vertices as before. In this integral, the only singularities of the integrand are contained in the jet function. Again, to approximate this integral, we will drop the small terms in the argument of the progator, and pick up only the large numerator component of the jet,

$$I(z) \;\sim\; \int d^4y\, S_\mu(z)\, \bar{D}^{\mu\nu}(z-y)\, \beta_\nu\, \beta'_\rho\, J^\rho(y)\;, \tag{2.5.12}$$

with $\beta^2 = \beta'^2 = 0$ and $\beta\cdot\beta' = 1$. Suppose the jet is in the plus-direction, then following our power counting, $z^- \gg y^-$ and $z_\perp^2 \gg y_\perp^2$ such that

$$(z-y)^2 = 2(z^+ - y^+)z^- - z_\perp^2 + \mathcal{O}(\lambda^{1/2})\;. \tag{2.5.13}$$

Thus, this time we write the propagator connecting the soft part to a jet as

$$\begin{aligned} D^{\mu\nu}(z-y)\,\beta_\nu \;&=\; \beta^\mu\, D^{+-}(y-z)\;, \\ \bar{D}^{+-}(z-y) \;&=\; \frac{\partial}{\partial y^+}\int_\infty^{y^+} d\sigma\, D^{+-}(z-\sigma\,\beta) \;\equiv\; \partial_{y^+}\mathscr{D}(z,y^+) \end{aligned} \tag{2.5.14}$$

Using the steps above, we integrate by parts in Eq. (2.5.12), and then add to the integrand the derivatives with respect to other components of y^μ as well. In this way, we obtain

$$I(z) \;\sim\; \int d^4y\, S_\mu(z)\, \beta^\mu\, \mathscr{D}(y,z)\,\big(-\partial_\nu J^\nu(y)\big)\;. \tag{2.5.15}$$

We see that the jets are connected to the soft part also by "scalar polarized" gluons, which can be factored from the jets by using the Ward identity given in Eq. (2.5.10). The formal proof of factorization into hard, soft, and jet functions in coordinate space now follows the momentum-space procedure, and requires only the *hard-collinear* and *soft-collinear* approximations described here.

2.5.3 Eikonal approximation

Having described the *hard-collinear* and *soft-collinear* approximations above to factorize the contributions from different subdiagrams at the leading singularity, we can now think of another approximation to simplify the computation of the leading term. One may make an approximation to the integrals keeping only the leading contribution on a pinch surface where the fermion lines are taken on the lightcone, and neglecting the sub-leading contributions coming away from that pinch surface by imposing the results of the Landau conditions inside the integrands.

As an example, let us again take the fermionic vertex function. The solutions to Landau equations with collinear fermions set the transverse coordinates and the minus (plus) coordinates of the positions of the fermion-gluon vertices on the plus-line (minus-line) to zero as well as time-ordering them. These conditions can be imposed inside the integrand by replacing the fermion propagators along the plus line with

$$S_F(x^2) \;=\; \not{\partial}\,\Delta_F(x^2) \;\to\; \theta(x^+)\,\delta(x^-)\,\delta^2(x_\perp)\,\gamma\cdot\beta\;, \tag{2.5.16}$$

with $\beta = \delta^{\mu+}$ while for those along the minus line, in the direction $\beta' = \delta^{\mu-}$, x^+ and x^- are exchanged. This is actually the coordinate-space version of the well-known eikonal approximation, which is based on assuming the gluons are soft and neglecting their squared momenta in the fermion propagators. The eikonal approximation originates from geometrical optics, where it corresponds to the small wavelength limit in which the trajectories of light are given by light rays as in classical theory. One might have derived the form of the fermion propagators also by taking the Fourier transform of the eikonal propagator in momentum space for a massless fermion moving in the direction $\beta^\mu = \delta^{\mu+}$,

$$\int \frac{d^4k}{(2\pi)^4}\,\frac{i}{\beta\cdot k + i\epsilon}\,e^{-ik\cdot x} \;=\; \theta(x^+)\,\delta(x^-)\,\delta^2(x_\perp)\;. \tag{2.5.17}$$

Let us apply this eikonal approximation to the one-loop vertex diagram as an

example,

$$\Gamma^{(1)}_{\text{eik}} = \int d^4y_2\, d^4y_1\, \theta(x_2^+ - y_2^+)\, \theta(y_2^+)\, \theta(y_1^-)\, \theta(x_1^- - y_1^-) \times \delta(y_2^-)\, \delta^2(y_{2,\perp})\, \delta(y_1^+)\, \delta^2(y_{1,\perp}) \frac{1}{(-(y_2 - y_1)^2 + i\epsilon)} \,, \tag{2.5.18}$$

where we have suppressed the numerical factors and dropped the delta-functions of the external lines. The result, after introducing the parameters λ and σ with $\beta'^{\nu} = \delta^{\nu -}$,

$$\Gamma^{(1)}_{\text{eik}} = \int_0^{x_2^+} d\lambda \int_0^{x_1^-} d\sigma\, \frac{1}{(-2\beta \cdot \beta' \lambda\, \sigma + i\epsilon)} \,, \tag{2.5.19}$$

is exactly equal to a first-order diagram of a Wilson line with a cusp at the origin, which begins at the point x_1^μ *pointing* in the direction of β', then changes its direction to β at the origin, and later ends at x_2^μ. The parameters λ, σ are simply relabelings for y_2^+ and y_1^- that give the locations where the gluon is attached to the Wilson line, and of course, are integrated over. This equality between the diagrams of a cusped path ordered exponential and of the vertex function after the eikonal approximation also holds at higher orders, because the theta functions simply order the attachments to the eikonals while the integrations over any other vertices are the same in both cases. Therefore, we may approximate the vertex function by a Wilson line calculation at any given order in perturbation theory [33, 57]. The power counting for the path ordered exponentials is not exactly the same with that for the vertex function with partonic lines, but is very similar and gives the same bound for their overall degree of divergence, which we will present in Appendix A.2 to avoid repetition. Having seen that path-ordered exponentials of constant velocities correspond to the eikonal approximation for energetic partons, we will now investigate them further in the next chapter.

2.6 Discussion

The coordinate-space singularities of Feynman integrals in a massless gauge theory have a direct interpretation in terms of physical processes, in which classical massless particles propagate freely between points in space-time, where they scatter by local interactions. The singularities occur only if these particles move on the lightcone. The condition for pinches in the coordinate integrals is interpreted as momentum conservation for these scattered particles with the identification of their momenta from their coordinates. This interpretation is the same as the interpretation given by Coleman and Norton [46] to Landau

equations in momentum space [45].

The pinches in the coordinate integrals for the vertex function occur when a group of lines get mutually collinear forming jets as in momentum space. There are also pinches from "zero" lines when some set of internal vertices move to the origin $x \to 0$ reflecting a short-distance singularity, where these zero lines or vertices with vanishing components define a hard function in coordinate space. There are also end-point singularities in the integrals over Feynman parameters $\alpha \to 0$, which define the soft function in coordinate space. An important difference from the momentum space is that the soft function is finite in coordinate space when the external points of the vertex function (x_1 and x_2 above) are kept at finite distances. The collinear divergences are of ultraviolet nature in coordinate space, and require $D < 4$ in dimensional regularization; while no infrared regulation is needed since the coordinates of the external particles provide the natural infrared cut-off.

By the power counting arguments developed above, vertex functions in coordinate space are found to be at worst logarithmically divergent at higher orders, relative to the lowest order results. Similarly, after the eikonal approximation, the path ordered exponentials have the same bound for their overall degree of divergence. The requirement for a divergence in both cases is that the hard and soft subdiagrams must not be directly connected, and they can only interact through the jets. Two jets on the lightcone in different directions can only have a hard interaction at the origin and interact softly at later times. This illustrates in coordinate space the factorization of short and long-distance dynamics in field theories. We have also explained the *hard-collinear* and *soft-collinear* approximations that are needed for the formal implementation of factorization in coordinate space.

Chapter 3

Webs and Surfaces

The contents of this chapter is published in Ref. [33].

3.1 Introduction

Gauge field path-ordered exponentials [59–61] or Wilson lines, represent the interaction of energetic partons with relatively softer radiation in gauge theories. For constant velocities, ordered exponentials of semi-infinite length correspond to the eikonal approximation for energetic partons. Classic phenomenological applications of ordered exponentials include soft radiation limits in deeply inelastic scattering [62] and parton pair production and electroweak annihilation [63–65]. They appear as well in the treatment of parton distributions [66, 67]. In all these cases, the electroweak current is represented by a color singlet vertex at which lines in the same color representation but with different velocities are coupled. This vertex is often referred to as a cusp.

Cusps also appear as vertices in polygons formed from Wilson lines [58], which have been studied extensively in the context of their duality to scattering amplitudes in $\mathcal{N} = 4$ SYM theory [43, 44, 68–71]. In the strong coupling limit of this theory, gauge-gravity duality relates the cusp and polygons to the exponentials of two-dimensional surface integrals. Surfaces bounded by open and closed paths of ordered exponentials are also a classic ingredient in lattice [61] and large-N_c [72] paradigms for confinement in quantum chromodynamics.

In this chapter, we show that in any gauge theory with massless vector bosons the cusp matrix element for lightlike Wilson lines can be expressed as the exponential of an integral over a two-dimensional surface, a result with applications as well to polygons formed from ordered exponentials. The corresponding integrand is an infrared finite function of the gauge theory coupling, evaluated for each point on the surface at a scale given by the invariant

distance from that point to the cusp vertex. This result extends to all orders in perturbation theory.

The set of all virtual corrections for the cusp [57] is formally identical to a vacuum expectation value, and can be written as

$$\Gamma^{(f)}(\beta_1,\beta_2) = \left\langle 0 \left| T\left(\Phi^{(f)}_{\beta_2}(\infty,0)\, \Phi^{(f)}_{\beta_1}(0,-\infty) \right) \right| 0 \right\rangle , \tag{3.1.1}$$

in terms of constant-velocity ordered exponentials,

$$\Phi^{(f)}_{\beta_i}(x+\lambda\beta_i,x) = \mathcal{P}\exp\left(-ig\int_0^\lambda d\lambda' \beta_i\cdot A^{(f)}(x+\lambda'\beta_i) \right) . \tag{3.1.2}$$

Here f labels a representation of the gauge group and β_i is a four-velocity, taken lightlike in the following. The combination of ordered exponentials in Eq. (3.1.1) corresponds to a partonic process with spacelike momentum transfer. For correspondence to a timelike process like pair creation, $\Phi^{(f)}_{\beta_1}(0,-\infty)$ can be replaced by $\Phi^{(\bar{f})}_{\beta_1}(\infty,0)$. Corrections to partonic scattering [73–83] involve the coupling of more than two ordered exponentials at a point [84, 85]. Here, we study the all-orders properties of the single cusp and of polygons with sequential cusps, computed perturbatively in coordinate space.

Perturbative corrections to the unrenormalized cusp, Eq. (3.1.1) are scaleless, and hence vanish in dimensional regularization. The ultraviolet poles of (3.1.1) determine the anomalous dimension of the cusp, and can be used to define a renormalized expansion, both for the cusp and for polygons formed from ordered exponentials of finite length [58, 84]. For the cusp in an asymptotically free theory, however, neither its ultraviolet nor its infrared behavior can be considered as truly physical. At very short distances, dynamics is perturbative and recoil cannot be neglected. At very long distances, dynamics is nonperturbative, and dominated by the hadronic spectrum. In this discussion, we will regard the cusp as an interpolation between these asymptotic regimes. We will concentrate on the structure of the integrals in the intermediate region, although we also discuss their renormalization.

We begin in Sec. 3.2 with a review of exponentiation for products of ordered exponentials, a result that extends to arbitrary products of such lines and to closed loops. Section 3.3 recalls the coordinate space picture of exponentiation in terms of web diagrams and introduces the cancellation of subdivergences of webs. It is in this discussion that a surface interpretation of the exponent emerges. We provide a two-loop illustration of subdivergence cancellation, motivate its generalization to all orders, and give an all-orders prescription for the calculation of the cusp exponent. In Sec. 3.4, we apply these ideas to

multi-cusp polygonal Wilson loops.

3.2 Exponentiation and webs in momentum-space

The cusp has long been known [86–88] to be the exponential of a sum of special diagrams called webs, which are irreducible by cutting two eikonal lines. We represent this result as

$$\Gamma(\beta_1, \beta_2, \varepsilon) \;=\; \exp E(\beta_1, \beta_2, \varepsilon)\,, \tag{3.2.1}$$

in $D = 4 - 2\varepsilon$ dimensions. The exponent E equals a sum over web diagrams, d, each given by a group factor multiplied by a diagrammatic integral,

$$E(\beta_1, \beta_2, \varepsilon) \;=\; \sum_{webs\ d} \overline{C}_d\, \mathcal{F}_d(\beta_1, \beta_2, \varepsilon)\,, \tag{3.2.2}$$

where $\mathcal{F}_d$ represents the momentum- or coordinate-space integral for diagram d. The coefficients of these integrals, $\overline{C}_d$ are modified color factors. Two-loop examples are shown in Fig. 3.1.

In momentum space we can write the exponent E as the integral over a single, overall loop momentum that runs through the web and the cusp vertex, assuming that all loop integrals internal to the web have already been carried out. The web is defined to include the necessary counterterms of the gauge theory [66,84,89,90]. Taking into account the boost invariance of the cusp for massless loop velocities, and the invariance of the ordered exponentials under rescalings of the velocities β_i, we have for the exponent the form,

$$E(\beta_1, \beta_2, \varepsilon) = \int \frac{d^D k}{(2\pi)^D}\, \frac{\beta_1 \cdot \beta_2}{k \cdot \beta_1\, k \cdot \beta_2}\, \frac{1}{k^2}\, \bar{w}\left(\frac{k^2}{\mu^2}, \frac{k \cdot \beta_1\, k \cdot \beta_2}{\mu^2 \beta_1 \cdot \beta_2}, \alpha_s(\mu^2, \varepsilon), \varepsilon\right). \tag{3.2.3}$$

In addition, the webs themselves are renormalization-scale independent,

$$\mu \frac{d}{d\mu}\, \bar{w}\left(\frac{k^2}{\mu^2}, \frac{k \cdot \beta_1\, k \cdot \beta_2}{\mu^2 \beta_1 \cdot \beta_2}, \alpha_s(\mu^2, \varepsilon), \varepsilon\right) = 0\,. \tag{3.2.4}$$

This renormalization scale invariance allows us to choose μ^2 equal to either of the kinematic arguments in the web. A further important property of webs is the absence of collinear and soft subdivergences in the sum of all web diagrams. That is, in Eq. (3.2.3), collinear poles are generated only when k^2 and either $k \cdot \beta_1$ or $k \cdot \beta_2$ vanish, infrared poles only when all three vanish and the overall

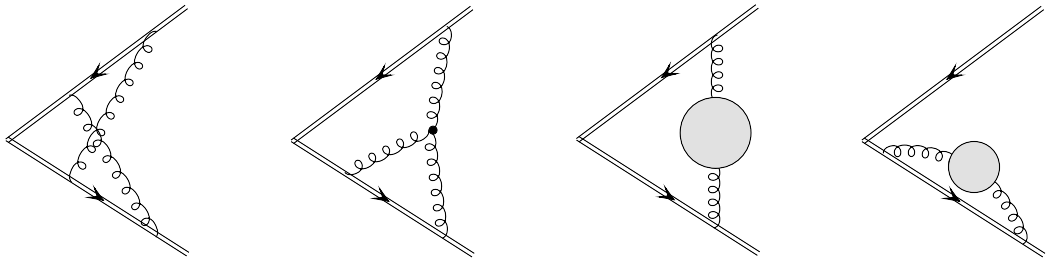

Figure 3.1: Two-loop web diagrams, referred to in the text as: (a) E_{cross}, (b) E_{3g}, (c)–(d) E_{se}. Web diagram (a) has the modified color factor, $C_a C_A/2$, where a refers to the representation of the Wilson lines. For diagram (a), the web color factor differs from its original color factor, while all other color factors are the same as in the normal expansion. Diagrams related by top-bottom reflection are not shown.

ultraviolet poles only when all components of k diverge. Equation (3.2.3) thus organizes the same double poles found in the corresponding partonic form factors [90–94]. Arguments for these properties in momentum space are given in Ref. [90], based on the factorization of soft gluons from fast-moving collinear partons. These considerations suggest that when embedded in an on-shell amplitude or cross section, the web acts as a unit, almost like a single gluon, dressed by arbitrary orders in the coupling. In the following, we observe that this analogy can be extended to coordinate space.

The form given above, in terms of webs, is for the unrenormalized cusp. When renormalized by the minimal subtraction of ultraviolet poles, the exponent E can be written in the form [36],

$$E_{\text{ren}}(\alpha_s(\mu^2),\varepsilon) = -\frac{1}{2}\int_0^{\mu^2}\frac{d\xi^2}{\xi^2}\left[\Gamma_{\text{cusp}}\Big(\alpha_s\left(\xi^2\right)\Big)\,\log\left(\frac{\mu^2}{\xi^2}\right) \;-\; G_{\text{eik}}(\alpha_s\left(\xi^2\right))\right], \tag{3.2.5}$$

where μ^2 is the renormalization scale, and where, here and below, we have set $\beta_1 \cdot \beta_2 = 1$. At order α_s^n, the leading pole behavior of this exponent is proportional to $\Gamma^{(1)}_{\text{cusp}}\,\alpha_s^n(1/\varepsilon)^{n+1}$, with $\Gamma^{(1)}_{\text{cusp}}(\alpha_s/\pi)$ the one-loop cusp anomalous dimension. Nonleading poles are generated from higher orders in Γ_{cusp}, from G_{eik}, and from the ε-dependence of the running coupling in D dimensions [91]. After renormalization in this manner, the cusp is a sum of infrared poles in one-to-one correspondence with the ultraviolet poles that are subtracted. The

cusp anomalous dimension is given to two loops by

$$\begin{aligned}\Gamma_{\text{cusp, a}} &= \left(\frac{\alpha_s}{\pi}\right) C_a \left[1 + \left(\frac{\alpha_s}{\pi}\right) K\right] , \\ K &= \left(\frac{67}{36} - \frac{\pi^2}{12}\right) C_A - \frac{5}{18} n_f T_f , \end{aligned} \tag{3.2.6}$$

with $C_a = 4/3, 3$ for $a = q, g$ for QCD, n_f the number of fermion flavors, and $T_f = 1/2$. At one loop, G_{eik} is zero, and we will derive its two-loop form below. Equation (3.2.5) gives all the poles of the cusp, when reexpanded in terms of the coupling at any fixed scale. We note that for timelike kinematics, the renormalization scale μ^2 should be chosen negative [36].

3.3 Webs and surfaces in coordinate space

3.3.1 The unrenormalized exponent and its surface interpretation

The coordinate-space analog of Eq. (3.2.3) is a double integral over two parameters, σ and λ that measure distances along the Wilson lines β_1 and β_2, respectively, with a new web function, w, which depends on these variables through the only available dimensionless combination, $\lambda\sigma\mu^2$,

$$E = \int_0^\infty \frac{d\lambda}{\lambda} \int_0^\infty \frac{d\sigma}{\sigma}\, w(\alpha_s(\mu^2, \varepsilon), \lambda\sigma\mu^2, \varepsilon) . \tag{3.3.1}$$

Here and below, we choose timelike kinematics. We emphasize that we are interested primarily in the form and symmetries of the integrand, rather than its convergence properties. Nevertheless, to separate infrared and ultraviolet poles in the integration, it is necessary that the integrand, w in Eq. (3.3.1) be free of both infrared and ultraviolet divergences at $\varepsilon = 0$ in renormalized perturbation theory (aside from the renormalization of the cusp itself). As we shall see below, Eq. (3.3.1) with a finite web function leads to a renormalized cusp that is fully consistent with the momentum space form, Eq. (3.2.5). In this construction, all ε poles of the exponent, and therefore the cusp, are then associated with the integrals over λ and σ in (3.3.1).

A direct, coordinate-space demonstration of the finiteness of the web function is interesting in its own right, and will be described in detail elsewhere [34]. Formally, such a demonstration is necessary to extend the proof of renormalizability for cusps connecting massive lines [84] to the massless case [58]. Here, we simply mention the essential ingredients of such an argument.

Diagram by diagram, one may use the analytic structure of the coordinate integrations [48] combined with a coordinate-space power-counting technique to identify the most general singular subregions in coordinate space [32]. In coordinate space, nonlocal ultraviolet subdivergences arise when a subset of vertices line up at finite distances from the cusp along either of the lightlike Wilson lines, while other, "soft" vertices remain at finite distances. Such subdiagrams factorize, however, in much the same manner as in momentum space [53–55]. Once in factorized form, combinatoric arguments show that divergent integrals cancel when all web diagrams are combined at a given order [34] in coordinate space, in much the same way as in the momentum-space treatment of Ref. [90]. Finally, taking λ and σ, as the positions of vertices in the web diagrams furthest from the cusp, there are no soft (infinite wavelength) divergences from integrations over the internal vertices of webs in coordinate representation, as shown in Ref. [32].

As we shall shall illustrate below, it is possible to implement the cancellation of subdivergences at fixed positions, λ and σ, along the ordered paths, specified by the vertices furthest from the cusp. Once this is done and the subdivergences thereby eliminated, the integrals over all vertices of the web diagrams converge on scales set by λ and σ in (3.3.1), and the web acts as a unit. Singular behavior of the cusp arises as λ and/or σ vanish, and in these limits all web vertices approach the directions of β_1 or β_2 together, as in Fig. 3.2(a). This is the perturbative realization of the web as a geometrical object. Subdivergent configurations that cancel are illustrated in Fig. 3.2(b).

The web function w constructed this way is again a renormalization group invariant, so that in (3.3.1), we may shift the renormalization scale to the product $(\lambda\sigma)^{-1}$, which results in an expression with the coupling running as the leading vertices move up and down the Wilson lines,

$$E \;=\; \int_0^\infty \frac{d\lambda}{\lambda} \int_0^\infty \frac{d\sigma}{\sigma}\, w\left(\alpha_s\left(1/\lambda\sigma\right), \varepsilon\right) \,. \tag{3.3.2}$$

In this all-orders form, dependence on the product $\lambda\sigma$ is entirely through the running coupling, aside from the overall dimensional factor. For $\mathcal{N} = 4$ SYM theory, Eq. (3.3.2) for the cusp holds as well at strong coupling [68, 69, 95], where the coordinates λ and σ also parameterize a surface. The generality of these results can be traced to the symmetries of the problem [95]. It is interesting to note, however, that in the strong coupling analysis, the product of internal coordinates $\lambda\sigma$, which serves as the renormalization scale in Eq. (3.3.2), relates the plane of the Wilson lines to a minimal surface in five dimensions.

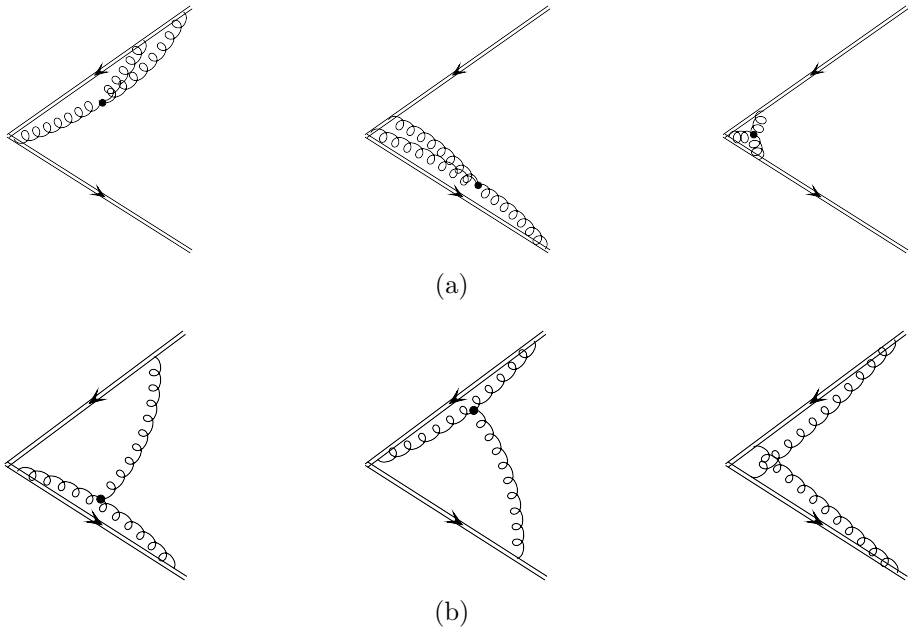

Figure 3.2: Representation of singular regions for a two-loop web diagram. (a) Single-scale regions, characteristic of webs. (b) Multiple-scale regions, associated with subdivergences that cancel in the sum of web diagrams.

3.3.2 Web renormalization in coordinate space

To derive a renormalized exponent for the cusp in coordinate space, we will find it useful to expand the unrenormalized web function in (3.3.2) in explicit powers of ε,

$$E(\varepsilon) \;=\; \sum_{n=0}^{\infty} \varepsilon^n \int_0^\infty \frac{d\lambda}{\lambda} \int_0^\infty \frac{d\sigma}{\sigma}\, w_n\left(\alpha_s\left(1/\lambda\sigma\right)\right) , \tag{3.3.3}$$

where w_n is the coefficient of ε^n, noting that the coupling retains implicit ε dependence. As noted above, the renormalized exponent is determined by the ultraviolet poles of these scaleless integrals. With this in mind, consistency with momentum space pole structure in Eq. (3.2.5) then clearly requires

$$w_0\left(\alpha_s\left(1/\lambda\sigma\right)\right) \;=\; -\,\frac{1}{2}\,\Gamma_{\text{cusp}}\Big(\alpha_s\left(1/\lambda\sigma\right)\Big) \,. \tag{3.3.4}$$

For finite values of λ and σ, only w_0 contributes to the unrenormalized integral in the $\varepsilon \to 0$ limit. To determine the renormalized cusp integral, however, we must take into account contributions from the boundaries $\lambda = 0$ and $\sigma = 0$,

which produce poles that can compensate explicit powers of ε in Eq. (3.3.3). Such boundary contributions from terms $\varepsilon^n w_n$ with $n > 0$ in Eq. (3.3.3) generate the anomalous dimension $G_{\rm eik}$ in the renormalized form, Eq. (3.2.5).

To compute $G_{\rm eik}$, we recall that the running coupling $\alpha_s(1/\lambda\sigma)$ remains a function of ε when reexpanded in terms of the coupling at any fixed scale, μ, which we represent as

$$\begin{aligned}\alpha_s(1/\lambda\sigma) &= \alpha_s(\mu^2)\,(\mu^2\lambda\sigma)^\varepsilon \left(1 + \frac{\alpha_s(\mu^2)}{4\pi}\,\frac{b_0}{\varepsilon}\,\left[(\mu^2\lambda\sigma)^\varepsilon - 1\right] + \ldots\right) \\ &\equiv \bar\alpha_s\left(\alpha_s(\mu^2), (\mu^2\lambda\sigma)^\varepsilon, \varepsilon\right)\,, \end{aligned} \tag{3.3.5}$$

where we exhibit only the dependence to order α_s^2, which is all we need here, and where $b_0 = (11/3)C_A - (4/3)n_f T_f$. The subleading anomalous dimension $G_{\rm eik}$ is found from single poles in $E(\varepsilon)$ after the λ and σ integrations. These can arise at any order by combinations of an overall factor ε^n in (3.3.3) with poles in the expansion of the coupling, (3.3.5). To identify such terms, we may conveniently take $\sigma < \lambda$ and multiply by 2, and reexpand $\alpha_s(1/\lambda\sigma)$ in terms of $\alpha_s(1/\lambda^2)$, schematically,

$$\begin{aligned} E(\varepsilon) &= -\frac{1}{2}\int_0^\infty \frac{d\lambda}{\lambda}\int_0^\infty \frac{d\sigma}{\sigma}\,\Gamma_{\rm cusp}\big(\alpha_s\left(1/\lambda\sigma\right)\big) \\ &\quad + 2\sum_{n=1}^\infty \varepsilon^n \int_0^\infty \frac{d\lambda}{\lambda}\int_0^\lambda \frac{d\sigma}{\sigma}\,w_n\left(\bar\alpha_s\left(\alpha_s(1/\lambda^2), (\sigma/\lambda)^\varepsilon, \varepsilon\right)\right)\,. \end{aligned} \tag{3.3.6}$$

The renormalized exponent is defined as the remainder when all ultraviolet poles are subtracted minimally at an arbitrary, fixed scale μ. Leading and nonleading poles are then generated by

$$\begin{aligned} E_{\rm ren}(\varepsilon, \alpha_s(\mu^2)) &= -\frac{1}{2}\int_{1/\mu}^\infty \frac{d\lambda}{\lambda}\int_{1/\mu}^\infty \frac{d\sigma}{\sigma}\,\Gamma_{\rm cusp}\big(\alpha_s\left(1/\lambda\sigma\right)\big) \\ &\quad + \int_{1/\mu}^\infty \frac{d\lambda}{\lambda}\,G_{\rm eik}\left(\alpha_s(1/\lambda^2)\right)\,, \end{aligned} \tag{3.3.7}$$

where the integrals are now defined by infrared renormalization ($\varepsilon < 0$). Simple changes of variables transform this expression into the renormalized cusp momentum-space integrals given in Eq. (3.2.5).

3.3.3 Lowest orders

The lowest order expression for Eq. (3.3.1) already illustrates the nontrivial relationship between the renormalization scale and the positions of the vertices.

It is found directly from the coordinate-space gluon propagator in Feynman gauge,

$$\begin{aligned} D^{\mu\nu}(x^2) &= \int \frac{d^Dk}{(2\pi)^D}\, e^{-ik\cdot x}\, \frac{-i\, g^{\mu\nu}}{k^2 \,+\, i\epsilon} \\ &= \frac{\Gamma(1-\varepsilon)}{4\pi^{2-\varepsilon}}\, \frac{-g^{\mu\nu}}{(-x^2+i\epsilon)^{1-\varepsilon}}\,. \end{aligned} \tag{3.3.8}$$

The resulting expression for the unrenormalized exponent is

$$\begin{aligned} E^{(\mathrm{LO})} &= -\, C_F\, \frac{\Gamma(1-\varepsilon)}{2} \int_0^\infty \frac{d\lambda}{\lambda}\, \frac{d\sigma}{\sigma} \left(\frac{\alpha_s(\mu^2)}{\pi}\right) (2\pi\lambda\sigma\mu^2)^\varepsilon\,, \qquad (3.3.9) \\ &= -\, \frac{C_F}{2} \left(1 \,+\, \varepsilon^2\, \frac{\pi^2}{12}\right) \int_0^\infty \frac{d\lambda}{\lambda}\, \frac{d\sigma}{\sigma} \left(\frac{\alpha_s(\mu^2)}{\pi}\right) (2\pi e^{\gamma_E}\lambda\sigma\mu^2)^\varepsilon\,, \end{aligned}$$

where in the second form we have expanded the integrand to order ε^2. The corresponding renormalized exponent is

$$E^{(\mathrm{LO})}_{\mathrm{ren}} = -\, C_F\, \frac{\Gamma(1-\varepsilon)}{2} \int_{1/\mu}^\infty \frac{d\lambda}{\lambda} \int_{1/\mu}^\infty \frac{d\sigma}{\sigma} \left(\frac{\alpha_s(\mu^2)}{\pi}\right) (2\pi\lambda\sigma\mu^2)^\varepsilon\,, \tag{3.3.10}$$

which is precisely Eq. (3.3.7) to lowest order. Here and below, for definiteness we choose the Wilson lines in fundamental representation.

At two loops, the diagrams of Fig. 3.1 can be used to illustrate both the cancellation of subdivergences in the sum of web diagrams, and the manner in which we identify the parameters λ and σ, which together define the position of the web function. Our calculations are carried out with ultraviolet regularization ($D < 4$). These coordinate-space integrals have appeared in the literature before, of course, and the calculations we exhibit below are closely related to those of Refs. [58] and [43,44], also carried out in dimensional regularization. We present them again, however, in a form that shows explicitly how the cancellation of subdivergences occurs at fixed positions for the web along the lightlike paths, already in the unrenormalized forms.

The calculation of the crossed-ladder diagram, Fig. 3.1(a), is particularly simple in coordinate space. It is just the integral of two gluon propagators over the eikonal parameters,

$$\begin{aligned} E_{\mathrm{cross}} \;=\; \mathcal{N}_{\mathrm{cross}}(\varepsilon) \int_0^\infty d\lambda_2 \int_0^{\lambda_2} d\lambda_1 \int_0^\infty d\sigma_2 \int_0^{\sigma_2} d\sigma_1 \\ \times\, \frac{1}{(2\lambda_2\sigma_1+i\epsilon)^{1-\varepsilon}}\, \frac{1}{(2\lambda_1\sigma_2+i\epsilon)^{1-\varepsilon}}\,, \end{aligned} \tag{3.3.11}$$

where the prefactor is given by

$$\mathcal{N}_{\rm cross}(\varepsilon) \;\equiv\; -\left(\frac{\alpha_s}{\pi}\right)^2 C_A C_F \,\frac{\Gamma^2(1-\varepsilon)}{2}\,(\pi\mu^2)^{2\varepsilon}\;. \tag{3.3.12}$$

For the color factor in this web diagram, we keep only the $C_A C_F/2$ contribution, as mentioned above. For $\varepsilon > 0$, we choose to integrate over the inner eikonal parameters, and identify $\lambda_2 \equiv \lambda$ and $\sigma_2 \equiv \sigma$ in the general form of Eq. (3.3.2), giving

$$E_{\rm cross} = -\left(\frac{\alpha_s}{\pi}\right)^2 C_A C_F \,\frac{\Gamma^2(1-\varepsilon)}{8\,\varepsilon^2}\,(2\pi\mu^2)^{2\varepsilon}\int_0^\infty \frac{d\lambda\; d\sigma}{(\lambda\sigma)^{1-2\varepsilon}}\;. \tag{3.3.13}$$

This expression has overall double ultraviolet poles in addition to two scaleless (surface) integrals along the Wilson lines. The singular behavior of the coefficient arises from $\lambda_1 \ll \lambda$ and $\sigma_1 \ll \sigma$, a "subdivergent" configuration, in which the two gluons approach different Wilson lines. The contributions from these regions will be cancelled by corresponding terms from the three-gluon diagrams.

We now turn to the diagrams with a three-gluon coupling, one of which is shown in Fig. 3.1(b), referred to below as E_{3g}. In the expression for E_{3g}, we introduce upper limits, Λ and Σ on the two paths. For the simple cusp, we will take the limit $\Lambda, \Sigma \to \infty$. We return to the finite case in the discussion of polygons.

After evaluation of the three-gluon vertex, using $\beta_2^2 = 0$, E_{3g} can be written as

$$\begin{aligned}
E_{3g} =\; & \mathcal{N}_{3g}(\varepsilon)\int d^Dx \int_0^\Sigma d\sigma\,\frac{1}{(-x^2+2\sigma x\cdot\beta_1+i\epsilon)^{1-\varepsilon}} \\
\times\Bigg[&\int_0^\Lambda d\lambda_1\int_{\lambda_1}^\Lambda d\lambda_2\,\frac{1}{(-x^2+2\lambda_1 x\cdot\beta_2+i\epsilon)^{1-\varepsilon}}\,\frac{2x\cdot\beta_2(1-\varepsilon)}{(-x^2+2\lambda_2 x\cdot\beta_2+i\epsilon)^{2-\varepsilon}} \\
&-\int_0^\Lambda d\lambda_2\int_0^{\lambda_2} d\lambda_1\,\frac{2x\cdot\beta_2(1-\varepsilon)}{(-x^2+2\lambda_1 x\cdot\beta_2+i\epsilon)^{2-\varepsilon}}\,\frac{1}{(-x^2+2\lambda_2 x\cdot\beta_2+i\epsilon)^{1-\varepsilon}}\Bigg] \\
=\; & \mathcal{N}_{3g}(\varepsilon)\int d^Dx \int_0^\Sigma d\sigma\,\frac{1}{(-x^2+2\sigma x\cdot\beta_1+i\epsilon)^{1-\varepsilon}} \\
\times\Bigg[&\int_0^\Lambda d\lambda_2\,\frac{1}{(-x^2+2\lambda_2 x\cdot\beta_2+i\epsilon)^{1-\varepsilon}}\int_0^{\lambda_2} d\lambda_1\,\frac{\partial}{\partial\lambda_1}\left(\frac{1}{(-x^2+2\lambda_1 x\cdot\beta_2+i\epsilon)^{1-\varepsilon}}\right) \\
&-\int_0^\Lambda d\lambda_1\,\frac{1}{(-x^2+2\lambda_1 x\cdot\beta_2+i\epsilon)^{1-\varepsilon}}\int_{\lambda_1}^\Lambda d\lambda_2\,\frac{\partial}{\partial\lambda_2}\left(\frac{1}{(-x^2+2\lambda_2 x\cdot\beta_2+i\epsilon)^{1-\varepsilon}}\right)\Bigg]\;,
\end{aligned} \tag{3.3.14}$$

where in this case the numerical prefactor is

$$\mathcal{N}_{3g}(\varepsilon) \;=\; -i\left(\frac{\alpha_s}{\pi}\right)^2 C_A C_F \,\frac{\Gamma^3(1-\varepsilon)}{8\pi^{2-\varepsilon}}\,(\pi\mu^2)^{2\varepsilon}\;. \tag{3.3.15}$$

In the second equality of Eq. (3.3.14), we isolate two total derivatives, in the variables λ_1 and λ_2. We shall carry out these two integrals first, at fixed values of the other path parameters and of x^μ.

There is a suggestive way of interpreting the total derivatives in Eq. (3.3.14), starting by recognizing that the "propagator" for the Wilson line is a step function, for example, $\theta(\lambda)$, with "equation of motion" $\partial_\lambda\theta(\lambda) = \delta(\lambda)$. In these terms, the λ_1 or λ_2 integrals over total derivatives can also be thought of as the result of integration by parts and the use of the equation of motion. In the term with $\partial/\partial_{\lambda_2}$, the equation of motion sets $\lambda_2 = \lambda_1$ and $\lambda_2 = \Lambda$. As $\Lambda \to \infty$ for fixed x^μ, the term with $\lambda_2 = \Lambda$ vanishes as a power for any $\varepsilon < 1/2$. The vanishing of such contributions, through the cancellation of propagators, is an ingredient in the gauge invariance of the cusp, which generalizes to the gauge invariance of partonic amplitudes [22,96]. We shall take the limit $\Lambda \to \infty$ first, at fixed values of the remaining integration variables after using the eikonal equation of motion. We will confirm below that this prescription gives a gauge invariant result for the cusp after summing over diagrams. We will evaluate the term from $\lambda_2 = \Lambda$, which by itself is gauge dependent, in Appendix B.2.

Returning to Eq. (3.3.14), we now integrate over the total-derivative integrals, λ_1 in the first term and over λ_2 in the second, and get,

$$\begin{aligned} E_{3g} \;&=\; \mathcal{N}_{3g}(\varepsilon)\int d^Dx \int_0^\Sigma d\sigma\,\frac{1}{(-x^2+2\sigma x\cdot\beta_1+i\epsilon)^{1-\varepsilon}} \\ &\quad\times\int_0^\Lambda d\lambda\left[-\frac{1}{(-x^2+i\epsilon)^{1-\varepsilon}}\,\frac{1}{(-x^2+2\lambda x\cdot\beta_2+i\epsilon)^{1-\varepsilon}}\right. \\ &\qquad\qquad +\frac{2}{(-x^2+2\lambda x\cdot\beta_2+i\epsilon)^{2-2\varepsilon}} \\ &\qquad\qquad \left.-\frac{1}{(-x^2+2\lambda x\cdot\beta_2+i\epsilon)^{1-\varepsilon}}\,\frac{1}{(-x^2+2\lambda x\cdot\beta_2+i\epsilon)^{1-\varepsilon}}\right] \\ &\equiv\; E_{3s} \;+\; 2\,E_{\rm pse} \;+\; E_{\rm end}\,. \end{aligned} \tag{3.3.16}$$

Here we have relabeled the remaining parameters as σ and λ in both terms. The three terms identified in the second relation correspond to the three terms in square brackets of the first relation. These terms involve scalar propagators only, and are represented by Fig. 3.3. We refer to the first term in brackets as

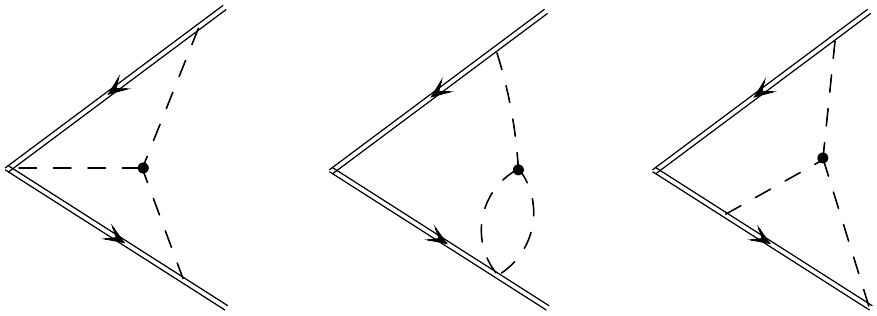

(a) (b) (c)

Figure 3.3: (a) 3-scalar diagram (b) Pseudo-self-energy diagram (c) End-point diagram.

the 3-scalar integral, E_{3s} (Fig. 3.3(a)), in which the end of one of the scalar propagators is fixed at the cusp by the eikonal equation of motion. We will call the second term the "pseudo-self-energy", E_{pse} (Fig. 3.3(b)), since two scalar propagators form a loop and attach to the Wilson line at the same point. Finally, the third term, $E_{\rm end}$ (Fig. 3.3(c)), in which $\lambda_2 = \Lambda$ for finite Λ will be referred to as the "end-point" diagram for this case. As noted above, the cusp itself is defined without the end-point diagram, but we will return to it in our discussion of Wilson line polygons below.

We can identify the sources of subdivergences in the expressions of Eq. (3.3.16) by finding points where the x^μ integral is pinched between coalescing singularities [32]. In the 3-scalar term E_{3s}, the integration contours of the light cone component $\beta_1 \cdot x$ and two-dimensional transverse components $x_\perp$ are pinched when $x^\mu = \zeta\beta_1^\mu$, with $0 < \zeta < \sigma$, and also when $x^\mu = \eta\beta_2^\mu$, with $0 < \eta < \lambda$. For fixed λ and σ these are the singular subdivergences referred to above, in which the point x^μ approaches the path in the β_1 or β_2 directions, respectively. In either case two lines are forced to the light cone on one of the Wilson lines, while the third line may attach anywhere on the opposite-moving line. There is no corresponding pinch in the pseudo-self-energy term, and this diagram, along with the self-energy diagrams, has only a single ultraviolet pole at fixed λ and σ, which is removed by the standard renormalization of the gauge theory.

The integration of the 3-scalar term has been in the literature for a long time, but some details are given in Appendix B.1, to derive it as a coefficient

times the scaleless integrals over parameters λ and σ. We find

$$E_{3s} = \left(\frac{\alpha_s}{\pi}\right)^2 C_A C_F \, \frac{\Gamma(1-2\varepsilon)\Gamma(1+\varepsilon)\Gamma(1-\varepsilon)}{16\,\varepsilon^2} \, (2\pi\mu^2)^{2\varepsilon} \int_0^\infty \frac{d\lambda \; d\sigma}{(\lambda\sigma)^{1-2\varepsilon}} \; . \tag{3.3.17}$$

We have taken the upper limits to infinity at this point, because we are interested in the (unrenormalized) cusp integral.

The pseudo-self-energy term in Eq. (3.3.16) inherits the entire ultraviolet divergence of the diagram E_{3g}, Fig. 3.1(b) at fixed λ and σ, and requires a counterterm that is part of the web, rather than cusp, renormalization. The result is

$$\begin{aligned} E_{\rm pse} = &- \left(\frac{\alpha_s}{\pi}\right)^2 C_A C_F \, \frac{1}{16\,\varepsilon} \int_0^\infty \frac{d\lambda \, d\sigma}{\lambda\sigma} \\ &\times \left[\frac{\Gamma^2(1-\varepsilon)}{1-2\varepsilon}(2\pi\mu^2\lambda\sigma)^{2\varepsilon} - \Gamma(1-\varepsilon)(2\pi\mu^2\lambda\sigma)^{\varepsilon}\right] , \end{aligned} \tag{3.3.18}$$

with the same scaleless integral times a single-scale constant. Finally, for the gluon self-energy diagrams, Figs. 3.1(c)–(d), we use the renormalized one-loop gluon Green function in coordinate space. The result for the self-energy contribution, $E_{\rm se}$ of Fig. 3.1(c), where the gluon connects both Wilson lines, can be written as

$$\begin{aligned} E_{\rm se} = &- \left(\frac{\alpha_s}{\pi}\right)^2 C_F \frac{1}{8\varepsilon} \int_0^\infty \frac{d\lambda \, d\sigma}{\lambda\sigma} \\ &\times \left[\frac{\Gamma^2(1-\varepsilon)}{1-2\varepsilon}\left\{\frac{(5-3\varepsilon)C_A - 4T_f n_f(1-\varepsilon)}{3-2\varepsilon}\right\}(2\pi\mu^2\lambda\sigma)^{2\varepsilon}\right. \\ &\left. - \Gamma(1-\varepsilon)\left\{\frac{5C_A - 4T_f n_f}{3}\right\}(2\pi\mu^2\lambda\sigma)^{\varepsilon}\right] \; + \; E_{\rm long} \, , \end{aligned} \tag{3.3.19}$$

where the (unrenormalized) longitudinal part of the Green function is given by

$$\begin{aligned} E_{\rm long} = &- \left(\frac{\alpha_s}{\pi}\right)^2 C_F \, \frac{\Gamma^2(1-\varepsilon)}{32\,\varepsilon^2\,(1+\varepsilon)(1-2\varepsilon)} \left\{\frac{(5-3\varepsilon)C_A - 4T_f n_f(1-\varepsilon)}{3-2\varepsilon}\right\} \\ &\times \int_0^\infty d\lambda \, d\sigma \; \frac{\partial}{\partial\lambda} \, \frac{\partial}{\partial\sigma} \left[(\pi\mu^2(\beta_2\lambda - \beta_1\sigma)^2)^{2\varepsilon}\right] . \end{aligned} \tag{3.3.20}$$

The function $E_{\rm long}$ comes from the coordinate space transform of the $q^\mu q^\nu$ term in the gluon self energy, and reduces to total derivatives in both σ and λ. In momentum space, the $q^\mu q^\nu$ terms decouple from the gauge invariant cusp

algebraically in the sum over diagrams, assuming that the external Wilson lines carry no momentum. To define such derivative terms in coordinate space for the cusp requires the introduction of small but nonzero β_1^2 and β_2^2, and with this infrared regularization, the longitudinal term above cancels the corresponding term for the self-energy diagram of Fig. 3.1(d), up to end-point contributions analogous to $E_{\rm end}$ in Eq. (3.3.16), which we have discarded in the calculation of the cusp contribution from E_{3g} above. We will once again neglect such terms for the purposes of this calculation, but will return to this question in the next subsection.

To check the finiteness and structure of the sum of these two-loop web diagrams, we expand them in ε, keeping all terms that can contribute ultraviolet poles to the cusp. The (two) three-gluon diagrams plus the crossed ladder gives

$$\begin{aligned} E_{\rm cross} \,+\, 2E_{3s} \,=\, & \frac{1}{8}\left(\frac{\alpha_s}{\pi}\right)^2 C_F C_A \left(\frac{\pi^2}{3} + 2\varepsilon\,\zeta_3 + \mathcal{O}(\varepsilon^2)\right) \\ & \times \left(2\pi e^{\gamma_E}\mu^2\right)^{2\varepsilon} \int_0^\infty \frac{d\lambda\; d\sigma}{(\lambda\sigma)^{1-2\varepsilon}}\,. \end{aligned} \tag{3.3.21}$$

Thus, as anticipated, the ultraviolet poles from the subdivergences of the web cancel, leaving only the overall scaleless integrals, whose singular behavior can be associated with hard, soft, and collinear configurations for all of the lines of the web together. The π^2 term will contribute to $\Gamma_{\rm cusp}$ and the $\varepsilon\zeta_3$ term to $G_{\rm eik}$. We next expand the integrands of $E_{\rm se}$ and $E_{\rm pse}$ at two loops, Eqs. (3.3.19) and (3.3.18) to order ε,

$$\begin{aligned} E_{\rm se} \,+\, 4E_{\rm pse} = & -\left(\frac{\alpha_s}{\pi}\right)^2 C_F \frac{1}{8}\int_0^\infty \frac{d\lambda\, d\sigma}{\lambda\sigma} \\ & \left[\left\{1 + \varepsilon^2\frac{\pi^2}{12}\right\}\frac{1}{\varepsilon} b_0 \left[(2\pi\mu^2 e^{\gamma_E}\lambda\sigma)^{2\varepsilon} - (2\pi\mu^2 e^{\gamma_E}\lambda\sigma)^{\varepsilon}\right]\right. \\ & + \left\{\left(\frac{67}{9}\,C_A - \frac{20}{9} n_f T_f\right)\right. \\ & \left.\left. + \,\varepsilon\left(\frac{404}{27} C_A - \frac{112}{27} n_f T_f + \frac{\pi^2}{12} b_0\right)\right\}(2\pi\mu^2 e^{\gamma_E}\lambda\sigma)^{2\varepsilon}\right]\,. \end{aligned} \tag{3.3.22}$$

The terms proportional to b_0/ε serve to evolve the one-loop web, Eq. (3.3.10) to the scale $1/\lambda\sigma$ times constants.

Combining Eqs. (3.3.21) and (3.3.22), we find the explicit terms in the web expansion, Eq. (3.3.3). In a scheme where logs of factors $2\pi e^{\gamma_E}$ are absorbed

into the definition of $\alpha_s(1/\lambda\sigma)$, we have for the terms in Eq. (3.3.3),

$$\begin{aligned} w_0(\alpha_s) &= -\frac{\alpha_s}{2\pi}\,C_F - \left(\frac{\alpha_s}{\pi}\right)^2 \frac{C_F}{2}\left(\left[\frac{67}{9}-\frac{\pi^2}{3}\right]C_A - \frac{20}{9}n_f T_f\right) + \dots\,, \\ w_1(\alpha_s) &= -\left(\frac{\alpha_s}{\pi}\right)^2 \frac{C_F}{8}\left(\left[\frac{404}{27}-2\zeta_3\right]C_A - \frac{112}{27}n_f T_f + \frac{\zeta_2}{2}\,b_0\right) + \dots\,, \\ w_2(\alpha_s) &= -\frac{\alpha_s}{2\pi}\,C_F\,\frac{\pi^2}{12} + \dots\,, \end{aligned} \tag{3.3.23}$$

where omitted terms are higher order in α_s or do not contribute to the cusp ultraviolet poles. The term linear in ε begins at order α_s^2, but the single pole also gets a contribution from the ε^2 term at one loop, when combined with the running of the coupling. With these results in hand, we can return to Eq. (3.3.3) and expand $\alpha_s(1/\lambda\sigma)$ in terms of the coupling at a fixed scale, $\alpha_s(\mu^2)$ using (3.3.5). This enables us to derive the single ultraviolet pole in E to order α_s^2, and hence the anomalous dimension $G_{\rm eik}$ at two loops,

$$G_{\rm eik} = \frac{1}{2}C_F C_A \left(\frac{\alpha_s}{\pi}\right)^2 \left[\left\{\frac{101}{27}-\frac{11}{72}\pi^2-\frac{1}{2}\,\zeta_3\right\}C_A + \left\{\frac{28}{27}-\frac{\pi^2}{18}\right\}n_f T_f\right]. \tag{3.3.24}$$

In Sec. 3.4, we will see the close relation of this result to the "collinear anomalous dimension" derived long ago in Ref. [58] for a closed polygon of Wilson lines of finite size.

3.3.4 Web integrals, end-points, and gauge invariance

A self-contained coordinate-space derivation of Eq. (3.3.1), generalizing the renormalization analysis of Ref. [84] for massive Wilson lines, will be given elsewhere [34]. Here, however, we will generalize our prescription for the calculation of the gauge-invariant cusp anomalous dimension. As we have seen, this requires us to find in coordinate space the analog of the action of momentum-space Ward identities that ensure the gauge invariance of the S-matrix [22,96].

In the following brief but all-orders discussion we follow Ref. [97] and write the exponent as a sum over the numbers, e_a, of gluons attached to the two Wilson lines, of velocity β_a, $a = 1, 2$. We note, however, that the argument extends to any number of lines. The web diagrams are integrals over the positions $\lambda_j\beta_2$ and $\sigma_k\beta_1$ of these ordered vertices of a function $\mathcal{W}_{e_1,e_2}(\{\lambda_j\},\{\sigma_k\})$, which includes the integrals over all the internal vertices of the corresponding web

diagrams. In the notation of Ref. [97] we then have at nth order ($n \geq e_1 + e_2$),

$$E^{(n)} = \sum_{e_2=1}^{n-1} \sum_{e_1=1}^{n-e_2} \prod_{j=1}^{e_1} \int_{\lambda_{j-1}}^{\infty} d\lambda_j \prod_{k=1}^{e_2} \int_{\sigma_{k-1}}^{\infty} d\sigma_k \, \mathcal{W}^{(n)}_{e_1,e_2}\left(\{\lambda_j\},\{\sigma_k\}\right) , \quad (3.3.25)$$

with $\lambda_0, \sigma_0 \equiv 0$. Here we expand functions as $E = \sum(\alpha_s/\pi)^n E^{(n)}$. We can use the notation of Eq. (4.4.1) to generalize our treatment of the three-gluon diagram and self-energy diagrams above. First, we isolate those contributions to $\mathcal{W}^{(n)}_{e_1,e_2}\left(\{\lambda_j\},\{\sigma_k\}\right)$ that are of the form of total derivatives in the largest path parameters, λ_{e_1}, σ_{e_2}, *and* whose upper limits vanish when the end-points of ordered exponentials are taken to infinity for fixed values of the internal vertices of the web. We represent this separation as,

$$\begin{aligned}\mathcal{W}^{(n)}_{e_1,e_2}\left(\{\lambda_j\},\{\sigma_k\}\right) = &\frac{\partial}{\partial\,\lambda_{e_1}} \mathcal{X}^{(\lambda)(n)}_{e_1,e_2}\left(\{\lambda_j\},\{\sigma_k\}\right) + \frac{\partial}{\partial\,\sigma_{e_2}} \mathcal{X}^{(\sigma)(n)}_{e_1,e_2}\left(\{\lambda_j\},\{\sigma_k\}\right) \\ &+ \frac{\partial}{\partial\,\lambda_{e_1}} \frac{\partial}{\partial\,\sigma_{e_2}} \mathcal{X}^{(\lambda\sigma)(n)}_{e_1,e_2}\left(\{\lambda_j\},\{\sigma_k\}\right) + \overline{\mathcal{W}}^{(n)}_{e_1,e_2}\left(\{\lambda_j\},\{\sigma_k\}\right) ,\end{aligned} \quad (3.3.26)$$

where the $\mathcal{X}^{(I)}$, $I = \lambda, \sigma, \lambda\sigma$, are functions whose derivatives are taken by λ_{e_1}, σ_{e_2} or both, and which vanish when λ_{e_1} and/or σ_{e_2} are taken to infinity with other integration variables held fixed. The function $\overline{W}$ is the remaining web integrand. To determine the cusp, we evaluate the total derivatives at the lower limits, $\lambda_{e_1} = \lambda_{e_1-1}$, $\sigma_{e_2} = \sigma_{e_2-1}$ or both, discarding the upper limits, as $E_{\rm end}$ in the two-loop case above. We then relabel the largest remaining λ_j integral (either λ_{e_1} or λ_{e_1-1}) as λ, and integrate over the rest of the λ_j, up to λ. The σ_k parameters are treated in just the same way. In this manner, we find for the web function in Eq. (3.3.1), the form

$$\begin{aligned}w\left(\alpha_s(1/\lambda\sigma,\varepsilon),\lambda\sigma\mu^2,\varepsilon\right) = &\sum_{e_2=1}^{n-1} \sum_{e_1=1}^{n-e_2} \prod_{j=1}^{e_1} \int_{\lambda_{j-1}}^{\lambda} d\lambda_j \prod_{k=1}^{e_2} \int_{\sigma_{k-1}}^{\sigma} d\sigma_k \, \delta(\lambda_{e_1} - \lambda)\, \delta(\sigma_{e_2} - \sigma) \\ \times \Big[&- \delta(\lambda_{e_1-1} - \lambda) \mathcal{X}^{(\lambda)(n)}_{e_1,e_2}\left(\{\lambda_j\},\{\sigma_k\}\right) - \delta(\sigma_{e_2-1} - \sigma) \mathcal{X}^{(\sigma)(n)}_{e_1,e_2}\left(\{\lambda_j\},\{\sigma_k\}\right) \\ &+ \delta(\lambda_{e_1-1} - \lambda)\, \delta(\sigma_{e_2-1} - \sigma) \mathcal{X}^{(\lambda\sigma)(n)}_{e_1,e_2}\left(\{\lambda_j\},\{\sigma_k\}\right) + \overline{\mathcal{W}}^{(n)}_{e_1,e_2}\left(\{\lambda_j\},\{\sigma_k\}\right) \Big] .\end{aligned} \quad (3.3.27)$$

Once web diagrams are summed over at any order, this form is gauge invariant,

and produces the same cusp integrand for finite lines as for infinite lines. This is because the infinitesimal gauge variation of a product of Wilson lines as in Eq. (3.1.1) produces a ghost propagator ending on the ends of the lines, which vanishes when those lines are taken to infinity [22, 96]. Even if the ends of the lines are at finite distances, the prescription to discard the upper limit of total derivatives automatically removes these gauge variations. When the end-points, which generalize $E_{\rm end}$ in Eq. (3.3.16) in our discussion above, are at finite distances, however, we must keep these terms and combine them with the remainder of the diagrams of the graph to derive the full, gauge invariant result.

3.4 Applications to polygon loops

The above reasoning leads to a number of interesting results for polygonal closed Wilson loops [43, 44, 68, 69]. These amplitudes also exponentiate in perturbation theory in terms of webs [43, 44]. To this observation we may apply once again the lack of subdivergences for webs.

Generic diagrams for quadrilateral loops are shown in Figs. 3.4 and 3.5. In Fig. 3.4, for example, the ath vertex of the polygon represents a cusp vertex that connects two Wilson lines, of velocity β_{a-1} and β_a, with $\beta_0 \equiv \beta_4$.

Exponentiation in coordinate space implies that the logarithm of a polygon P is a sum of the web configurations illustrated by the figures,

$$\ln P \;=\; \sum_{\text{cusps } a} W_a \;+\; \sum_{\text{sides } \{a+1,a\}} W_{a+1,a} \;+\; W_{\rm plane}\,. \tag{3.4.1}$$

The first terms organize webs associated entirely with one of the cusps of the polygon, constructed in terms of the coordinate webs identified above. Because each edge is of finite length, we must now retain the additional gauge-variant

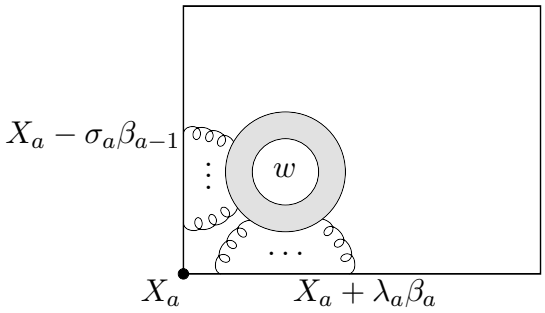

Figure 3.4: A single-cusp web W_a, in the sum of Eq. (3.4.1).

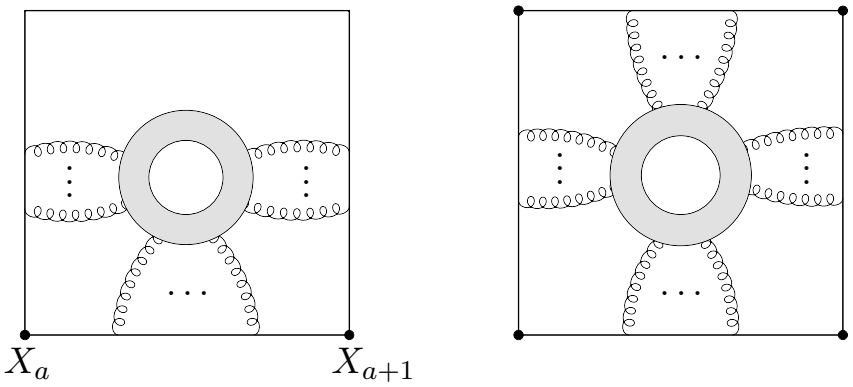

(a) (b)

Figure 3.5: (a) A 'side' web $W_{a+1,a}$ in of Eq. (3.4.1), in this case associated with the lightlike side between X_a and X_{a+1}. (b) A web that contributes to $W_{\rm plane}$ in Eq. (3.4.1).

terms associated with the end-point contributions ($E_{\rm end}$ above), which are to be combined with gauge-variant end-points from webs connecting three or four sides to derive a gauge-invariant result. The cancellation of subdivergences in webs implies that after a sum over diagrams, only the cusp poles and a single, overall collinear singularity survives [34, 43, 44]. There remains a finite contribution from webs that connect all four (or in general more) of the Wilson lines, and these are represented by the final term in (3.4.1).

Evidently, the single-cusp contribution, $W_a(\beta_a, \beta_{a-1})$ has the same gauge-invariant integrand as for the finite Wilson lines in Eq. (3.3.2), in terms of the lengths L_a of the sides of the polygon, between vertices a and $a+1$

$$W_a(\beta_a, \beta_{a-1}, L_a, L_{a-1}) \;=\; \int_0^{L_a} \frac{d\lambda_a}{\lambda_a} \int_{-L_{a-1}}^{0} \frac{d\sigma_a}{\sigma_a}\, w(\alpha_s(1/\lambda_a\sigma_a, \varepsilon), \varepsilon)\,. \quad (3.4.2)$$

The web function w for the cusp can depend only on the scalar products of the velocities, and we may assume for simplicity that these are all of the same order.

The two-cusp contributions connect three sides, and the only available singular configuration is when all lines in the web are parallel to the side between the two adjacent vertices. The only invariants on which the web can then depend are of the form $L_a\eta$, with L_a the length of this side, and η a typical distance of vertices in the web from the side. As a result, the general

form of the $W_{a+1,a}$ in Eq. (3.4.1) is

$$W_{a+1,a}(L_a) \;=\; \int_0^{L_a} \frac{d\eta}{\eta}\; w_{a+1,a}\left(\alpha_s(\eta L_a, \varepsilon)\right) \;, \tag{3.4.3}$$

for a function $w_{a+1,a}(\alpha_s)$, where we assume all the sides are of a similar length. Finally, for the diagrams, in which the web is stretched out between more than three sides of a polygon (in this case, the web is connected to all four sides of the quadrilateral), $W_{\rm plane}$, the only scale available is the area of the quadrilateral, and these web contributions are an expansion in the coupling evaluated at the inverse area, with finite coefficients.

The two-loop diagrams for all of these topologies were computed in [43,44]. We note that in the results quoted there, the cusp anomalous dimension does not appear until all diagrams of the topologies of W_a and $W_{a+1,a}$ are combined. Following the prescription for the web integrand given above, however, the two-loop cusp is associated entirely with the diagrams dressing a single corner, W_a, precisely because the gauge-variant end-point contributions $E_{\rm end}$ of Eq. (3.3.16) are not included in that object. For polygons, these gauge-variant terms at two loops, or any order, cancel contributions from the two-cusp contributions $W_{a+1,a}$, which also give rise to gauge-variant terms that cancel those from planar diagrams. These gauge-variant terms contain subdivergences in general. The complete result, of course, is gauge invariant and corresponds at two loops to the full calculation in Refs. [58] and [43,44].

For polygons, the renormalization group equation has been given in [58],

$$\frac{d}{d\,\ln\mu^2}\,P_{\rm ren} \;=\; -\frac{1}{2}\,\sum_a \Gamma_{\rm cusp}(\alpha_s(\mu^2))\,\ln(\mu^2 L_a L_{a-1}\beta_a\cdot\beta_{a-1}) - \Gamma_{\rm co}\left(\alpha_s(\mu^2)\right)\;, \tag{3.4.4}$$

where the L_a and μ-dependence of the first term is characteristic of cusps with lightlike Wilson lines [57], and where the second term, $\Gamma_{\rm co}$ was called the collinear anomalous dimension in Ref [58]. Aside from overall factors associated with the number of sides of the polygon, the collinear anomalous dimension for the quadrilateral is identical to $G_{\rm eik}$ in Eq. (3.3.24), except for the coefficient of ζ_3, which differs due to extra diagrams that connect three sides of the quadrilateral.

Polygons of this sort have been studied in the context of a duality to scattering amplitudes in conformal theories [43, 44, 68]. Here, we consider a four-sided polygon that projects to a square in the x_1/x_2 plane, with side X, as in Figs. 3.4–3.5. In four dimensions, the loop starts at the origin, travels along the plus-x_1 direction for a 'time' $X^0 = X$, then changes direction to x_2 for time X, and then moves backwards in time and space, first in the x_1 direction,

then x_2, back to the origin. We can now use the coordinates x_1 and x_2 to define parameters λ_a and σ_a for each of the cusp integrals W_a in Eq. (3.4.2),

$$\begin{aligned} \sigma_1 &= -x_2\,, & \lambda_1 &= x_1\,, \\ \sigma_2 &= x_1 - X\,, & \lambda_2 &= x_2\,, \\ \sigma_3 &= x_2 - X\,, & \lambda_3 &= X - x_1\,, \\ \sigma_4 &= -x_1\,, & \lambda_4 &= X - x_2\,. \end{aligned} \tag{3.4.5}$$

In this notation, we can add the four cusp web integrals of Eq. (3.4.2), to get a single integral over x_1 and x_2. The web functions, of course, depend on the particular forms of λ and σ above. We find

$$\sum_{a=1}^{4} W_a(\beta_a, \beta_{a-1}) \;=\; \int_0^X dx_1 \int_0^X dx_2 \, \frac{(X-x_2)[(X-x_1)w_1 + x_1 w_2] + x_2[x_1 w_3 + (X-x_1)w_4]}{x_1(X-x_1)x_2(X-x_2)}\,, \tag{3.4.6}$$

where $w_a \equiv w(\alpha_s(\lambda_a(x_1,x_2)\sigma_a(x_1,x_2)))$. For a conformal theory, all dependence on the σ_a and λ_a is in the denominators and we can sum over a to get a result in terms of a constant web function w_0. Changing variables to $y_a = 1 - 2x_a/X$, we derive the unregularized form found from the analysis of extremal two-dimensional surfaces embedded in a five-dimensional background in [68],

$$\sum_{a=1}^{4} W_a(\beta_a, \beta_{a-1}) \;=\; \int_{-1}^{1} dy_1 \int_{-1}^{1} dy_2 \, \frac{4w_0}{(1-y_1^2)(1-y_2^2)}\,, \tag{3.4.7}$$

to which we should add the collinear and finite multi-cusp contributions of Fig. 3.5.

3.5 Conclusions

We have found that when the massless cusp is analyzed in coordinate space, it is naturally written as the exponential of a two-dimensional integral. The integrand, a web function, depends on the single invariant scale through the running of the coupling, which for a theory that is conformal in four dimensions agrees with strong-coupling results [68, 69, 95]. This agreement extends to aspects of closed, polygonal Wilson loops. These results do not rely on a planar limit [72], but it is natural to conjecture that for large N_c the integral

may take on an even more direct interpretation in terms of surfaces for non-conformal theories.

Chapter 4

Regularization, Subtractions, and Factorization in Coordinate Space

This chapter of the thesis is based on research (in joint work with George Sterman) that has not been published yet [34].

4.1 Introduction

For many purposes, scattering amplitudes and the expectation values of gauge theory Wilson lines may be studied in momentum space or coordinate space, although most fixed-order computations are carried out in momentum space. At the same time, a coordinate-space perspective may serve as a bridge between scattering amplitudes and observables, often those involving jets [98,99]. Similarly, analyses in coordinate space have played a central role in correspondences between gauge theories and gravity [69], and dual conformal symmetries for select supersymmetric theories make a direct correspondence between choices of momenta for amplitudes and assignments of the vertices of certain polygonal Wilson loops [43, 100]. These considerations suggest that it may be useful to reexamine some of the all-orders properties of perturbative scattering amplitudes and cross sections that have been derived primarily from a momentum-space analysis [7, 53] in terms of coordinate-space integrals. In this spirit, we argued in Ref. [33] that the cusp formed by two Wilson lines can be written in a geometrical form to all orders in perturbation theory, as a surface integral over an ultraviolet finite function of the running coupling, whose scale varies with position on the surface. The surface integrand itself is found from the web diagrams of the cusp [86–88], which will play a role

in our discussion below. A more general analysis of partonic amplitudes was undertaken in Ref. [32], which examined the structure of coordinate-space singularities of massless gauge theories, by analyzing the pinch singularities of Feynman integrals in coordinate space [48] and developing a power counting procedure to identify leading and nonleading behavior.

In this chapter we will apply and extend the results of Chapter 2 (published in Ref. [32]), where it was found, for example, that in renormalized matrix elements of the form

$$G^{\nu}(x_1, x_2) \;=\; \left\langle 0 \left| T\left(\phi(x_2)\, J^{\nu}(0)\, \phi^{\dagger}(x_1)\right)\right| 0\right\rangle \;, \tag{4.1.1}$$

singularities occur only when the external points are on the light cone with respect to the interaction vertex, that is, only at $x_I^2 = 0$, $I = 1, 2$, and that divergences in coordinate-space integrals are logarithmic, relative to tree level. It was also argued that integrals in such "leading regions" factorize into hard, soft, and jet functions as for the well-known factorizations of momentum space [31, 54, 55].

In coordinate space, the collinear and short-distance divergences are both of ultraviolet nature [32], requiring $D < 4$ in dimensional regularization, while the factorized soft function is finite when the external points are kept at finite distances from each other. In contrast to short-distance singularities, collinear ultraviolet divergences are by their very nature nonlocal, and are not removed by the standard renormalization procedures for quantum field theory. It is natural, however, to expect that they may be treated by analogy to collinear singularities in momentum space, where they are infrared, requiring $D > 4$, for example, and are factorized into universal functions. To derive and interpret the corresponding factorization properties for coordinate-space amplitudes, it is necessary to introduce a subtraction procedure directly in coordinate space, similar to constructions in momentum space [31, 54, 55]. The subtractions will enable us to reorganize perturbative amplitudes for gauge theories in a manner that makes their singularity structure and factorization properties manifest, after using the Ward identities of the theory.

We work in Feynman gauge, to preserve Lorentz invariance and causality in the physical space-time structure of the amplitudes we study. Our construction is for gauge theory amplitudes in fixed-angle scattering, and so must deal with the non-trivial complication that in gauge theories with massless particles almost any subdiagram may produce collinear singularities or take part in the underlying short-distance process, in different parts of the integration space. This is in contrast to lowest-order electroweak processes like Drell-Yan, where the hard scattering is uniquely associated with a specific vertex.

Building on the results and analysis of Chapter 2 (Ref. [32]), we will analyze

the ultraviolet structure of multiparton coordinate-space Green functions in configurations related to fixed-angle scattering,

$$G_N(x_1,\ldots,x_N) \;=\; \langle 0|T\left(\phi_N(x_N)\cdots\;\phi_1(x_1)\right)|0\rangle\,. \tag{4.1.2}$$

These Green functions, of course, are not gauge invariant, but as we will observe, their leading singularities in coordinate space have essentially the same gauge invariance properties as S-matrix amplitudes, as a result of the same Ward identities.

The arguments that we give below carry over almost without change from coordinate space to momentum space, and we provide in this way a new all-orders analysis of factorization for scattering amplitudes in massless QCD and related theories in Feynman gauge. Our work thus complements the momentum-space analyses carried out in physical gauge long ago in Ref. [101] for scattering amplitudes. See also Ref. [102], which uses physical gauges to analyze a large set of amplitudes and observables involving outgoing jets. Our analysis of field theory perturbative amplitudes, based on an all-orders subtraction procedure to isolate, organize and cancel singular behavior, can also play a role in improving and extending existing factorization proofs for electroweak annihilation [31, 54, 55], jet and single-particle inclusive cross sections in hadron-hadron collisions [103].

We also study the closely-related multieikonal products of path-ordered exponentials, or Wilson lines [59–61], which we represent as

$$\Phi^{[f]}_{\dot\xi_C}(y,x) = P\,\exp\left[\int_0^\infty d\tau\,\dot\xi_C(\tau)\cdot A^{(f)}\left(\xi_C(\tau)\right)\right]\,. \tag{4.1.3}$$

Wilson lines that correspond to partonic amplitudes have constant velocities, $\dot\xi_C = \beta_C$, and are color matrices, in representations labelled f here. A four-Wilson line multieikonal vertex, for example, is defined by a constant matrix, c_M in color space that links the color indices at a point [73, 84, 101],

$$\begin{aligned}\Gamma^{[\mathrm{f}]}_{4,M\{r_k\}} = \sum_{\{d_i\}}\langle 0|\,\Phi^{[f_4]}_{\beta_4}(\infty,0)_{r_4,d_4}\;\Phi^{[f_3]}_{\beta_3}(\infty,0)_{r_3,d_3}\\ \times\,(c_M)_{d_4d_3,d_2d_1}\;\Phi^{[f_2]}_{\beta_2}(0,-\infty)_{d_2,r_2}\;\Phi^{[f_1]}_{\beta_1}(0,-\infty)_{d_1,r_1}\,|0\rangle\,.\end{aligned} \tag{4.1.4}$$

For the eikonal Wilson lines of this expression, constant velocities β_I label the curves, which we can choose to be $\xi_J(\tau_J) = \beta_J\tau_J$ (outgoing) or $\xi_I(\tau_I) = -\beta_I\tau_I$ (incoming). The curves meet at the origin, either from infinity in the past or to infinity in the future. In momentum space, Wilson lines appear as linear,

"eikonal" propagators. The corresponding coordinate-space propagators are simply step functions, ordering the connections of gluons to the exponential. As a specific application below, we will use our subtraction scheme to confirm the ultraviolet finiteness of the cusp web integrand [33].

We begin Sec. 4.2, with a review of the sources of ultraviolet poles in the coordinate-space calculation of multieikonal and partonic amplitudes [32, 48]. We go on to define a series of subtractions [53, 104] adapted to coordinate integrals, and show how they eliminate singularities and enable factorization to all orders in perturbation theory by methods similar to the treatment of infrared logarithms in momentum space. Section 4.3 deals with the special case of the two-eikonal amplitude, the singlet "cusp". We will relate the subtraction procedure of Sec. 4.2 directly to the logarithm of the cusp, given by the so-called web prescription. In this context, the ultraviolet finiteness of the web function, as discussed in Chapter 3 (published in Ref. [33]) is confirmed. We then turn in Sec. 4.4 to general, fixed-angle partonic and multieikonal amplitudes, and derive their factorization properties in Feynman gauge. We conclude with a summary and comments on possible developments.

4.2 Regularization of collinear singularities in coordinate space

We begin with a review of the results of Ref. [32] regarding the coordinate-space singularities of partonic and eikonal amplitudes, after perturbative renormalization. We follow this with an iterative construction of a set of nonlocal ultraviolet subtractions, adapted in analogy to the BPHZ momentum-space renormalization procedure [104], in the spirit of the all-orders, all-logs treatment of infrared divergences in momentum space in Ref. [53] for infrared divergences. In the subsequent sections, we will relate this additive regularization to the renormalization and factorization properties of eikonal and partonic amplitudes in coordinate space.

4.2.1 Leading regions, ultraviolet divergences and gauge invariance

The most general singular regions of coordinate-space integrals from which divergences arise were determined by the analysis of the analytic structure of coordinate-space integrals and the development of a corresponding power-counting technique in Ref. [32]. Divergences arise from pinches in the integrations over the positions of internal vertices considered as variables in complex

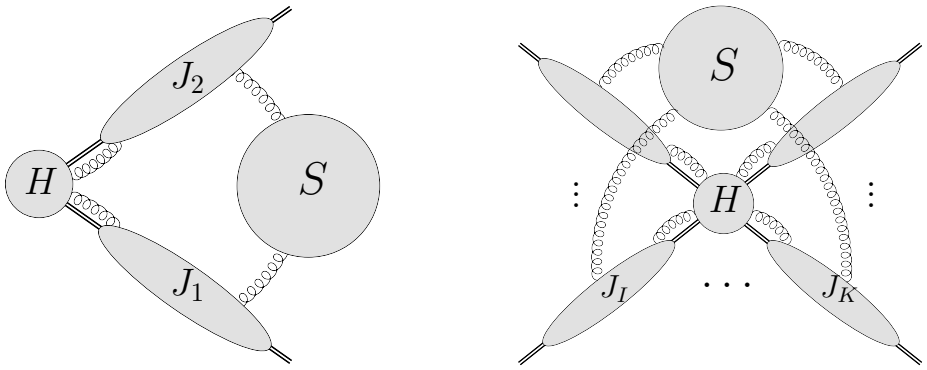

Figure 4.1: Leading pinch surfaces represented by soft, jet and hard subdiagrams for (a) cusp and (b) a typical multieikonal or multi-parton amplitude. Gluon lines represent arbitrary number of connections between the subdiagrams. In (b) the double line represents either Wilson lines or partonic propagators connected to the external vertices.

coordinate space. This is the direct analog of pinches in loop momenta in momentum space [35, 47, 53]. As in momentum space, at each such leading region, the diagram describes a physical processes with classical propagation for all lines that connect vertices that are lightlike separated, while soft lines can connect vertices with arbitrary separations. We will refer to a manifold in coordinate space with a definite set of lines pinched on the lightcone as a pinch surface (PS). (We use this notation in the same sense as "PSS" in Ref. [53].)

In Ref. [32] it was shown that at such pinch surfaces, diagrams are characterized by subdiagrams of soft, jet-like and short-distance (hard) sets of lines, as depicted in Fig. 4.1, which is similar to the familiar structure of diagrams at pinch surfaces (PSs) in momentum space in direct QCD treatments [31, 47, 53–55] and in soft-collinear effective theory [74, 105]. In the case of the massless cusp, for example (Fig. 4.1(a)), nonlocal ultraviolet subdivergences occur when subsets of vertices align along the Wilson lines, configurations that define jet subdiagrams. Other vertices remain at finite distances from both Wilson lines and the cusp in the soft subdiagram, while the remaining vertices move to the cusp and form the hard subdiagram [33]. The same factorization into the same types of subdiagrams also occurs for multieikonal vertices with more Wilson lines and in partonic amplitudes in coordinate space whenever a single point in spacetime is related to a set of external positions by lightlike distances, as illustrated in Fig. 4.1(b). (We assume that no pair of external vertices is related by a lightlike distance, and that the positions

of external vertices do not allow physical processes with multiple hard scatterings.) At these leading regions or PSs, one can make the coordinate-space soft-collinear and hard-collinear approximations, as defined in Ref. [32], which lead to the factorization of these subregions by the application of the Ward identities in the same way as in momentum space [31, 54, 55]. We will give the expressions for these approximants for a leading PS in the definition of the subtraction terms below. We use the term "leading" below to denote an ultraviolet logarithm or a pole in the dimensionally regulated case, and where necessary to distinguish PS that produce such divergences from those that do not.

Before giving more details, we pause to observe that, to participate in the physical picture associated with pinch surfaces requires that the "external" propagators, beginning at the positions of fields, x_I in Eq. (4.1.2), be on the light cone with respect to the position of the physical hard scattering. The hard scattering may be mediated, for example, by exchange of a gluon in QCD or by an electroweak current. For multieikonal amplitudes, we can always fix the vertex joining the eikonal lines at the origin. In the case of partonic scattering, with external fields ϕ_I at points x_I, as in Eq. (4.1.2), we consider $2 \to N$ scattering, where x_1^0, x_2^0 are large and negative and all x_I^0, $I > 2$ are large and positive. In this case, the requirement of a physical process allows hard scattering at a single, unique point, which, by translation invariance may also be taken as the origin. In this coordinate system, all $x_I^2 = 0$ at the pinch surfaces, and we may identify velocity vectors by $\beta_I^\mu \equiv x_I^\mu / x_I^0$ for each external field. These β_I fix the directions of jets in the reduced diagrams of Fig. 4.1(b), for partonic scattering amplitudes, in the same way as the Wilson lines fix jet directions for multieikonal amplitudes. For an amplitude with several Wilson lines or external partonic fields, we denote the velocity of the Ith line by β_I, with $\beta_I^2 = 0$. For each such line we introduce an additional, "complement" vector, $\bar{\beta}_I$, $\bar{\beta}_I^2 = 0$, normalized by $\beta_I \cdot \bar{\beta}_I = 1$. The leading singularity of the diagram requires that the leading behavior of each external propagator remains uncancelled. We may think of this as the analog of the requirement that the S-matrix is the residue of the leading pole in every external line.

The foregoing considerations on external propagators enable us to argue that the leading behavior in coordinate space is gauge invariant, once external vector fields are projected onto transverse polarizations. This may be seen from the diagrammatic proof of the gauge invariance of the S-matrix [56]. In momentum space, an infinitesimal gauge transformation produces a sum of terms in which either external propagators are cancelled, or vectors are projected onto scalar polarizations, proportional to their own momentum. The Fourier transformations of these relations are contributions in which an

external propagator is replaced by a four dimensional delta function, fixing its position at an internal vertex, or the divergence is taken of an external vector field, and hence a gradient of the external propagator. The former case gives a suppression by x_I^2 relative to leading behavior, while the latter is eliminated by the same transverse projection that defines the S-matrix.

4.2.2 Variables, power counting and neighborhoods for pinch surfaces

In the analysis of the pinch singularities of the coordinate-space integrals, the soft, jet, and hard regions were determined by the identification of "intrinsic" and "normal" variables, which parametrize a pinch surface and its normal space, respectively [32, 47, 53]. At a pinch surface, normal variables vanish as a distance scaling factor, $\lambda \to 0$ while intrinsic variables remain finite. At lowest order in normal variables, the propagator denominators of jet lines are linear in normal, those of the hard lines are quadratic in normal variables, and the soft lines are of zeroth order in normal variables. (Our specific choices of normal variables for the amplitudes under consideration will be described shortly.) Power counting can be performed by factoring out the lowest powers of λ from each factor of the *homogenous* integrand and the integration measure for each normal variable,

$$s_i = \lambda s_i' \,. \tag{4.2.1}$$

Then, near a pinch surface, the integral for some quantity $g(q_k)$, depending on external parameters q_k has the form [32],

$$\begin{aligned} g(q_k) \sim \int_0^{d_0} d\lambda \lambda^{p-1} \int \prod_i ds_i' \, \delta \left(1 - \sum_i |s_i'|^2 \right) \\ \times \int \prod_j dr_j \Big(\bar{I}_g(s_i', r_j, q_k) + \mathcal{O}(\lambda^\eta) \Big) \,, \end{aligned} \tag{4.2.2}$$

where $\eta > 0$ and where the integrals over the intrinsic variables r_j of the homogenous integrand $\bar{I}_g$ should be finite or have similar pinch surfaces as subsets of the s_i' and possibly intrinsic variables vanish. The scale d_0, which quantifies the maximum distance from the pinch surface, may be thought of as arbitrary at this point. The analysis of the homogeneous integrand determines the choice of normal variables near each PS [32]. As found in the power counting in Ref. [32], the leading overall degree of divergence is $p = 0$ for pinch surfaces of both eikonal and partonic amplitudes, relative to lowest

order, indicating logarithmic divergences of their integrals in coordinate space.

In these terms, leading regions are characterized by

1. Gluon propagators attaching the soft subdiagram to jet K are contracted only to the jet velocity vector, β_K.

2. Gluon propagators attaching the soft subdiagram to jet subdiagram K depend on the positions, $z^{(K)\mu}$ of the jet vertices to which they attach only through a vector that depends on a single coordinate: $\bar{\beta}_K \cdot z^{(K)} \beta_K^\mu$. The arguments of such propagators are given by

$$\begin{aligned} D^{\mu\nu}(x - z^{(K)})\, J_\nu(z^{(K)}) &= \frac{g^{\mu\nu}}{[-(x-z)^2 + i\epsilon]^{1-\varepsilon}}\, J_\nu(z^{(K)}) \\ &\to \frac{\beta_K^\mu \bar{\beta}_K^\nu}{[-2\,\bar{\beta}_K \cdot (x - z^{(K)})\,\beta_K \cdot x + x_\perp^2 + i\epsilon]^{1-\varepsilon}}\, J_\nu(z^{(K)})\,, \end{aligned} \tag{4.2.3}$$

   with x the position of a soft vertex, or in the case of a gluon exchanged between Wilson lines or jets, a point on the other line or in the other jet. We have dropped terms that are of order $\lambda^{1/2}$ near the pinch surface, where the denominator is finite. It is then convenient to define coordinates that link the soft and jet subdiagram in convolution for each vertex position, $z^{(K)}$,

$$\begin{aligned} d^D z^{(K)} &\equiv d\tau^{(K)}\, d^{D-1} z^{(K)}\,, \\ \tau^{(K)} &= \bar{\beta}_K \cdot z^{(K)}\,. \end{aligned} \tag{4.2.4}$$

   Here, only $\tau^{(K)}$ is an intrinsic variable, while $\beta_K \cdot z^{(K)}$ and $z_\perp^{(K)2}/\bar{\beta}_K \cdot z^{(K)}$ can be chosen as normal variables for this jet. We will refer to Eq. (4.2.3) as the soft-collinear approximation. For the special case of $z^{(K)}$ a vertex on the Kth Wilson line, we can identify $z^{(K)\mu} = \tau^{(K)} \beta_K^\mu$.

3. Gluon propagators attaching jet subdiagram J_I to the hard subdiagram are contracted only to the complementary vector, $\bar{\beta}_I^\mu$.

4. Gluon propagators attaching jet subdiagram I to the hard subdiagram depend on the coordinates, $y^{(I)}$ of the hard vertices to which they attach

by vector $\beta_I \cdot y^{(I)} \bar{\beta}_I^\mu$, and may be approximated as

$$\begin{aligned} D^{\mu\nu}(z - y^{(I)})\, H_\nu(y^{(I)}) &= \frac{g^{\mu\nu}}{[-(z-y^{(I)})^2 + i\epsilon]^{1-\varepsilon}}\, H_\nu(y^{(I)}) \\ &\to \frac{\bar{\beta}_I^\mu \beta_I^\nu}{[-2\,\beta_I \cdot (z - y^{(I)})\,\bar{\beta}_I \cdot z + z_\perp^2 + i\epsilon]^{1-\varepsilon}}\; H_\nu(y^{(I)})\,. \end{aligned} \tag{4.2.5}$$

Notice the similarity between this approximation, which we refer to as the hard-collinear approximation, and the soft-collinear approximation, Eq. (4.2.3). We have dropped terms that are of order $\lambda^{3/2}$ near the pinch surface, where the denominator is $\mathcal{O}(\lambda)$. Then, similarly to Eq. (4.2.4) we define

$$\begin{aligned} d^D y^{(I)} &\equiv d\zeta^{(I)}\; d^{D-1} y^{(I)}\,, \\ \zeta^{(I)} &= \beta_I \cdot y^{(I)}\,. \end{aligned} \tag{4.2.6}$$

In the hard subdiagram, all components of the positions y^μ are normal variables. In the generic case, where all components of y^μ appear linearly in the denominators of jet lines shown in Eq. (4.2.5), all of these components are naturally taken to scale linearly in λ. When there are precisely two incoming and two outgoing jets at the pinch surface hard scattering, however, one spacelike component of y^μ, which we may call $y_{\rm out}$, does not appear in any factor $\beta_I \cdot y$, $I = 1, \ldots, 4$. Rather, it appears quadratically in every propagator attached to the vertex at y^μ. This coordinate defines the direction normal to the scattering plane in a center-of-momentum frame of the physical picture at the pinch surface. In this case, the single variable $y_{\rm out}$ scales as $\lambda^{1/2}$, and the integral is correspondingly enhanced. This enhancement is also a feature of the lowest-order, tree-level scattering, however, and does not change the logarithmic nature of radiative corrections [32], which are the focus of our discussion.

5. In the case of partonic amplitudes, a leading PS requires that (exactly) one partonic propagator attaches each jet subdiagram to the hard scattering with a physical (transverse) polarization for fermions or vectors. For these propagators, the corresponding hard-collinear approximation may be represented as

$$\Delta^{\alpha\beta}(z - y^{(I)})\; H_\beta(y^{(I)}) \quad \to \quad \Delta^{\alpha\beta}(z)\; \mathcal{T}_\beta{}^{\beta'} H_{\beta'}(y^{(I)})\,, \tag{4.2.7}$$

where $\mathcal{T}_\beta{}^{\beta'}$ is an appropriate projection for the leading physical polarizations with $\Delta^{\alpha\beta}$ the corresponding propagator, depending on the spin of the field. The action of this approximation is to fix the position of the partonic field that initiates the jet subdiagram to the origin, which is the position of the hard scattering when the external points x_I approach the light cone.

In summary, for a partonic amplitude with hard scattering at the origin and external points on the light cone $x_I^2 \to 0$, *all* pinch surfaces are specified by a list of vertices $\{z_\mu^{(K)}\}$ that specify jet subdiagram J_K, and a list of vertices $\{y_\mu\}$ that specify the hard subdiagram H, while the remaining vertices $\{x_\mu\}$ specify the soft subdiagram S. From these lists of vertices, we find the normal variables of an arbitrary pinch surface ρ,

$$\{s_i^{(\rho)}\} \;=\; \left\{ \left\{ \beta_K \cdot z^{(K)},\, \frac{z_\perp^{(K)2}}{\bar{\beta}_K \cdot z^{(K)}} \right\}, \{y_\mu\} \right\}, \tag{4.2.8}$$

that is, the opposite-moving and the square of the perpendicular components normalized by the longitudinal distance for each vertex in each jet, and all components of vertices in the hard subdiagram. All other independent components are intrinsic variables,

$$\{r_j^{(\rho)}\} \;=\; \left\{ \{x_i^\mu\},\, \{\beta_K \cdot z^{(K)}\} \right\}. \tag{4.2.9}$$

We emphasize that the number of pinch surfaces is finite for any diagram of finite order, and is determined simply by the ways of assigning vertices to the jet, soft and hard subdiagrams.

The choice of subdiagrams can be pictured directly in coordinate space. In Fig. 4.2, each point represents the projection of the position of an interaction vertex in some very high-order diagram onto the plane defined by two non-collinear Wilson lines, for example. The closed curves represent the jets and hard scatterings in a transparent fashion. The normal variables for vertices in either jet are given simply by their distances to the corresponding lines in this diagram, and normal variables for vertices in the hard function are their distances from the origin, as in Eq. (4.2.8). We denote these subdiagrams by $S^{(\rho)}$, $J_I^{(\rho)}$ and $H^{(\rho)}$, respectively. We suppress their explicit orders, which are implicit in the choice of PS ρ. It is also clear from the figure that assignments of vertices to jet, hard and soft subdiagrams are shared by many diagrams, that is, all the perturbative diagrams that are found by connecting the points in the figure.

To organize integrals in the presence of this large but finite number of pinch

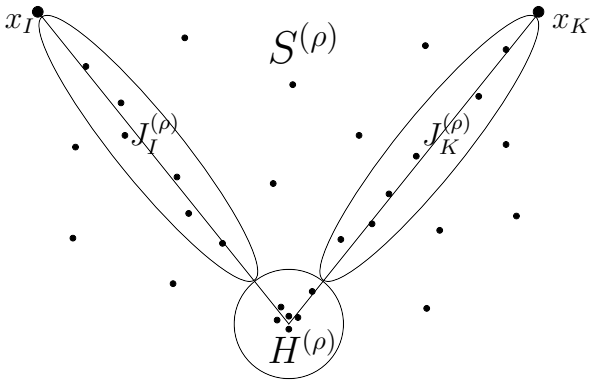

Figure 4.2: Representation of the arrangement of vertices near a leading pinch surface ρ directly in coordinate space and their assignments to jet, $J_I^{(\rho)}$, hard, $H^{(\rho)}$, and soft, $S^{(\rho)}$ subdiagrams. For every region, the direction of the jet $J_I^{(\rho)}$ is determined by the relative position of the external point x_I with respect to the position of the hard scattering.

surfaces, we define a neighborhoods $n[\rho]$ of pinch surfaces (PS) ρ by requirements on normal variables, $s_i^{(\rho)}$, given in Eq. (4.2.8), and intrinsic variables $r_j^{(\rho)}$ from Eq. (4.2.9),

$$\begin{aligned}
\sum_i |s_i^{(\rho)}|^2 &\leq d_0^2\,, \\
|r_j^{(\rho)}|^2 &\geq \left(\sum_i |s_i^{(\rho)}|^2\right)^{\delta_j} d_0^{2-2\delta_j} \\
&\geq \lambda^{2\delta_j}\left(\sum_i |s_i'^{(\rho)}|^2\right)^{\delta_j} d_0^{2-2\delta_j}\,,
\end{aligned} \tag{4.2.10}$$

for some finite distance scale d_0. A power $0 < \delta_j < 1/2$ is chosen for each intrinsic variable $r_j^{(\rho)}$, and the $s_i'^{(\rho)}$ are rescaled normal variables, Eq. (4.2.1). The inequalities for power δ_j ensures that the leading terms involving normal variables in the soft-collinear and hard-collinear approximations, Eqs. (4.2.3) and (4.2.5), remain dominant by a power over the first corrections to these approximations, which are relatively suppressed by $\lambda^{1/2}$ in both cases. With this definition, the soft-collinear and hard-collinear approximations associated with pinch surface ρ remain accurate for $\lambda \to 0$ in Eq. (4.2.2) throughout neighborhood $n(\rho)$. We can think of Eq. (4.2.10) as specifying the closed curves of Fig. 4.2.

4.2.3 Approximation operators and region-by-region finiteness

We will now employ the approximations identified above to define a set of approximation operators, denoted t_ρ, one for each leading pinch surface ρ. Each operator t_ρ is defined to act on any diagram $\gamma^{(n)}$ that possesses the corresponding PS and to give an expression that corresponds to the leading, singular behavior of $\gamma^{(n)}$ in the neighborhood of PS ρ. As is always the case in discussions of renormalization, the operator t_ρ is defined only up to a finite ambiguity, which specifies a regularization, and eventually a renormalization scheme. We may, for example, think of minimal subtraction schemes, but for our purposes it will be most useful to define subtractions similar to those employed in proofs of factorization [53].

We define the action of the approximation operator as precisely the soft-collinear and hard-collinear approximations given above in Eqs. (4.2.3) and (4.2.5) respectively, given schematically by

$$\begin{aligned} t_\rho \gamma^{(n)} \quad \equiv \quad & \prod_I \int d\tau^{(I)} \; S^{(\rho)}_{\{\mu_I\}}(\tau^{(I)}) \; \beta_I^{\mu_I} \bar{\beta}_{I,\mu'_I} \\ & \times \int d\zeta^{(I)} \int d^{D-1} z^{(I)} \; J_I^{(\rho)\mu'_I\nu'_I}(z^{(I)}, \zeta^{(I)}) \; \bar{\beta}_{I,\nu'_I} \beta_I^{\nu_I} \\ & \times \int d^{D-1} y^{(I)} \; H^{(\rho)}_{\{\nu_I\}}(y^{(I)}) \, . \end{aligned} \tag{4.2.11}$$

In this expression, each vector index and vertex position, for example, μ_I and $z^{(I)}$, represents arbitrary numbers of such indices for gluons connecting the subdiagrams specific to this leading region, $S^{(\rho)}$, $J_I^{(\rho)}$ and $H^{(\rho)}$. As mentioned above, the "soft-collinear" and "hard-collinear approximations" defined for coordinate-space integrals in [32] are equivalent to approximations with similar names in discussions of factorization in momentum space [31, 106]. In this case, however, the approximation isolates ultraviolet divergences in the neighborhood of the PS in coordinate space, so long as the soft-collinear and hard-collinear approximations apply. We represent this result by

$$t_\rho \, \gamma^{(n)}\big|_{\text{div } n[\rho]} \;=\; \gamma^{(n)}\big|_{\text{div } n[\rho]} \;, \tag{4.2.12}$$

where the subscript "div $n[\rho]$" represents the divergent UV behavior, from short-distance and/or collinear configurations of region ρ where the soft-collinear and hard-collinear approximations apply. We will explore the consequences of this relation by introducing the concept of nested pinch surfaces, in the following discussion. We emphasize first, however, that the equality (4.2.12)

refers to the result of an integral over the neighborhood, $n[\rho]$ of PS ρ, where the approximation is accurate, but the definition $t_\rho \gamma^{(n)}$ refers to the full integral, extended over the full integration region in coordinate space, including other PSs and regions where t_ρ no longer gives a good approximation to the integrand.

As in any multi-loop diagram, multiple ultraviolet divergences can arise from sets of vertices that approach the hard scattering or the collinear directions in partonic amplitudes, or the cusp and/or the Wilson lines in multi-eikonal amplitudes, at different rates, just as loop momenta may go to infinity faster in some subdiagrams than in others. As for the renormalization of Green functions, we can classify sets of divergences as either nested or overlapping, in terms of the limiting process in coordinate space.

Nesting in coordinate space can be classified directly in terms of pinch surfaces. We say PS ρ_1 is nested in PS ρ_2 when some subset of vertices in ρ_1 approaches the light cone and/or the origin faster than other vertices in ρ_2, while others remain fixed. The smaller nested PS has larger subdiagrams with vertices near the light cone (jets) or the origin (hard subdiagram). Otherwise, we will say that the PSs are overlapping.

To be specific, for two leading pinch surfaces, ρ_1 is a nested subsurface of ρ_2, denoted

$$\rho_1 \subseteq \rho_2 \,, \tag{4.2.13}$$

if and only if

$$\begin{aligned} H^{(\rho_2)} &\subseteq H^{(\rho_1)} \,, \\ H^{(\rho_2)} \cup J_I^{(\rho_2)} &\subseteq H^{(\rho_1)} \cup J_I^{(\rho_1)} \,, \end{aligned} \tag{4.2.14}$$

for all jets J_I. That is, the jet and/or hard subdiagrams grow as the dimension of the pinch surface decreases. The equality holds only when $\rho_1 = \rho_2$, in which case all these relations are equalities. Otherwise, we say that ρ_1 is contained in ρ_2. Without specifying their ordering, we say that ρ_1 and ρ_2 nest. The subsurface, or nesting, relation is transitive,

$$\rho_3 \subset \rho_2 \text{ and } \rho_2 \subset \rho_1 \;\Rightarrow\; \rho_3 \subset \rho_1 \,. \tag{4.2.15}$$

We note that the smaller the pinch surface in the sense of Eq. (4.2.14), the *larger* the number of its normal variables, and the smaller the number of its intrinsic variables. Another way of putting this is that smaller pinch surfaces have the larger "codimension". We will denote any fully nested set with M_N pinch surfaces by $N = \{\sigma_1 \subset \sigma_2 \subset \cdots \subset \sigma_{M_N}\}$, and the set of all such nested

sets for diagram γ as $\mathcal{N}[\gamma]$.

We now use nesting of pinch surfaces and the definitions of neighborhoods above to help us construct a set of regions in coordinate space that cover all pinch surfaces, and in each of which an operator, t_ρ gives a valid approximation to the singular behavior of the diagram. Our choice for this "reduced neighborhood" is

$$\hat{n}[\rho] \;=\; n[\rho] \backslash \cup_{\sigma \supset \rho} \left(n[\rho] \cap n[\sigma] \right) \,. \tag{4.2.16}$$

By construction, region $\hat{n}[\rho]$ is the neighborhood $n[\rho]$ where the soft- and hard-collinear approximations of PS ρ remain accurate, less its intersection with the neighborhoods $n[\sigma]$ of all larger pinch surfaces, $\sigma \supset \rho$. Pinch surface σ has more intrinsic (and fewer normal) variables than pinch surface ρ, and one or more of the instrinsic variables of σ are normal variables of ρ, and in neighborhood $n[\sigma]$ the normal variables of ρ that are instrinsic variables of σ do not vanish rapidly enough to produce a divergence. Although pinch surface ρ is a subpace of lower dimension in surface σ, the neighborhoods $n[\rho]$ and $n[\sigma]$ are of the same dimension, and $\rho \subset \sigma$ does *not* imply that $n[\rho] \subset n[\sigma]$. The neighborhoods $\hat{n}[\rho]$ cover all pinch surfaces without duplication.

Not all pairs of regions can satisfy the nesting criterion, Eq. (4.2.14). We say two pinch surfaces are overlapping when $\rho \not\subset \sigma$ and $\sigma \not\subset \rho$, which we denote as

$$\rho \;\phi\; \sigma \,. \tag{4.2.17}$$

By definition, if $\rho \;\phi\; \sigma$, then ρ and σ cannot appear any set N of nested PSs of γ. The overlap relation, ϕ has a property analogous to transitivity of nesting, Eq. (4.2.15), which also follows easily from the defining properties of nesting, Eq. (4.2.14),

$$\begin{aligned} \text{given}: &\qquad \sigma_1 \subset \sigma_2 \subset \sigma_3 \,,\; \sigma_3 \;\phi\; \rho \text{ and } \sigma_1 \;\phi\; \rho \\ \text{then}: &\qquad \sigma_2 \;\phi\; \rho \,. \end{aligned} \tag{4.2.18}$$

Any pair of PSs is either nested or overlapping. Note that the pinch surface where all vertices are in the hard subdiagram is nested with all other pinch surfaces, so that no pair of pinch surfaces is fully disjoint.

As we have seen, each pinch surface, and corresponding neighborhood is associated with a distinct matching of the list of vertices to the jet, hard and soft subdiagrams. In these terms, we can give an explicit form for the requirement of Eq. (4.2.12), that the divergences from PS ρ are equal for $\gamma^{(n)}$

and $t_\rho \gamma^{(n)}$,

$$
\begin{aligned}
t_\rho \gamma^{(n)}\big|_{\text{div } \hat{n}[\rho]} \;-\; \gamma^{(n)}\big|_{\text{div } \hat{n}[\rho]} \;=\; & \\
\prod_I \int d\tau^{(I)} \int d\zeta^{(I)} \int d^{D-1} z^{(I)} \int d\zeta^{(I)} \int d^{D-1} y^{(I)}\, \Theta(\hat{n}[\rho]) & \\
\times \Big[S^{(\rho)}_{\{\mu_I\}}(\tau^{(I)})\, \beta_I^{\mu_I}\, \bar{\beta}_{I,\mu_I'}\, J_I^{(\rho)\mu_I'\nu_I'}(z^{(I)}, \zeta^{(I)})\, \bar{\beta}_{I,\nu_I'} \beta_I^{\nu_I}\, H^{(\rho)}_{\{\nu_I\}}(y^{(I)}) & \\
-\; S^{(\rho)}_{\{\mu_I\}}(z^{(I)})\, J_I^{(\rho)\mu_I\nu_I}(z^{(I)}, y^{(I)})\, H^{(\rho)}_{\{\nu_I\}}(y^{(I)}) \Big] \;\Big|_{\text{div } \hat{n}[\rho]} & \\
=\; 0\,, &
\end{aligned}
\tag{4.2.19}
$$

where $\Theta(\hat{n}[\rho])$ restricts the integration to reduced neighborhood $\hat{n}[\rho]$, Eq. (4.2.16). This integral over the reduced nieghborhood converges because of the accuracy of the soft-collinear and hard-collinear approximations in the entire neighborhood $n[\rho]$, and therefore in the smaller neighborhood, $\hat{n}[\rho]$.

Equation (4.2.19) is the main result we will use for applications in the following sections, treating the neighborhood of each PS separately. As a more general result, however, we will show that all divergent contributions to amplitudes can be written without restriction to specific regions, by a construction involving nested subtractions [53], which we now discuss.

4.2.4 Nested subtractions

The quantities $t_\rho \gamma$, Eq. (4.2.11), can also be thought of as counterterms for ultraviolet divergences associated with Wilson lines and/or the limits $x_I^2 \to 0$ in the partonic matrix elements, Eq. (4.1.2). Following the reasoning of [53], we define an n-loop regulated version of $\gamma^{(n)}$ by

$$
R^{(n)}\, \gamma^{(n)} \;=\; \gamma^{(n)} \;+\; \sum_{N \in \mathcal{N}[\gamma^{(n)}]} \prod_{\rho \in N} \big(- t_\rho \big)\, \gamma^{(n)}\,, \tag{4.2.20}
$$

so that we may write for the full nth order amplitude, $\Gamma^{(n)} = \sum \gamma^{(n)}$,

$$
\Gamma^{(n)} \;=\; -\sum_{\gamma^{(n)}} \sum_{N \in \mathcal{N}[\gamma^{(n)}]} \prod_{\sigma \in N} \big(- t_\sigma \big)\, \gamma^{(n)} \;+\; R^{(n)}\, \Gamma^{(n)}\,. \tag{4.2.21}
$$

The sets N of PSs σ include not only "proper" pinch surfaces, but also those for which the pinch surfaces involve setting all vertices of the diagram on the light cone or at the hard scattering. These products are ordered with the larger PSs to the right of smaller PSs. As in Eq. (4.2.11), the approximation

operators act on the diagram over the full integration region, not restricted to the neighborhood of the corresponding pinch surface. Thus, the first appoximation operators t_ρ to act on γ involve the fewest points on the light cones or at short distances.

We will argue that the nesting, from regions to subregions, eliminates double counting, allowing the subtractions t_ρ for each leading region PS ρ to be extended from $\hat{n}[\rho]$ to the full space, as in the momentum space discussion described in Ref. [53]. We can also think of individual subtractions acting region by region; the purpose of the nested products is to cancel the action of subtractions outside their corresponding reduced neighborhoods $\hat{n}[\rho]$. In summary, we claim that for each diagram $\gamma^{(n)}$, the action of $R^{(n)}$ is to remove divergences from every leading pinch surface ρ,

$$R^{(n)}\,\gamma^{(n)}|_{\text{div }\hat{n}[\rho]} \;=\; 0\,. \tag{4.2.22}$$

Combining this result with the definition of nested subtractions in Eq. (4.2.21) and the requirement Eq. (4.2.19), we find

$$\begin{aligned}\sum_{N^\rho\neq\rho}\left(\prod_{\sigma\in N^\rho}(-t_\sigma)\;+\;\prod_{\sigma\in N^\rho\backslash\rho}(-t_\sigma)\right)\gamma^{(n)}\big|_{\text{div }\hat{n}[\rho]}\\ +\;\sum_{\bar{N}^\rho}\prod_{\sigma\in\bar{N}^\rho}(-t_\sigma)\,\gamma^{(n)}\big|_{\text{div }\hat{n}[\rho]}\;=\;0\,.\end{aligned} \tag{4.2.23}$$

That is, for (4.2.22) to hold in each neighborhood $\hat{n}[\rho]$, the divergent parts of *all* subtraction terms *except* for $t_\rho\Gamma$ alone must cancel (or vanish) in region $\hat{n}[\rho]$ defined by Eq. (4.2.16).

Thus, to prove the absence of divergences in $R^{(n)}\Gamma^{(n)}$ for an arbitrary $\hat{n}[\rho]$, we must examine all nestings in Eq. (4.2.21). We consider separately those nestings denoted N^ρ that include ρ, along with the set $N^\rho\backslash\rho$, in which region ρ can nest but is excluded, and finally the set of nestings, denoted, $\bar{N}^\rho$, in which ρ cannot nest because $\rho\,\phi\,\sigma$ for at least one element $\sigma\in\bar{N}^\rho$.

It is worth noting the relationship between the subtraction approach here, and the momentum space "strategy of regions" [107]. In the latter, approximations tailored to regions of loop momenta that are the sources of leading behavior are also extended to all of loop momentum space. We are doing something very similar here; each of the subtraction terms in each nesting is associated with a particular PS, but we extend each such exppression over the full coordinate integration space. The list of PSs specifies the list of regions about which to expand. By showing that all double counting is eliminated in the sum over all nestings, we will verify in this section that the sum of

subtractions is an acceptable representation of the original amplitude, up to well-defined finite corrections. In Sec. 4.4, we will show that the sum over nestings is also equivalent to a single factorized expression in coordinate space for both multieikonal and partonic amplitudes, by using the exponentiation properties of webs.

We start with those nestings, N^ρ in which ρ appears along with at least one other PS. For all such nestings, in neighborhood $\hat{n}[\rho]$, the term corresponding to nesting N^ρ cancels the nesting, $N^\rho \backslash \rho$. This is because the action of t_ρ is equivalent to the identity in region $\hat{n}[\rho]$, so that

$$\sum_{N^\rho \neq \rho} \left(\prod_{\sigma \in N^\rho} (-t_\sigma) + \prod_{\sigma \in N^\rho \backslash \rho} (-t_\sigma) \right) \gamma^{(n)} \Big|_{\text{div } \hat{n}[\rho]} = 0 \,, \tag{4.2.24}$$

where, as in Eq. (4.2.12), the subscript "div $\hat{n}[\rho]$" on the right-hand side refers to the sum of all divergent parts from the integral over $\hat{n}[\rho]$. This implies that the proof of Eq. (4.2.22) requires that we show that the sum of all overlapping subtractions cancels independently,

$$\sum_{\bar{N}^\rho} \prod_{\sigma \in \bar{N}^\rho} (-t_\sigma) \, \gamma^{(n)} \Big|_{\text{div } \hat{n}[\rho]} = 0 \,. \tag{4.2.25}$$

Here, nestings $\bar{N}^\rho$ in Eq. (4.2.21) are not consistent with a leading region ρ because one or more of the regions σ overlap with ρ. Because we are interested in singular contributions, we need to consider only those nestings, $\bar{N}^\rho$ that are divergent in region ρ, and we will use this condition below.

To motivate our approach, we consider an arbitrary nesting $\bar{N}^\rho$ that contains elements σ that overlap with PS ρ. Because of the transitive nature of nesting, Eq. (4.2.15), we can partition the PSs $\sigma_i \in \bar{N}^\rho$ into three ordered sets [53]: those that are larger than ρ, those that are smaller than ρ and those that overlap with ρ,

$$\bar{N}^\rho = N_L \cup N_\phi \cup N_S \,, \tag{4.2.26}$$

with

$$\begin{aligned} N_L[\rho] &= \{\sigma_j \supset \rho\} \,, \\ N_\phi[\rho] &= \{\sigma_k \; \phi \; \rho\} \,, \\ N_S[\rho] &= \{\sigma_l \subset \rho\} \,, \end{aligned} \tag{4.2.27}$$

where all $\sigma_j \supset \sigma_k \supset \sigma_l$. Note that the set $N_S[\rho]$ may include the element, σ_γ, corresponding to the smallest PS of diagram γ, where all of its vertices are in $H^{(\sigma_\gamma)}$ and move to the cusp or multieikonal vertex at the PS.

In the following, we will identify an "induced" PS σ_{ind}, which is intermediate between the sets $N_\phi[\rho]$ and $N_S[\rho]$ in Eq. (4.2.27). This PS, $\sigma_{\rm ind}$ will be a proper subregion of both region ρ and of every element $\sigma_k \in N_\phi$. It will at the same time contain every element $\sigma_l \in N_S[\rho]$, including the case when it equals the *largest* element of $N_S[\rho]$. The induced region, $\sigma_{\rm ind}[\sigma_i, \rho]$ will be constructed to act as the identity on $t_{\sigma_i}\gamma^{(n)}$ in neighborhood $\hat{n}[\rho]$ up to finite corrections,

$$\left[\left(-t_{\sigma_{\rm ind}[\sigma_i,\rho]} \right) \left(-t_{\sigma_i} \right) \gamma^{(n)} \; + \; \left(-t_{\sigma_i} \right) \gamma^{(n)} \right] \Big|_{\rm div \;\; \hat{n}[\rho]} \;\; = \;\; 0 \,, \quad (4.2.28)$$

for every PS σ_i included in $N_\phi[\rho]$. That is, the integral of this combination over region $\hat{n}[\rho]$ is nondivergent, and the resulting integral confined to $\hat{n}[\rho]$ should be considered as a finite contribution to the full diagram. Equation (4.2.28) assures that in region $\hat{n}[\rho]$, nestings that include PS $\sigma_{\rm ind}$ cancel with those that do not include $\sigma_{\rm ind}$.

The induced PS $\sigma_{\rm ind}[\sigma, \rho]$ is defined as usual by its hard, jet and soft subdiagrams. These subdiagrams are determined in turn by the subdiagrams of PSs σ and ρ in the following manner,

$$H^{(\sigma_{\rm ind})} \;\; = \;\; \left[\; H^{(\sigma)} \cup H^{(\rho)} \; \cup \prod_{I,K,\, I \neq K} \left(J_I^{(\sigma)} \cap J_K^{(\rho)} \right) \; \right]_{\rm connected} \,, \quad (4.2.29)$$

$$J_I^{(\sigma_{\rm ind})} \;\; = \;\; J_I^{(\sigma)} \cup J_I^{(\rho)} \setminus H^{(\sigma_{\rm ind})} \,, \quad (4.2.30)$$

$$\begin{aligned} S^{(\sigma_{\rm ind})} \;\; &= \;\; S^{(\sigma)} \cap \; S^{(\rho)} \\ &= \;\; \gamma \setminus \left(H^{(\sigma_{\rm ind})} \cup \prod_I J_I^{(\sigma_{\rm ind})} \right) \,. \end{aligned} \quad (4.2.31)$$

As indicated in the first relation, an induced PS is found only when the union of the hard subdiagrams and adjacent intersections of jets is itself connected. For consistency, we also demand that the soft subdiagram be connected only to jet subdiagrams and not to the hard subdiagram by the power counting of Ref. [32]. We note that although the construction is symmetric in σ and ρ, only the approximant t_σ has been applied to the diagram. The construction (4.2.29)–(4.2.31) "favors" hard subdiagrams $H^{(\sigma_{\rm ind})}$ and then jet subdiagrams $J_I^{(\sigma_{\rm ind})}$ compared to the soft subdiagram $S^{(\sigma_{\rm ind})}$. That is, we go from larger to smaller PSs.

Much of the subtlety in this construction involves "overlapping jets" in different directions, in which some subsets of lines shift from one lightcone in σ to another lightcone in ρ. Many such subdiagrams, $J_I^{(\sigma)} \cap J^{(\rho)}$, are possible, and are defined by the list of PSs of each diagram γ. We now observe an important

result, which follows from the action of the approximation operator t_σ. In the integral $t_\sigma\gamma$, including the approximation operator for region σ, certain PSs are modified. We find that PSs involving overlaps $J_I^{(\sigma)} \cap J_K^{(\rho)}$ are replaced by PSs where the lines in $J_I^{(\sigma)} \cap J_K^{(\rho)}$ are either pinched at the origin, or move only in the direction $\bar\beta_I$ (of the jet in region σ), complementary to the direction of $J_I^{(\sigma)}$ and independent of direction β_K (of the jet in region ρ).

To see how such "complementary" collinear singularities, along with pinches at the origin, occur, and why there are no other singularities in $J_I^{(\sigma)} \cap J_K^{(\rho)}$, we consider a gluon line in $J_K^{(\sigma)}$, attached at one end to an arbitrary vertex at a point y in $J_K^{(\rho)}$, $K \neq I$, and at the other end to a vertex x that is in $J_I^{(\sigma)} \cap J_K^{(\rho)}$. Because this line is not in $J_I^{(\sigma)}$, it must be in $S^{(\sigma)}$. For the denominator of this line, the action of t_σ is then

$$\begin{aligned} -(y-x)^2 + i\epsilon \;&\to\; -(y - (x\cdot\bar\beta_I)\beta_I)^2 + i\epsilon \\ &=\; -y^2 + 2(x\cdot\bar\beta_I) y\cdot\beta_I + i\epsilon\,. \end{aligned} \tag{4.2.32}$$

When y approaches the collinear configuration, $y \propto \beta_K$, $y - x$ is lightlike if and only if $x \cdot \bar\beta_I = 0$ or $x = 0$. These conditions require that the vertex in $J_I^{(\sigma)} \cap J_K^{(\rho)}$ be either on the $\bar\beta_I$ lightcone, or at the origin.

The foregoing result has consequences for the couplings of soft lines that would attach to lines in subdiagrams $J_I^{(\sigma)} \cap J_K^{(\rho)}$. The power counting described in Ref. [32] shows that for leading behavior at PS ρ, that is, ultraviolet divergence, the soft polarization tensor ($g^{\mu\nu}$ for us) of a line connected to a jet subdiagram must contract with vectors proportional to the direction of the jet lines on the light cone to which they attach. The action of t_σ applies the soft-collinear approximation, Eq. (4.2.11), appropriate to region σ, in which soft lines couple to jet lines moving in direction β_I. As we have seen, however, in region ρ the jet lines of $J_I^{(\sigma)} \cap J_K^{(\rho)}$ move in the complementary, $\bar\beta_I$, direction. This leads to a relative suppression, which eliminates UV divergences in this region. To illustrate the point, consider a PS σ where a soft gluon is attached to a jet fermion line at point z. The resulting product on the fermion line after the action of t_σ is of the form

$$S(z'' - z)\,\gamma\cdot\bar\beta_I\,S(z - z')\,, \tag{4.2.33}$$

with $S(y)$ the coordinate-space fermion propagator,

$$S(y) = \frac{\Gamma(2-\varepsilon)}{2\pi^{2-\varepsilon}} \frac{\gamma\cdot y}{(-y^2 + i\epsilon)^{2-\varepsilon}}\,, \tag{4.2.34}$$

in $D = 4 - 2\varepsilon$ dimensions. The product in Eq. (4.2.33) is suppressed relative

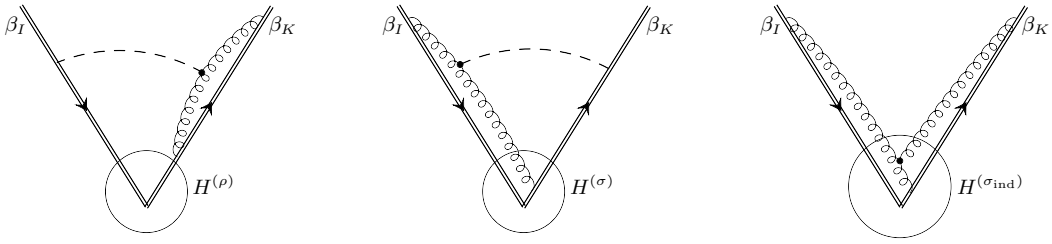

Figure 4.3: Example of nested overlapping subdivergences, involving jets at two loops for the cusp. Dashed lines represent soft lines, and circles denote hard subdiagrams. The hard subdiagram of the rightmost figure is $H^{(\sigma_{\rm ind})}$, from Eq. (4.2.29) applied to the diagrams on the left.

to leading behavior when $z'' - z$ and $z - z'$ are in the $\bar{\beta}_I$ direction. Similar suppressions hold for three-gluon and other relevant vertices (See Ref. [32].) In summary, after the action of the soft approximation t_σ, any lines in $S^{(\sigma)} \cap S^{(\rho)}$ are coupled to $J_I^{(\sigma)} \cap J_K^{(\rho)}$ through the combination $\bar{\beta}_{I\mu_I} J_I^{(\sigma)\mu_I\nu_I}(z)$ and are not UV divergent in region ρ, where internal lines are either parallel to $\bar{\beta}_I$ in region, $\rho \neq \sigma$ or shrink to the origin. This result is an important ingredient in showing the consistency of the construction outlined above for induced PSs,.

An example of the construction of Eq. (4.2.29) applied to the cusp is shown in Fig. 4.3, where the circles isolate the hard subdiagrams $H^{(\sigma)}$, $H^{(\rho)}$ and $H^{(\sigma_{\rm ind})}$. The gluon line in these diagrams attaching the three-gluon vertex to the inner vertex on the β_K Wilson line appears in different jets in the overlapping regions, and so appears in the hard subdiagram in the induced PS. In region ρ, after the action of t_σ, this line is pinched in the $\bar{\beta}_I$ direction or at the origin, independent of β_K, and the diagram gives examples both of a pinch in the "complementary direction" and of a pinch at the origin.

Figure 4.4 illustrates Eq. (4.2.29) with a case when the hard scattering subdiagrams of σ and ρ PSs are disjoint, but are connected in the sense of Eq. (4.2.29), through the overlaps of jet subdiagrams. In the figure, the hard scattering may be associated with the propagator connecting the vertices y_1 and y_2 (PS σ) when $y_1 \to y_2 \to 0$, while y_3 and y_4 remain at finite distances from each other, or alternately when $y_3 \to y_4 \to 0$ (PS ρ), where y_1 and y_2 remain at finite distances. At PS ρ, the lines (y_1, y_3) and (y_2, y_4) are in the jet subdiagrams associated with external points x_1 and x_2 respectively. At PS σ, they are in the jet subdiagrams associated with external points x_3 and x_4. These two regions cannot be nested. The action of t_σ, however, decouples the internal integrals of the hard subdiagram (y_1, y_2) from the σ jet functions, because these vertices are where physically-polarized parton lines attach to the hard scattering at PS σ, and are hence set to the origin, as in Eq. (4.2.7). In

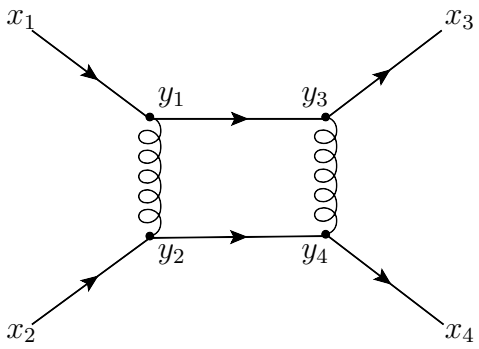

Figure 4.4: An example of non-overlapping hard subdiagrams that lead to a connected induced hard subdiagram.

the neighborhood of PS ρ, on the other hand, y_3 and y_4 are set to the origin. When the integral of $t_\sigma \gamma$ is taken into region ρ, the lines $y_1 - y_3$ and $y_2 - y_4$ are squeezed to the origin, and we are led precisely to PS σ_{ind} of Eq. (4.2.29), where all the vertices $y_1, \ldots, y_4$ shrink to the origin.

We now turn to general arguments on how the construction of Eqs. (4.2.29)–(4.2.31) satisfies Eq. (4.2.28), which states that the combination $t_{\sigma_{\text{ind}}} t_\sigma \gamma$ is a good approximation to $t_\sigma \gamma$ near PS ρ, where $\sigma \in N_\phi[\rho]$. We must verify that:

- (i) The hard-collinear approximation should hold for lines that connect each $J_I^{(\sigma_{\text{ind}})}$ to $H^{(\sigma_{\text{ind}})}$.
- (ii) The soft-collinear approximation should hold for lines that connect $S^{(\sigma_{\text{ind}})}$ to each $J_I^{(\sigma_{\text{ind}})}$.
- (iii) Configurations in which lines from $S^{(\sigma_{\text{ind}})}$ attach to $H^{(\sigma_{\text{ind}})}$ can be neglected. That is, whenever the construction of Eqs. (4.2.29)–(4.2.31) produces such a PS, this configuration should not be associated with a divergence.
- (iv) Configurations for which the construction gives a multiply-connected subdiagram $H^{(\sigma_{\text{ind}})}$ must also be finite.

These four criteria are met as follows.

- (i) There are two classes of collinear lines from any jet $J_I^{(\sigma_{\text{ind}})}$ that attach to $H^{(\sigma_{\text{ind}})}$ in the construction of Eqs. (4.2.29)–(4.2.30), whose elements are distinguished by the vertices in $H^{(\sigma_{\text{ind}})}$ to which they attach. According to Eq. (4.2.29), this vertex is either in the union of the two hard subdiagrams, $H^{(\sigma)} \cup H^{(\rho)}$ or in one of the jet intersections $J_I^{(\sigma)} \cap J_K^{(\rho)}$. These two sets of vertices are disjoint.

1. First, consider a vertex of $H^{(\sigma_{\rm ind})}$ that is in $H^{(\sigma)} \cup H^{(\rho)}$, and to which a line from $J_I^{(\sigma_{\rm ind})}$ attaches. Any external line of $H^{(\sigma)} \cup H^{(\rho)}$ must be an external line of either $H^{(\sigma)}$ or $H^{(\rho)}$ (or both), and hence must be in $J_I^{(\sigma)}$ or $J_I^{(\rho)}$ (or both). (By Eq. (4.2.30) these lines are certainly in $J_I^{(\sigma_{\rm ind})}$.) Jet lines in this class connect $J_I^{(\sigma)}$ to $H^{(\sigma)}$ or $J_I^{(\rho)}$ to $H^{(\rho)}$ (or both). If the line in question connects $J_I^{(\sigma)}$ to $H^{(\sigma)}$, the hard-collinear approximation is already imposed by t_σ; if it connects $J_I^{(\rho)}$ to $H^{(\rho)}$, $t_{\sigma_{\rm ind}}$ will then apply the hard-collinear approximation, which is accurate at PS ρ for this line.

2. Second, the vertex that connects jet lines of $J^{(\sigma_{\rm ind})}$ to $H^{(\sigma_{\rm ind})}$ may be in the intersection $J_I^{(\sigma)} \cap J_K^{(\rho)}$. Such vertices cannot be connected to lines that are in $J_I^{(\rho)}$, because in region ρ, any vertex that connects to collinear lines in both $J_I^{(\rho)}$ and $J_K^{(\rho)}$ is in $H^{(\rho)}$. This would reduce to the case we have just discussed. The only other possibility for an I-jet line in $\sigma_{\rm ind}$ is a line in $S^{(\rho)}$, that is, soft in region ρ, which is attached to $J_K^{(\rho)}$, but is also in $J_I^{(\sigma)}$. Such lines are attached by the vertex in question to $J_I^{(\sigma)} \cap J_K^{(\rho)}$, $K \neq I$, but are not themselves in it. By Eq. (4.2.30), these lines are in $J_I^{(\sigma_{\rm ind})}$.

   We now consider such a line, which is in $J_I^{(\sigma)}$, and is also attached to $J_K^{(\rho)} \cap J_I^{(\sigma)}$ from $S^{(\rho)}$. As we have seen below Eq. (4.2.32), however, the only pinch surfaces of $J_K^{(\rho)} \cap J_I^{(\sigma)}$ on the light cone are in the $\bar\beta_I$ direction after the action of t_σ. The gluons from $S^{(\rho)}$ therefore couple to velocity $\bar\beta_I$, which is identical to the hard-collinear approximation for their attachment to $H^{(\sigma_{\rm ind})}$, given by Eq. (4.2.5). Thus, the hard-collinear approximation of $t_{\sigma_{\rm ind}}$ is again accurate at PS ρ.

- (ii) By Eq. (4.2.31), a line in $S^{(\sigma_{\rm ind})}$ must be in both $S^{(\sigma)}$ and $S^{(\rho)}$, and hence must be a soft line in region ρ. Lines in $S^{(\sigma_{\rm ind})}$ that attach to the jets $J_I^{(\sigma_{\rm ind})}$ must, by Eq. (4.2.30), attach to vertices that are either in $J_I^{(\sigma)}$ or $J_I^{(\rho)}$. In the former case, the soft-collinear approximation is already carried out by t_σ; in the latter case, the soft-collinear approximation of $t_{\sigma_{\rm ind}}$ is accurate in ρ.

- (iii) The diagrammatic construction of Eqs. (4.2.29)–(4.2.31) can result in soft lines attached to the hard scattering. This can happen when a line is part of both $S^{(\sigma)}$ and $S^{(\rho)}$, and is hence part of $S^{(\sigma_{\rm ind})}$ by Eq. (4.2.31), and connects to a vertex that is in both $J_I^{(\sigma)}$ and $J_K^{(\rho)}$, with $K \neq I$, which by (4.2.29) is a vertex in $H^{(\sigma_{\rm ind})}$. We give a four-loop

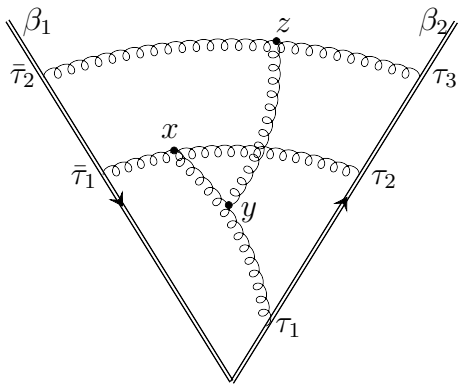

Figure 4.5: Four-loop example illustrating the two overlapping jets defined by Eq. (4.2.35).

example in Fig. 4.5, where the two overlapping jets and the induced hard function are determined by the set of vanishing normal variables

$$\begin{aligned} J_1^{(\sigma)} &: \{\beta_1 \cdot x, \beta_1 \cdot y, \tau_1\} \\ J_2^{(\rho)} &: \{\beta_2 \cdot x, \beta_2 \cdot y\} \\ H^{(\sigma_{\rm ind})} &: \{x^\mu, y^\mu, \tau_1\}\,. \end{aligned} \tag{4.2.35}$$

In this case, the soft gluon that would be connected to the hard function $H^{(\sigma_{\rm ind})}$ is the line $z-y$. In this and all related cases, such contributions are suppressed in region ρ, because, as shown above, when lines in $S^{(\sigma)} \cap S^{(\rho)}$ are coupled to $J_I^{(\sigma)} \cap J_K^{(\rho)}$, the corresponding PS ρ is suppressed.

In the example in Fig. 4.5, we immediately see that the terms that remain after the action of t_σ are suppressed, because t_σ replaces the polarization of gluon $z-y$ by the complementary light-cone direction, $\bar{\beta}_1$ at vertex y, giving a product of the form $\bar{\beta}_{1\mu_1'} J_1^{(\sigma)\mu_1'\nu_1'}(y)$ for jet J_1, which is suppressed in region ρ. After the action of t_σ, in the neighborhood of PS ρ, however, the lines in subdiagram $J_1^{(\sigma)} \cap J_2^{(\rho)}$ to which the soft lines attach can have pinch singularities only in precisely the $\bar{\beta}_1$ direction, even if $\bar{\beta}_1 \neq \beta_2$. The line $\tau_2\beta_2 - x$ in the figure illustrates this point.

- (iv) For amplitudes involving physical processes with both incoming and outgoing external partons or Wilson lines, there are in general disconnected hard subdiagrams at pinch surfaces, as illustrated by the diagram of Fig. 4.6(a), where the solid lines represent fermion or Wilson lines. Such pinch surfaces, however, are not associated with leading singular behavior, because, as in momentum space [53], the Ward identities of

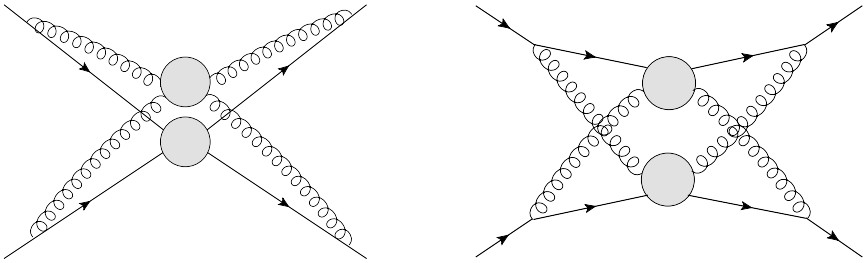

(a) (b)

Figure 4.6: Examples of disconnected hard subdiagrams.

the theory require that each jet subdiagram is connected to the hard subdiagram by at least one line that is not scalar polarized. Similar suppressions are described for cross sections in Refs. [108] and [109]. We may therefore assume that leading pinch surfaces for partonic amplitudes involve at most a single, connected hard scattering. Similarly, for multieikonal amplitudes, the local multieikonal vertex must be part of every hard subdiagram, so that the union of hard parts in (4.2.29) is always connected. For partonic amplitudes, however, it is still possible that disconnected subdiagrams $H^{(\sigma)}$ and $H^{(\rho)}$ mediate the hard scattering in overlapping regions, as we have seen in the example of Fig. 4.4, where the construction of Eq. (4.2.29) led to a connected $H^{(\sigma_{\text{ind}})}$. We must, however, confirm that disconnected hard scatterings that might result from the construction of the induced PS are suppressed.

The induced hard scattering may fail to be connected if either a connected component of $J_I^{(\sigma)} \cap J_K^{(\rho)}$ is disconnected from the hard subdiagrams or if the hard subdiagrams $H^{(\sigma)}$ and $H^{(\rho)}$ are themselves disconnected, and not connected by intersecting jet subdiagrams, as required in Eq. (4.2.29). (As we have seen, the latter is only possible in partonic scattering amplitudes.) We treat these cases in turn.

Consider the case in which a connected subdiagram $X \in J_I^{(\sigma)} \cap J_K^{(\rho)}$ of the overlap between $J_I^{(\sigma)}$ and $J_K^{(\rho)}$ is not directly connected to the either $H^{(\sigma)}$ or $H^{(\rho)}$. Each external line of this intersection can be in $S^{(\sigma)}$ and $J_K^{(\rho)}$ or in $S^{(\rho)}$ and $J_I^{(\sigma)}$, or in both $S^{(\sigma)}$ and $S^{(\rho)}$. We have seen that lines in $S^{(\sigma)}$ are suppressed when attached to $J_I^{(\sigma)} \cap J_K^{(\rho)}$. Therefore, all lines external to subdiagram X must be in $S^{(\rho)}$. But such an arrangement is not consistent with the requirement of a physical process at the PS, in which each jet subdiagram $J_K^{(\rho)}$ must be connected and must include one external parton field or Wilson lines. We conclude that $t_\sigma \gamma$ is suppressed

at all PSs ρ that would produce induced PSs of this type. For amplitudes defined by products of Wilson lines, this is the only possibility, because every hard subdiagram will include the multi-eikonal vertex at which the Wilson lines connect. For these amplitudes, the union of $H^{(\sigma)}$ and $H^{(\rho)}$ is always connected.

The induced hard part $H^{(\sigma_{\rm ind})}$, however, will remain disconnected under Eq. (4.2.29) if (and only if) every path between the hard subdiagrams $H^{(\rho)}$ and $H^{(\sigma)}$ includes lines that are in $S^{(\sigma)}$ and/or $S^{(\rho)}$. This requirement, however, turns out to eliminate leading behavior in region ρ. The reason is illustrated by the example of Fig. 4.6(a), which at the PS σ describes the scattering of (massless) fermions. The alternative physical process, with a hard scattering involving gluons, would require the fermions to be in soft region $S^{(\rho)}$, a configuration that is always suppressed [32]. This reasoning applies to any order and diagram: restricting ourselves to fermion-fermion scattering to be specific, at any leading PSs, the fermions must only appear as jet lines, and as external lines of both hard subdiagrams $H^{(\sigma)}$ and $H^{(\rho)}$. But then, since the fermion lines are continuous, the hard subdiagrams must be connected by these jet lines, which must be in different directions in the two PSs. The definition of Eq. (4.2.29) is then guaranteed to give a connected hard subdiagram $H^{(\sigma_{\rm ind})}$. In a similar fashion, for external gluons, the role of fermion lines is taken by gluon lines that carry the external physical polarizations of the gluons. Such polarizations cannot be radiated into soft subdiagrams at leading PSs [32], and the same reasoning as for external fermions applies.

In summary, we have shown how to construct the induced leading region $\sigma_{\rm ind}[\sigma,\rho]$ and have confirmed that $t_{\sigma_{\rm ind}} t_\sigma \gamma$ is a good approximation to $t_\sigma\,\gamma$ in region ρ, so that Eq. (4.2.28) is satisfied. We note that showing Eq. (4.2.28) for $t_\sigma\gamma$ implies the same result for $t_\sigma\, t_{\sigma'}\gamma$ for any nested pair, $\sigma\subset\sigma'$, because the approximations in $t_{\sigma'}$ do not modify the list of pinch surfaces or power counting in region $\sigma_{\rm ind}$, which was all that was used in the discussion above. Therefore the same approximations in t_σ apply to both γ and $t_{\sigma'}\gamma$ in neighborhood $\hat{n}[\sigma]$.

We are now ready show that with this definition of $\sigma_{\rm ind}$, Eq. (4.2.22) is satisfied, that is, that all subtractions for overlapping regions cancel. To proceed, assuming that $N_\phi[\rho]$ is not empty, we construct the induced region for the pair ρ and the smallest region within $N_\phi[\rho]$, which we denote by $\sigma_{\phi\,\rm min}$. By construction, both ρ and $\sigma_{\phi\,\rm min}$ are larger in the sense of nesting, by Eq. (4.2.14), than every element in $N_S[\rho]$. In fact, $\sigma_{\rm ind}[\sigma_{\phi\,\rm min},\rho]$ is also larger than all elements of $N_S[\rho]$ in the sense of Eq. (4.2.14). To confirm this, consider a region τ in N_S. Because τ nests with both ρ and $\sigma_{\phi\,\rm min}$, the union of each jet in τ with

the hard subdiagram in τ contains the union of hard and each jet subdiagram in both ρ and $\sigma_{\phi\,\min}$. At the same time, τ can nest separately with both ρ and $\sigma_{\phi\,\min}$ only if all lines in the overlaps of different jets, $J_I^{(\sigma_{\phi\,\min})}$ and $J_K^{(\rho)}$ are contained within $H^{(\tau)}$. As a result $H^{(\sigma_{\rm ind}[\sigma_{\phi\,\min}])}$ is contained within $H^{(\tau)}$.

We conclude that the induced region $\sigma_{\rm ind}$ either contains all of the elements of $N_S[\rho]$ or is equal to the largest element in $N_S[\rho]$. At the same time, it is itself contained within region $\sigma_{\phi\,\min}$, the smallest of the regions in $N_\phi[\rho]$. Therefore, $\sigma_{\rm ind}[\sigma_{\phi\,\min},\rho]$ nests with all the elements of $\bar{N}^{(\rho)}$, and either $\sigma_{\rm ind}[\sigma_{\phi\,\min},\rho]$ is already contained in $\bar{N}^\rho$ or the set $N^{\sigma_{\rm ind}} \equiv \{\bar{N}^\rho, \sigma_{\rm ind}[\sigma_{\phi\,\min},\rho]\}$ is an acceptable nesting. At the same time, $t_{\sigma_{\rm ind}[\sigma_{\phi\,\min},\rho]} t_\sigma \gamma$ is a good approximation to $t_\sigma\gamma$, so that in region ρ Eq. (4.2.28) holds, and leading contributions cancel between arbitrary nesting $\bar{N}^\rho$ and its induced pair nesting $N^{\sigma_{\rm ind}}$. Thus, we have verified the cancellation of all terms in the sum over $\bar{N}^\rho$ in Eq. (4.2.25) and the ultraviolet finiteness of the subtracted diagram, Eq. (4.2.22), which is what we were after.

4.2.5 Factorization for the subtraction terms

In the following, we will use the term "leading region" to refer to both leading pinch surfaces and their corresponding reduced neighborhoods, except where a distinction is required for clarity.

The action of t_ρ is to perform the soft- and hard-collinear approximations on gluons that attach $S^{(\rho)}$ to the jet subdiagrams and gluons that attach the jet subdiagrams to the hard subdiagram of PS ρ, such that the leading singularity of γ in neighborhood $\hat{n}[\rho]$ is given by Eq. (4.2.11). Ref. [32] shows how the soft-jet and jet-hard gluon connections, approximated by their dominant polarization states as in Eq. (4.2.11), may be replaced by scalar polarizations (equivalent to longitudinal polarizations for massless particles). For the sake of brevity, let us illustrate the idea for a soft-jet connection, as specified by Eq. (4.2.3). The same reasoning also applies to the hard-collinear approximation. We start by rewriting the propagator given in Eq. (4.2.3) as

$$D^{\mu\nu}(x - \tau^{(K)}\beta^{(K)}) \;=\; \frac{\partial}{\partial \tau^{(K)}} \int_\infty^{\tau^{(K)}} d{\tau_K}' D^{\mu\nu}(z - \tau_K \beta^{(K)}) \;, \tag{4.2.36}$$

and integrate by parts in Eq. (4.2.11) such that the derivative now acts on the jet function. We can add the derivatives with respect to the other components of the jet vertex $z^{(K)}$ to the integrand, as these terms are total derivatives and vanish after the integration. The soft-collinear approximation, Eq. (4.2.3),

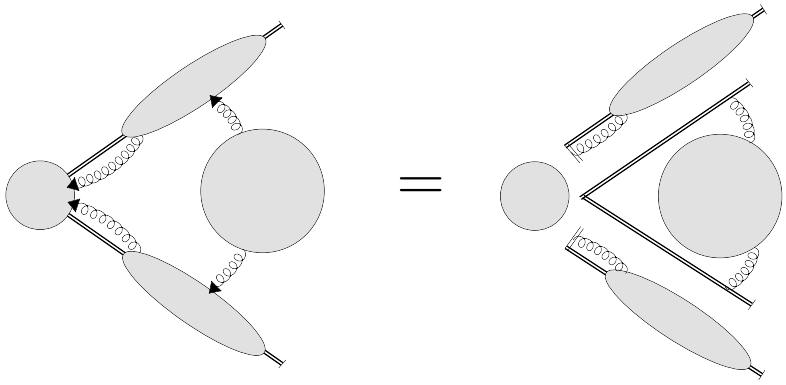

Figure 4.7: Factorization in a leading region illustrated for a vertex function, illustrating Eq. (4.2.38). Each line ending in an arrow represents arbitrary numbers of gluons in the soft-collinear or hard-collinear approximation defined in the text. As in Fig. 4.1, the double lines passing through the jet functions may represent either Wilson lines or partons.

then becomes [32]

$$D^{\mu\nu}(x-z^{(K)})\;J_\nu(z^{(K)}) \to \int_\infty^{\tau^{(K)}} d\tau_K D^{\mu\nu'}(z-\tau_K\beta^{(K)})\beta_{\nu'}\;\left(-\partial_\nu J^\nu(z^{(K)})\right)\,, \tag{4.2.37}$$

where the first factor is to be interpreted as the integral over an eikonal line in the jet direction $\beta^{(K)}$, with the parameter τ_K the position of the attachment of the soft line $z-\tau_K\beta^{(K)}$ to this eikonal. This summarizes the soft-collinear approximation defined in [32] for coordinate-space integrals, and can be carried out independently for each gluon to which we apply the soft-collinear or hard-collinear approximation.

Equation (4.2.37) is simply the Fourier transform of the soft approximation in momentum space to any order in perturbation theory, as discussed extensively in Refs. [31, 54, 55], for example. Replacing the jet-soft connections by scalar-polarized gluon lines that are associated with the scalar operator $\partial_\mu A^\mu(x)$ allows us to apply the gauge theory Ward identities. After the sum over all diagrams, the Ward identities then ensure the factorization of the soft lines from jet subdiagrams exactly in the same way as in momentum space in Refs. [31, 54, 55]. We note that the Ward identity we need for showing the factorization in the case of the cusp was given in the proof of renormalizability of smooth Wilson lines in Ref. [89].

Proceeding in this fashion, the action of t_ρ on amplitude G gives a factorized

form,

$$t_\rho \, \Gamma = \mathcal{S}_\rho \times \prod_I \, \mathcal{J}_{I,\rho} \times \mathcal{H}_\rho \ , \tag{4.2.38}$$

where the product $\times$ indicates a product in color space. In the spirit of the notation of Eq. (4.2.11) for individual subtracted diagrams, the factorized soft and jet functions may be represented as

$$\mathcal{S}_\rho \ = \ \int \overline{d\tau}_K \ S_{\rho,\{\mu_K\}}(\tau_K) \ \beta_K^{\mu_K} \ , \tag{4.2.39}$$

$$\mathcal{J}_{I,\rho} \ = \ \int \overline{d\zeta}_I \, J_{I,\rho}^{\nu'_I}(\zeta_I) \ \bar{\beta}_{I,\nu'_I} \ . \tag{4.2.40}$$

Relative to Eq. (4.2.11), the integrals over distances along light-cone directions, τ_K and ζ_I, originating from $\tau^{(K)}$ in Eq. (4.2.4) and $\zeta^{(I)}$ in Eq. (4.2.6), act only on the soft and jet functions, and are no longer in convolution with the jet and hard functions, respectively. These integrals are ordered along the relevant eikonals, which we indicate by an overline. The hard function $\mathcal{H}_\rho$ is an overall color factor, with no scalar-polarized external gluons, and hence no longer in convolution with the jet functions.

The factorized soft functions constructed this way are identical to multieikonal amplitudes, evaluated at the order of the soft subdiagram of the original diagrams in region ρ. This is the case whether we are analyzing a multieikonal or a partonic amplitude. The difference between the two cases is in the jet functions, which for multieikonal amplitudes are given by the square roots of the singlet cusp operators,

$$\mathcal{J}_I^{\mathrm{eik[f]}}(\varepsilon) = \left\langle 0 \left| T\left(\Phi_{\beta_I}^{[f]}(\infty,0) \, \Phi_{\bar{\beta}_I}^{[f]\dagger}(\infty,0) \right) \right| 0 \right\rangle^{1/2} , \tag{4.2.41}$$

which, as indicated by its argument, may be regulated dimensionally. For partonic amplitudes, the jet functions are given by square roots of vacuum expectation values of partonic fields, ϕ, recoiling against an eikonal in the conjugate color representation,

$$\mathcal{J}_I^{\mathrm{part[f_\phi]}}(x_I, \bar{\beta}_I) = \left\langle 0 \left| T\left(\phi(x_I) \, \phi^\dagger(0) \Phi_{\bar{\beta}_I}^{[f_\phi]\dagger}(\infty,0) \right) \right| 0 \right\rangle^{1/2} , \tag{4.2.42}$$

where f_ϕ is the color representation of parton ϕ, where again $\bar{\beta}_I$ is the complementary lightlike vector defined by x_I, and where x_I^2 serves as to regulate collinear singularities. In region ρ we identify the factorized functions with the

"leading" singularities of these matrix elements, where all vertices approach the light cone.

Because Eq. (4.2.38) holds for the appoximation operation associated with every leading PS ρ, independently of the order of the amplitude, a sum over all diagrams and regions produces a fully factorized amplitude, originally shown for fixed-angle scattering amplitudes in momentum space in Ref. [101],

$$\begin{aligned} \Gamma &= \mathcal{S} \times \prod_I \mathcal{J}_I^{\mathrm{eik[f]}} \times \mathcal{H}^{\mathrm{eik}} \,, \\ G &= \mathcal{S} \times \prod_I \mathcal{J}_I^{\mathrm{part[f_\phi]}} \times \mathcal{H}^{\mathrm{part}} \,, \end{aligned} \tag{4.2.43}$$

where now the jet functions depend on the regulators appropriate to the amplitude in question, x_I^2 in partonic amplitudes like Eq. (4.1.1), or ε in expectations of Wilson lines like Eq. (4.1.4). As noted above, in every leading region, the soft function is the same whether the jets are eikonal or partonic. The construction of the soft function in a manner that avoids double counting is discussed in Secs. 4.3 and 4.4, where we will make important use of the exponentiation properties of the cusp and multieikonal amplitudes.

4.3 Webs and regularization

In this section we give a detailed treatment of the simplest of the eikonal amplitudes, the "cusp", defined by Eq. (4.2.41), with a gauge-singlet vertex. Our goal is to relate the regularization procedure developed in the previous section, where we exhibited an expression for cusp and other amplitudes in terms of nested leading regions, Eq. (4.2.21), to the exponentiation properties of the cusp. We first recall the graphical interpretation of exponentiation.

4.3.1 Cusp webs and exponentiation

All multi-eikonal amplitudes, of the type of Eqs. (4.1.3) and (4.2.41) may conveniently be written as exponentials

$$\Gamma = \exp\ W \,, \tag{4.3.1}$$

where W is determined by a set of diagrammatic rules in terms of so-called web diagrams, which were first identified and analyzed for the special case of the cusp, the square of $\mathcal{J}_I^{\mathrm{eik}}$, Eq. (4.2.41). In all cases, the exponent W is a sum of diagrams with modified color factors. For the special case of the cusp, these diagrams, which we label by w, are (all) elements of the set of

diagrams that are irreducible under cuts of the two Wilson lines [86–88] (thus their name, "webs"). For the cusp, the exponent can be represented as

$$W \quad = \quad \sum_{\text{webs } w} \bar{C}\,(w)\,\mathcal{I}\,(w)\;, \tag{4.3.2}$$

with $\mathcal{I}(w)$ the corresponding diagrammatic integral over the positions of all the internal vertices of web w. Each web integral is mulitplied by a color factor $\bar{C}(w)$, modified from the factor $C(w)$ that would normally be associated with diagram w. It is possible to give a closed form for $\bar{C}(w)$ [79], but in the following discussion, we will use the recursive definition [87], given for each diagram by

$$\bar{C}\left(w^{(n)}\right) \;=\; C\left(w^{(n)}\right) \;-\; \sum_{d\in D} \prod_{w_i^{(n_i)}\in d} \bar{C}\left(w_i^{(n_i)}\right)\;, \tag{4.3.3}$$

where the $w_i^{(n_i)}$ are lower order webs, of order n_i, in the decompositions d of the original diagrams $\gamma^{(n)}$, contributing to $W^{(n)}$, into lower order webs, with $\sum_i n_i = n$. As usual, we denote the coefficient of $(\alpha_s/\pi)^n$ in W as $W^{(n)}$, and similarly for all other functions.

The sum in Eq. (4.3.3) is over all "proper" web decompositions $D[\gamma^{(n)}]$, not including $\gamma^{(n)}$ itself, and the right-hand side vanishes identically for diagrams $\gamma^{(n)}$ that are not webs, for which we have [87, 88]

$$\sum_{D[v]} \prod_{w_i\in D[v]} \bar{C}(w_i) \;=\; C(v)\,. \tag{4.3.4}$$

As a result, the nth-order coefficient $W^{(n)}$ to the sum of *all* diagrams that contribute to the cusp at the same order can be written as

$$W^{(n)} = \sum_{\gamma^{(n)}} \left(\gamma^{(n)} \;-\; \mathcal{I}(\gamma^{(n)}) \sum_{D[\gamma^{(n)}]} \prod_{w\in D[\gamma^{(n)}]} \bar{C}(w) \right)\,. \tag{4.3.5}$$

We will use this form below. The web prescription for W, the logarithm of the cusp was originally identified in momentum space [87, 88], but also has a very simple coordinate-space derivation [97]. Webs can be used to show the exponentiation of double logarithms and double poles, and of power corrections related to singularities in the perturbative running coupling [36, 66, 90–94]. They help organize calculations at two loops and beyond in the cusp and in closed Wilson loops [33, 44, 57]. As we shall review below, the concept of webs

can also be generalized beyond the color-singlet cusp and also as a starting point for a beyond-eikonal expansion [79, 97, 110, 111].

Considering the sum of virtual diagrams associated with a cusp vertex, web diagrams for massive eikonals (Wilson lines) have only a single, overall ultraviolet (and infrared) divergence [84], up to multiple poles associated with the running of the coupling. In the massless limit, they develop a double pole times the cusp anomalous dimension, again with higher-order poles that can be predicted by the running of the coupling order-by-order [36, 57, 90]. The treatment of vanishing mass in the cusp was developed in [57] in momentum space, employing physical gauges.

We will study the fully massless case. Each diagram w in Eq. (4.3.2) or (4.3.5) can be written as an integral over its "leading" vertices, that is, vertices at the furthest distances from the cusp vertex along each Wilson line,

$$W \quad = \quad \int_0 \frac{d\tau d\bar{\tau}}{\tau\,\bar{\tau}}\; f_W(\alpha_s(\mu^2), \mu^2\tau\bar{\tau}, \varepsilon)\,, \tag{4.3.6}$$

where in the absence of masses, the dependence of the integrand reduces to just a few variables. On a diagram-by-diagram basis, the integrals that define f_W have many subdivergences, involving jet and hard subdiagrams, which show up as logarithmic enhancements, as analyzed in Ref. [32]. For the sum of web diagrams we write

$$\begin{aligned} W \quad &= \quad \int_0 \frac{d\tau d\bar{\tau}}{\tau\,\bar{\tau}}\; f_W(\alpha_s(\mu), \mu^2\tau\bar{\tau}, \varepsilon) \\ &= \quad \int_0 \frac{d\tau d\bar{\tau}}{\tau\,\bar{\tau}}\; f_W(\alpha_s(1/\tau\bar{\tau}), 1, \varepsilon)\,. \end{aligned} \tag{4.3.7}$$

We may think of these integrals as cut off at some large length scale to avoid explicit infrared singularities. The integrand f_W is a renormalization scale independent function that is itself the result of all the remaining integrals, as in the two-loop example treated in detail in Ref. [33], where the interpretation of the result (4.3.7) is discussed. We shall refer to the sum over webs at fixed τ and $\bar{\tau}$ as the "web integrand", and we shall argue that after a sum over all diagrams, the full web integrand f_W is ultraviolet finite for $\varepsilon \to 0$. Renormalization for the web functions is then manifestly additive, and associated with the singular $\tau, \bar{\tau} \to 0$ limits of the integral. The connection between multiplicative renormalizability and the structure of web functions has been reviewed recently for both color-singlet cusps and multieikonal vertices in [110]. In Sec. 4.4, we will use the exponentiation in terms of webs to discuss factorization for multieikonal amplitudes, and also discuss subdivergences in web

integrands for these cases. In fact, we will identify a rather general argument that applies to cusp as well as multieikonal amplitudes. First, however, we shall discuss the web construction for the cusp in its own terms. Although the demonstration of finiteness below for the cusp function is in some ways more elaborate than the general discussion of Sec. 4.4, it is more explicit, and gives insight into the manner in which perturbative corrections conspire at each order to produce an ultraviolet-finite web function.

4.3.2 Subtractions, webs and decompositions

Consider the n-loop web, $W^{(n)}$ given in Eq. (4.3.5). In this equation, we add and subtract the sum over all nested subtractions subdivergences in the full n-loop cusp, $R^{(n)}\,\Gamma^{(n)}$, defined in Eq. (4.2.21). This gives

$$W^{(n)} \;=\; R^{(n)}\,\Gamma^{(n)} \;+\; \Delta W^{(n)}\,, \tag{4.3.8}$$

with

$$\begin{aligned}\Delta W^{(n)} \;=\; &-\sum_{\gamma^{(n)}}\sum_{N\in\mathcal{N}[\gamma^{(n)}]}\prod_{\rho\in N}(-t_\rho)\,\gamma^{(n)} \\ &-\sum_{\gamma^{(n)}}\mathcal{I}(\gamma^{(n)})\left(\sum_{D[\gamma^{(n)}]}\prod_{w\in D[\gamma^{(n)}]}\bar{C}(w)\right),\end{aligned} \tag{4.3.9}$$

which is the difference between the sum of subtractions for nth order diagrams and the subtractions in Eq. (4.3.5) that define the webs, also summed over all diagrams. In the following, we shall show that in every leading region ρ involving a subdivergence, $\Delta W^{(n)}$ is integrable. This in turn implies that the nth order web, Eq. (4.3.5), is itself integrable over all subspaces where individual diagrams are ultraviolet singular. Ultraviolet divergences can then arise only when all the vertices of the web approach the origin or the light cone together.

Let us thus consider $\Delta W^{(n)}$, Eq. (4.3.9), restricted to the neighborhood of ρ, which we denote by $\Delta W^{(n)}_\rho$. As we have seen in Eq. (4.2.22) and the subsequent discussion, in each region ρ the ultraviolet behavior of the vertex is well-approximated by the single subtraction term, $t_\rho\Gamma^{(n)}$, while all other nestings cancel. Then, up to nonsingular corrections, when restricted to the neighborhood of ρ, Eq. (4.3.9) becomes

$$\Delta W^{(n)}_\rho = -\sum_{\gamma^{(n)}}(-t_\rho)\gamma^{(n)}_\rho \;-\; \sum_{\gamma^{(n)}}\mathcal{I}(\gamma^{(n)}_\rho)\sum_{D[\gamma^{(n)}]}\prod_{w\in D[\gamma^{(n)}]}\bar{C}(w)\,. \tag{4.3.10}$$

We will now argue that the sum of diagrams in region ρ, the first sum on the right-hand side, cancels against those web decompositions ($D[\gamma^{(n)}]$) in the second sum, that "match" the structure of leading region ρ, and that other, "unmatched" contributions to the sum either cancel or are suppressed in region ρ. We begin our argument by recalling the result of using Ward identities in the first term, as discussed at the end of Sec. 4.2.

For definiteness, we assume that there is a non-trivial soft function, which we now denote by S_ρ, in region ρ, as in the factorized form, Eq. (4.2.38),

$$\begin{aligned} t_\rho \sum_{\gamma^{(n)}} \gamma_\rho^{(n)} &= S_\rho^{(n-m_\rho)} \times R_\rho^{(m_\rho)} \\ &= \sum_{s_\rho \in S_\rho} s_\rho^{(n-m_\rho)} \times \sum_{r_\rho \in R_\rho} r_\rho^{(m_\rho)} \,. \end{aligned} \tag{4.3.11}$$

In this rewriting of Eq. (4.2.38), the soft function S_ρ multiplies a "remainder" function, R_ρ, which (to avoid clutter) includes sums over the jet and hard subdiagrams in region ρ. Function $S_\rho = \sum s_\rho$ is the sum of the soft subdiagrams, s_ρ, of each $\gamma^{(n)}$ in region ρ, connected directly to β and $\bar{\beta}$ Wilson lines, and similarly for $R_\rho = \sum r_\rho$. We let m_ρ be the order of the remainder function in region ρ. In summary, in each leading region ρ, after a sum over all $\gamma^{(n)}$ Ward identities factorize the subdiagrams that make up S_ρ and R_ρ. The sum over all $\gamma^{(n)}$ in region ρ can then be replaced by independent sums over soft subdiagrams s_ρ and remainder subdiagrams r_ρ.

Next, we separate color and coordinate factors of each $s_\rho^{(n-m_\rho)}$ and $r_\rho^{(m_\rho)}$ in Eq. (4.3.11),

$$\begin{aligned} t_\rho \sum_{\gamma^{(n)}} \gamma_\rho^{(n)} &= S_\rho^{(n-m_\rho)} \times R_\rho^{(m_\rho)} \\ &= \sum_{s_\rho \in S_\rho} C\left(s_\rho^{(n-m_\rho)}\right) \mathcal{I}\left(s_\rho^{(n-m_\rho)}\right) \times \sum_{r_\rho \in R_\rho} C\left(r_\rho^{(m_\rho)}\right) \mathcal{I}\left(r_\rho^{(m_\rho)}\right) \,. \end{aligned} \tag{4.3.12}$$

This is the form that we will compare to the sum of web subtractions, the second sum in Eq. (4.3.9), which becomes

$$\begin{aligned} \Delta W_\rho^{(n)} &= \sum_{s_\rho \in S_\rho} C\left(s_\rho^{(n-m_\rho)}\right) \mathcal{I}\left(s_\rho^{(n-m_\rho)}\right) \sum_{r_\rho \in R_\rho} C\left(r_\rho^{(m_\rho)}\right) \mathcal{I}\left(r_\rho^{(m_\rho)}\right) \\ &\quad - \sum_{\gamma^{(n)}} \mathcal{I}(\gamma_\rho^{(n)}) \sum_{D[\gamma^{(n)}]} \prod_{w \in D[\gamma^{(n)}]} \bar{C}(w) \,. \end{aligned} \tag{4.3.13}$$

As indicated below Eq. (4.3.10), it is useful to split the set of decompositions, $D[\gamma^{(n)}]$ into the set of those that match the factorization of soft and remainder functions in the first term of this expression, and those that do not. More specifically, matched decompositions of a diagram $\gamma^{(n)}$ are those in which no web contains lines in *both* the soft subdiagram of $\gamma^{(n)}$, $s_\rho[\gamma^{(n)}]$, and the remainder subdiagram, $r_\rho[\gamma^{(n)}]$. Correspondingly, in unmatched decompositions, at least one web contains lines of both the soft subdiagram and the remainder in region ρ. In these terms, every decomposition of diagram $\gamma^{(n)}$ is either matched or unmatched in region ρ. We represent this division of decomposiitons for the second term in (4.3.13) as

$$\begin{aligned}
&\sum_{\gamma^{(n)}} \mathcal{I}_\rho(\gamma^{(n)}) \sum_{D[\gamma^{(n)}]} \prod_{w\in D[\gamma^{(n)}]} \bar{C}(w) \\
&\quad = \sum_{\gamma^{(n)}} \mathcal{I}_\rho(\gamma^{(n)}) \left(\sum_{D_{S_\rho\otimes R_\rho}[\gamma^{(n)}]} \prod_{w\in D_{S_\rho\otimes R_\rho}} \bar{C}(w) \;+\; \sum_{D_{S_\rho\cap R_\rho}[\gamma^{(n)}]} \prod_{w\in D_{S_\rho\cap R_\rho}} \bar{C}(w) \right) \\
&\quad \equiv\; w_\rho^{(n)}[S_\rho\otimes R_\rho] \;+\; w_\rho^{(n)}[S_\rho\cap R_\rho]\;,
\end{aligned} \tag{4.3.14}$$

where the first term on the right of the second equality represents the sum over the set of matched decompositions, $D_{S_\rho\otimes R_\rho}$ and the second is the sum over unmatched decompositions, $D_{S_\rho\cap R_\rho}$.

In the following, we will show that the matched decompositions cancel the factorized subtraction terms of Eq. (4.3.12) in region ρ,

$$\begin{aligned}
0 \;&=\; t_\rho \sum_{\gamma^{(n)}} \gamma_\rho^{(n)} \;-\; w_\rho^{(n)}[S_\rho\otimes R_\rho] \\
&=\; S_\rho^{(n-m_\rho)} \times R_\rho^{(m_\rho)} \;-\; w_\rho^{(n)}[S_\rho\otimes R_\rho] \\
&=\; \sum_{s_\rho\in S_\rho} C\left(s_\rho^{(n-m_\rho)}\right) \mathcal{I}\left(s_\rho^{(n-m_\rho)}\right) \sum_{r_\rho\in R_\rho} C\left(r_\rho^{(m_\rho)}\right) \mathcal{I}\left(r_\rho^{(m_\rho)}\right) \;-\; w_\rho^{(n)}[S_\rho\otimes R_\rho]\,,
\end{aligned} \tag{4.3.15}$$

while the unmatched decompositions are suppressed,

$$w_\rho^{(n)}[S_\rho\cap R_\rho] \;=\; 0\,. \tag{4.3.16}$$

Substituted into Eq. (4.3.13), these two results show that $\Delta W_\rho^{(n)} = 0$, so that the web integrand is free of ultraviolet subdivergences.

Before giving our arguments for the results (4.3.15) and (4.3.16), we recall that we have assumed that the leading region ρ has a nontrivial soft subdiagram, $S_\rho^{(n-m_\rho)}$. For the special case of a leading region with no soft subdiagram ($m_\rho = n$), and only jet and hard subdiagrams, we may pick any of the jet subdiagrams to take the place of $S_\rho^{(n-m_\rho)}$, with the same result. In the following, we shall suppress the orders of $S_\rho^{(n-m_\rho)}$ and $R_\rho^{(m_\rho)}$, since these are in principle fixed by the choice of region ρ.

4.3.3 Matched decompositions

It is clear that the sum over matched decompositions of Eq. (4.3.14), denoted $D_{S_\rho \otimes R_\rho}[\gamma^{(n)}]$ for each diagram $\gamma^{(n)}$, separates into two independent sums over the web decompositions of the soft and remainder subdiagrams of $\gamma^{(n)}$. Among these decompositions are the choices $s_\rho[\gamma^{(n)}]$ and $r_\rho[\gamma^{(n)}]$, the soft and remainder subdiagrams themselves, which appear along with all of the webs made of their decompositions. Using the general form for webs, Eq. (4.3.5), we can thus separate the color factors associated with the soft and the remainder subdiagrams,

$$\begin{aligned} w_\rho^{(n)}[S_\rho \otimes R_\rho] \;&=\; \sum_{\gamma^{(n)}} \mathcal{I}_\rho(\gamma^{(n)}) \left(\bar{C}\left(s_\rho[\gamma^{(n)}]\right) \;+\; \sum_{D\left[s_\rho[\gamma^{(n)}]\right]} \prod_{d \in D\left[s_\rho[\gamma^{(n)}]\right]} \bar{C}(d) \right) \\ &\qquad \times \left(\bar{C}\left(r_\rho[\gamma^{(n)}]\right) \;+\; \sum_{D\left[r_\rho[\gamma^{(n)}]\right]} \prod_{d' \in D\left[r_\rho[\gamma^{(n)}]\right]} \bar{C}(d') \right) \\ &= \sum_{\gamma^{(n)}} \mathcal{I}_\rho(\gamma^{(n)})\; C\left(s_\rho[\gamma^{(n)}]\right)\; C\left(r_\rho[\gamma^{(n)}]\right) \;, \end{aligned} \tag{4.3.17}$$

where in the second equality we have used Eq. (4.3.3) for web color factors. In effect, after the sum over matched decompositions, the web color factors of the soft and remainder functions revert to their normal form, the same as in the subtraction terms of Eq. (4.3.13). As usual the sum over $D[\gamma]$ of any diagram γ refers only to its proper web decompositions. Note that the color identity in (4.3.17) extends to all diagrams, γ. For a non-web v, for which $\bar{C}(v) = 0$, we recall Eq. (4.3.4).

Having factorized the product of color factors in the sum over matched

decompositions, we now turn to the coordinate integrals themselves. We reexpress the sum over diagrams $\gamma^{(n)}$ in Eq. (4.3.17) into independent sums over soft and remainder subdiagrams s_ρ and r_ρ, and then a sum over all possible connections of these subdiagrams to the eikonal lines, respecting the relative orderings, $O[s_\rho, r_\rho]$ of the connections of the gluons that attach s_ρ to the Wilson lines and those that connect r_ρ to the Wilson lines,

$$\sum_{\gamma^{(n)}} \mathcal{I}_\rho(\gamma^{(n)}) \;=\; \sum_{s_\rho \in S_\rho} \sum_{r_\rho \in R_\rho} \sum_{\substack{\text{eikonal} \\ \text{orderings O}}} \mathcal{I}_\rho(O[s_\rho, r_\rho])\,. \tag{4.3.18}$$

In (4.3.17), this gives

$$w_\rho^{(n)}[S_\rho \otimes R_\rho] \;=\; \sum_{s_\rho \in S_\rho} \sum_{r_\rho \in R_\rho} \sum_{\substack{\text{eikonal} \\ \text{orderings O}}} \mathcal{I}(O[s_\rho, r_\rho])\;\; C\,(s_\rho)\;\; C\,(r_\rho)\;. \tag{4.3.19}$$

To this result we apply the coordinate-space eikonal identity [97], applicable whenever we sum over all connections of a set of web subdiagrams that are attached to the eikonal line, respecting the order of gluon lines within each subdiagram,

$$\sum_{\substack{\text{eikonal} \\ \text{orderings O}}} \mathcal{I}(O[s_\rho, r_\rho, \dots]) \;=\; \mathcal{I}(s_\rho) \times \mathcal{I}(r_\rho) \times \cdots\,, \tag{4.3.20}$$

a "shuffle algebra" result that generalizes to any numbers of subdiagrams and any number of eikonal lines. In Eq. (4.3.19), this gives the desired result,

$$\begin{aligned} w_\rho^{(n)}[S_\rho \otimes R_\rho] \;&=\; \sum_{s_\rho \in S_\rho} \sum_{r_\rho \in R_\rho} \mathcal{I}(s_\rho)\; C\,(s_\rho)\;\; \mathcal{I}(r_\rho)\;\; C\,(r_\rho) \\ &=\; S_\rho \times R_\rho\,, \end{aligned} \tag{4.3.21}$$

which shows that (4.3.15) holds for the matched decompositions.

4.3.4 Unmatched decompositions

We now treat the unmatched decompositions of Eq. (4.3.14), whose sum we have denoted as $w_\rho^{(n)}[S_\rho \cap R_\rho]$. For any diagram $\gamma^{(n)}$, this sum includes those decompositions with at least one web that includes one or more line from the soft subdiagram $s_\rho[\gamma^{(n)}]$ and one or more line in $r_\rho[\gamma^{(n)}]$. For this discussion, we assume that the cancellation of subdivergences has been proven to order $n-1$.

From Eq. (4.3.14), we have for the unmatched decompositions

$$w_\rho^{(n)}[S_\rho \cap R_\rho] \;=\; \sum_{\text{all } \gamma^{(n)}} \mathcal{I}_\rho(\gamma^{(n)}) \sum_{D_{S_\rho\cap R_\rho}[\gamma^{(n)}]} \prod_{w\in D_{S_\rho\cap R_\rho}[\gamma^{(n)}]} \bar{C}(w)\;, \qquad (4.3.22)$$

with $D_{S_\rho\cap R_\rho}[\gamma^{(n)}]$ meaning $D[\gamma^{(n)}] \in \{S_\rho \cap R_\rho\}$.

By analogy to our analysis of the matched distributions, we will exchange the sum over diagrams $\gamma^{(n)}$ for sums over webs. In every element of the unmatched decompositions $D[\gamma^{(n)}] \in \{S_\rho \cap R_\rho\}$ of diagram $\gamma^{(n)}$ there is a non-empty decomposition that includes a subdiagram $u_\rho[\gamma^{(n)}]$ consisting of (one or more) webs that are not all in the soft subdiagram, and not all in the remainder of $\gamma^{(n)}$. In general, once subdiagram $u_\rho[\gamma^{(n)}]$ is fixed, there are also decompositions, $s'_\rho[\gamma^{(n)}]$ whose webs are proper subdiagrams of the soft subdiagram found by removing the unmatched webs of u_ρ from $\gamma^{(n)}$, $S'_\rho[\gamma^{(n)}\backslash u_\rho]$, and another subdiagram, $r'_\rho[\gamma^{(n)}]$, which is a subdiagram of the remainder $R_\rho[\gamma^{(n)}\backslash u_\rho]$. We can then write

$$\gamma_\rho^{(n)} \;=\; s'_\rho[\gamma^{(n)}] \cup r'_\rho[\gamma^{(n)}] \cup u_\rho[\gamma^{(n)}]\,. \qquad (4.3.23)$$

The sum over unmatched web decompositions of $\gamma^{(n)}$, then, can be reorganized as a sum over the independent decompositions of each of these subdiagrams. For decompositions of the soft and remainder subdiagrams, s'_ρ and r'_ρ, the diagrams themselves appear in these sums, along with all of their decompositions. For each unmatched subdiagram, u_ρ, however, only those decompositions are included that leave u_ρ an unmatched decomposition. The set of missing decompositions includes those that are matched to the soft and remainder subdiagrams of u_ρ, which we denote by $w_\rho[S[u_\rho] \otimes R[u_\rho]]$, with $S[u_\rho]$ the soft subdiagram of u_ρ, and $R[u_\rho]$ the corresponding remainder. This set also includes decompositions that have both matched and unmatched subdiagrams of lower order. By the inductive hypothesis, however, unmatched decompositions of lower order vanish. Therefore, by adding and subtracting matched decompositions $w_\rho[S[u_\rho] \otimes R[u_\rho]]$ only, we can derive a factor which consists of the difference between all decompositions of u_ρ and its matched decompositions, $w_\rho[S[u_\rho] \otimes R[u_\rho]]$. Doing the sum over all connections to the

Wilson lines, using (4.3.20) now gives

$$
\begin{aligned}
w_\rho^{(n)}[S_\rho \cap R_\rho] \;=\; & \left(\sum_{s'_\rho \in S'[\gamma^{(n)} \setminus u_\rho]} \mathcal{I}(s'_\rho) \right) \left(\sum_{r'_\rho \in R'[\gamma^{(n)} \setminus u_\rho]} \mathcal{I}(r'_\rho) \right) \left(\sum_{u_\rho \in U_\rho} \mathcal{I}(u_\rho) \right) \\
& \times \left(\bar{C}(s'_\rho) \;+\; \sum_{D\left[s'_\rho[\gamma^{(n)}]\right]} \prod_{d' \in D\left[s'_\rho[\gamma^{(n)}]\right]} \bar{C}(d') \right) \\
& \times \left(\bar{C}(r'_\rho) \;+\; \sum_{D\left[r'_\rho[\gamma^{(n)}]\right]} \prod_{d'' \in D\left[r'_\rho[\gamma^{(n)}]\right]} \bar{C}(d'') \right) \\
& \times \left(\bar{C}(u_\rho) \;+\; \sum_{D\left[u_\rho[\gamma^{(n)}]\right]} \prod_{d \in D\left[u_\rho[\gamma^{(n)}]\right]} \bar{C}(d) \;-\; w_\rho\left[S[u_\rho] \otimes R[u_\rho]\right] \right) ,
\end{aligned}
\tag{4.3.24}
$$

where the orders of each function are implicit. This leads to

$$
\begin{aligned}
w_\rho^{(n)}[S'_\rho \cap R'_\rho] \;=\; & \left(\sum_{s'_\rho \in S'_\rho[\gamma^{(n)} \setminus u_\rho]} s'_\rho \right) \left(\sum_{r'_\rho \in R'_\rho[\gamma^{(n)} \setminus u_\rho]} r'_\rho \right) \\
& \times \left(\sum_{u_\rho \in U_\rho} \left\{ u_\rho \;-\; w_\rho\left[S[u_\rho] \otimes R[u_\rho]\right] \right\} \right) \\
=\; & S'_\rho[\gamma^{(n)} \setminus u_\rho] \;\times\; R'_\rho[\gamma^{(n)} \setminus u_\rho] \;\times\; \left(U_\rho \;-\; w_\rho\left[S[U_\rho] \otimes R[U_\rho]\right]\right) .
\end{aligned}
\tag{4.3.25}
$$

The first factors on the right-hand side are factorized soft and remainder subdiagrams, while the third factor is a sum of all unmatched subdiagrams of the same nonzero order. The third factor vanishes by Eq. (4.3.15), which says that all subdivergences cancel against the sum of matched decompositions, up to order n. Thus, all unmatched decompositions cancel in region ρ, and we confirm Eq. (4.3.16) and hence the absence of subdivergences, Eq. (4.3.15) in the logarithm of the cusp amplitude [33].

4.4 Multieikonal and partonic amplitudes

The arguments of the previous section apply specfically to the cusp, where we have used the inductive construction of web color factors, Eq. (4.3.3). We go on now to study how the considerations above change for amplitudes with multiple Wilson lines connected at a local vertex, and to use their exponentiation properties to demonstrate factorization.

4.4.1 Cancellation of web subdivergences for large N_c

For a multieikonal vertex, Γ_a with $a > 3$ Wilson lines, and a consequent mixing of color tensors [84], it will be useful to use an alternative expression [97]. We label each web function with an index E, simply representing a list of the numbers of gluons attached to each Wilson line, $E \equiv \{e_1 \dots e_a\}$ for a Wilson lines. We then express each web $w_E^{(i)}$ as an integral $\mathcal{I}_E$ over integrand $\mathcal{W}_E^{(i)}$, of these diagrams, written as

$$\begin{aligned} w_E^{(i)} &= \prod_{\alpha=1}^{a} \prod_{j=1}^{e_\alpha} \int_{\tau_{j-1}^{(a)}}^{\infty} d\tau_j^{(\alpha)}\, \mathcal{W}_E^{(i)} \left(\{\tau_j^{(\alpha)}\} \right) \\ &\equiv \mathcal{I}_E \left[\mathcal{W}_E^{(i)} \right], \end{aligned} \tag{4.4.1}$$

where the $\tau_j^{(\alpha)}$ label the locations of the vertices coupling gluons to the ath Wilson line, ordered as $\tau_1^{(\alpha)} \le \tau_2^{(\alpha)} \le \dots \le \tau_{e_\alpha}^{(\alpha)}$. The functions $\mathcal{W}_E^{(i)}$ represent sums over all diagrams with the specified numbers of eikonal connections, and are symmetric under exchange, including color, of the gluons attached at each vertex $\tau_j^{(\alpha)}$. Summing over connections, E, we find the complete web as a sum of the $w_E^{(i)}$, and the amplitude is given by

$$\begin{aligned} \Gamma_a &= \exp\left[\sum_i W_a^{(i)} \right] \\ &= \exp\left[\sum_i \sum_E \mathcal{I}_E \left[\mathcal{W}_E^{(i)} \right] \right]. \end{aligned} \tag{4.4.2}$$

In these terms, we can write an iterative expression for the nth order web function with a Wilson lines as

$$W_a^{(n)} = \sum_E \sum_{\gamma_E^{(n)}} \left(\gamma_E^{(n)} - \left\{ \exp\left[\sum_{i=1}^{n-1} \sum_E \mathcal{I}_E \left[\mathcal{W}_E^{(i)} \right] \right] \right\}^{(n)} \right), \tag{4.4.3}$$

where the superscript on the exponential specifies the nth order in the expansion of the exponential of webs up to order $n-1$. In this expression, the functions $\mathcal{W}_E^{(i)}$ are ordered web integrands, whose color factors are matrices that do not commute in general. In the case of two (or three) Wilson lines, or in the "planar" limit of large N_c, however, these factors do commute [112], and the sum over orderings is equivalent to the modified color factor $\bar{C}(w_i)$ in Eq. (4.3.3) above.

We shall assume that each of the web functions $W_a^{(i)} = \sum_E \mathcal{I}_E[\mathcal{W}_E^{(i)}]$ for $i < n$ gets finite contributions only when all of its vertices are integrated over finite distances from the light cone, and when all of its vertices move to the light cone together. This is to say that all $W_a^{(i)}$, $i < n$ are free of subdivergences. We shall see under what conditions we may infer this result for $W_a^{(n)}$.

The regularization discussion of Sec. 4.2 applies as well to multieikonal vertices as to the cusp. Similarly, for any neighborhood $\hat{n}[\rho]$ for the diagrams of $W_a^{(n)}$, we may construct a difference $\Delta W_{a,\rho}^{(n)}$, by analogy to Eq. (4.3.10) above,

$$\begin{aligned}\Delta W_{a,\rho}^{(n)} &= \sum_E \sum_{\gamma_E^{(n)}} (-t_\rho)\gamma_E^{(n)} - \left\{ \exp\left[\sum_{i=1}^{n-1} \sum_E \mathcal{I}_E\,[\mathcal{W}_E^{(i)}] \right] \right\}_\rho^{(n)} \\ &= (-t_\rho)\Gamma_a^{(n)} - \left\{ \exp\left[\sum_{i=1}^{n-1} W_a^{(i)} \right] \right\}_\rho^{(n)} , \end{aligned} \tag{4.4.4}$$

where now the subscript ρ on the exponential term denotes the contribution of the integrals of the expanded exponential to region ρ, which defines a potential subdivergence of $W_a^{(n)}$. In any such region ρ, the hard function consists of some number $r_\rho < n$ vertices in the union of integrals implicit in monomials of webs found from the expansion of the exponential, which shrink to the origin or the light cone, along with the lines that connect them, while $n - r_\rho$ vertices are fixed at finite distances from the origin. The webs in Eq. (4.4.4), as defined in Eq. (4.4.1), are expressed as integrals over the positions of all vertices, including those that attach to the eikonal lines. As a result, we may separate additively the contribution to each web function in the exponential from the region where all of its vertices approach the light cone. We denote this contribution, which contains the only divergence in $W_a^{(i)}$, by $W_{a,\text{uv}}^{(i)}$. Because we assume that all webs commute, and that they have no subdivergences up

to order $n-1$, we may write the result of this separation as

$$\begin{aligned}\Delta W_{a,\rho}^{(n)} &= (-t_\rho)\Gamma^{(n)} - \left\{\exp\left[\sum_{i=1}^{n-1}[W_{a,\mathrm{fin}}^{(i)} + W_{a,\mathrm{uv}}^{(i)}]\right]\right\}_\rho^{(n)} \\ &= (-t_\rho)\Gamma^{(n)} - \left\{\exp\left[\sum_{i=1}^{n-1} W_{a,\mathrm{fin}}^{(i)}\right]\exp\left[\sum_{i=1}^{n-1} W_{a,\mathrm{uv}}^{(i)}\right]\right\}_\rho^{(n)} .\end{aligned} \tag{4.4.5}$$

where we define

$$W_{a,\mathrm{fin}}^{(i)} = W_a^{(i)} - W_{a,\mathrm{uv}}^{(i)} , \tag{4.4.6}$$

which in effect is a regulated version of the ith order web. The separation of the finite and ultraviolet factors of the web exponent is trivial when the web functions commute, but once commutators are included it requires the application of the Campbell-Baker-Hausdorf theorem. The situation is equivalent to that in the renormalization of multieikonal webs outlined in Ref. [97]. We shall return briefly to this question below, but here we continue with the case in which all web functions commute, and we find simply,

$$\Delta W_{a,\rho}^{(n)} = (-t_\rho)\Gamma_a^{(n)} - \left\{\exp\left[\sum_{i=1}^{n-1} W_{a,\mathrm{fin}}^{(i)}\right]\exp\left[\sum_{i=1}^{n-1} W_{a,\mathrm{uv}}^{(i)}\right]\right\}_\rho^{(n)} . \tag{4.4.7}$$

The restriction to region ρ now acts entirely on the exponential of the $W_{a,\mathrm{uv}}$ and picks out the order-r_ρ contribution to the exponential of webs. By definition, this is the full set of diagrams $\Gamma_a^{(r_\rho)}$ restricted to the neighborhood of the light cone. Similarly, the exponential of finite parts gives the finite integral of $\Gamma_a^{(n-r_\rho)}$, and we find

$$\Delta W_{a,\rho}^{(n)} = (-t_\rho)\Gamma_a^{(n)} - \sum_{r_\rho=1}^{n-1} \Gamma_{a,\mathrm{fin}}^{(n-r_\rho)}\,\Gamma_{a,\mathrm{uv}}^{(r_\rho)} . \tag{4.4.8}$$

Given the factorization of the full amplitude in region ρ, we conclude that $\Delta W_{a,\rho}$ is finite when integrated over the neighborhood $\hat{n}[\rho]$ of any PS. For large-N_c, then, the full multieikonal web is free of subdivergences, just as for the cusp. As anticipated above, the arguments we have given in this section, relying on exponentiation, are somewhat simpler than those based directly on the web construction itself.

4.4.2 Collinear factorization and web exponentiation beyond large N_c

Relaxing the commutativity of the web functions, we can still derive an important result for QCD and other theories beyond the planar approximation, that for an arbitrary multieikonal amplitude collinear singularities are color diagonal and enter the web function additively. This means that all subdivergences where some, but not all, vertices go to the light cone are cancelled in the webs. The steps are just the same as for the case where all webs commute, we only replace $W^{(i)}_{a,\mathrm{uv}}$ with $W^{(i)}_{a,\mathrm{co}}$, defined as the contribution where all vertices go to one or more of the light cones,

$$\Delta W^{(n)}_{a,\rho} \;=\; (-t_\rho)\Gamma^{(n)}_a \;-\; \left\{ \exp\left[\sum_{i=1}^{n-1} [W^{(i)}_{a,\mathrm{central}} + W^{(i)}_{a,\mathrm{co}}] \right] \right\}^{(n)}_{\rho} \;, \tag{4.4.9}$$

where $W^{(i)}_{a,\mathrm{central}}$ represents the remainder of the web function, where no vertex approaches the light cone, although in this case subsets of vertices may approach the origin. This additive separation is certainly true for $i = 1$, because the collinear and central singularities arise from different regions of the same integral. In addition, the sum of all $i = 1$ (one-loop) collinear singularities for any multieikonal vertex is color diagonal (the sum of Casimir invariants, one for each Wilson line).

We now assume that $W^{(i)}_{a,\mathrm{co}}$, $i < n$ is color diagonal and thus commutes with all $W^{(j)}_{a,\mathrm{central}}$. The same steps as for the fully commuting case then lead to a result analogous to Eq. (4.4.8),

$$\Delta W^{(n)}_{a,\rho} \;=\; (-t_\rho)\Gamma^{(n)}_a \;-\; \sum_{c_\rho=1}^{n-1} \Gamma^{(n-c_\rho)}_{a,\mathrm{central}}\, \Gamma^{(c_\rho)}_{a,\mathrm{co}} \;. \tag{4.4.10}$$

Given this result, all subdivergences involving collinear subdiagrams of order $i < n$ cancel, and the only remaining collinear divergences are those in which all vertices approach any set of the light cones. Again, these collinear singularities separate into color-diagonal factors, and we conclude that at order n the collinear singularities of the web function are additive. Thus, to all orders,

collinear singularities factor into a product in the amplitude,

$$\begin{aligned}\Gamma_a &= \exp\left[\sum_{i=1}^{\infty}\left(W^{(i)}_{a,\text{central}} + W^{(i)}_{a,\text{co}}\right)\right] \\ &= \exp\left[\sum_{i=1}^{\infty} W^{(i)}_{a,\text{central}}\right]\,\exp\left[\sum_{i=1}^{\infty} W^{(i)}_{a,\text{co}}\right]\,, \end{aligned} \tag{4.4.11}$$

where $W^{(i)}_{a,\text{co}}$ is the additive part of the ith order web function that includes its collinear singularities. In principle, we could define this function up to a constant by introducing the appropriate factorization scale. We will not need the details of such a construction, however, and simply assume this can be done. In the second equality, we use the color-diagonal nature of the collinear singularities. We note that for a identical Wilson lines, $W^{(i)}_{a,\text{co}} = a\, w^{(i)}_{\text{co}}$, with $w^{(i)}_{\text{co}}$ the contribution from a single such line. We can put the factorized expression Eq. (4.4.11) into a standard form, simply by multiplying and dividing by an appropriate power of a function whose collinear singularities match those of the exponential of $W^{(i)}_{a,\text{co}}$. For a jet function corresponding to direction β, let us denote this function by $J_I(\beta, n_\beta)$, where n_β is any other vector introduced in the definiton of J_I. As this notation suggests, there is considerable freedom in the choice of J_I. An acceptable choice for J_I, however, would be the square root of the cusp itself [42, 93, 113],

$$J^{\text{eik}}_I(\beta, n_\beta) \;\equiv\; \Gamma^{1/2}_{\text{cusp}}(\beta, \bar{\beta})\,, \tag{4.4.12}$$

where the square root reflects the symmetry between the vectors β and $\bar{\beta}$, giving the same collinear singularities associated with both directions in the cusp defined as in Eq. (4.2.41).

Once we have defined the jet functions, we may then reorganize the factorized multieikonal amplitude as

$$\Gamma_a \;=\; \left(\exp\left[\sum_{i=1}^{\infty} W^{(i)}_{a,\text{central}}\right]\frac{\exp\left[\sum_{i=1}^{\infty} W^{(i)}_{a,\text{co}}\right]}{\prod_{I=1}^{a} J^{\text{eik}}_I}\right)\,\prod_{I=1}^{a} J^{\text{eik}}_I\,. \tag{4.4.13}$$

Because the eikonal jets cancel all collinear singularities in the ratio, the ratio may be factorized into soft and hard eikonal subdiagrams, which are renormalized locally, in the same manner as for massive, or other non-lightlike

lines [79, 84, 97],

$$\left(\frac{\Gamma_a}{\prod_{I=1}^{a} J_I^{\rm eik}}\right) \;=\; \mathcal{S}_a \times \mathcal{H}_a^{\rm eik}\,, \tag{4.4.14}$$

which defines the product of soft and hard functions $\mathcal{S}$ and $\mathcal{H}$, each of which is free of collinear singularities. The hard function absorbs all of the short-distance singularities of the original amplitude, in addition to those resulting from the factors of $J_I^{\rm eik}$ in the denominator. This gives a definition for the product of soft and hard functions in Eq. (4.2.43), which we inferred from the singularity structure of $\Gamma^{(n)}$. We then rewrite the multieikonal amplitudes as

$$\begin{aligned} \Gamma_a \;&=\; \left(\frac{\Gamma_a}{\prod_{I=1}^{a} J_I^{\rm eik}}\right) \prod_{I=1}^{a} J_I^{\rm eik} \\ &\equiv\; \mathcal{S}_a \times \mathcal{H}_a \;\times \prod_{I=1}^{a} J_I^{\rm eik}\,. \end{aligned} \tag{4.4.15}$$

As emphasized in the discussion of Eq. (4.2.43), the factorized soft function, with collinear singularities removed, is the same for both eikonal and partonic amplitudes with the same velocities β_I and color representations.

Finally, we may use the results above to formulate factorized partonic amplitudes [101,102] in coordinate space. For partonic amplitudes with a external partons, we write

$$\begin{aligned} G_a \;&=\; \mathcal{S}_a \times \mathcal{H}_a \;\times \prod_{I=1}^{a} J_I^{\rm part} \\ &=\; \left(\frac{\Gamma_a}{\prod_{I=1}^{a} J_I^{\rm eik}}\right) \prod_{I=1}^{a} J_I^{\rm part}\,. \end{aligned} \tag{4.4.16}$$

Comparing to Eq. (4.2.43), this expression reproduces the factorized form in every leading region of the original amplitude G_a. The partonic jet functions or the eikonal function Γ_a introduces singularities that are not in G_a. These correspond to collinear subdiagrams in Γ_a and soft subdiagrams in $J_I^{\rm part}$. These singularities exponentiate and are cancelled independently by factors of $J_I^{\rm eik}$ in the denominator, when its web functions move into the collinear or soft region, respectively [114]. This cancellation only requires that the complementary eikonal vectors be chosen the same in the eikonal and partonic jet functions, Eqs. (4.2.41) and (4.2.42), respectively. Such contributions factorize precisely because of the exponentiation of the web functions which, as shown above, have

no subdivergences. With an appropriate determination of the hard function order-by-order, Eq. (4.4.16) reproduces all divergences in factorized form.

4.5 Conclusions

We have studied partonic matrix elements, along with the cusp and multieikonal amplitudes for massless Wilson lines, in coordinate space and Feynman gauge. In these amplitudes, ultraviolet collinear and short-distance divergences arise when sets of vertices approach either Wilson lines or the eikonal vertex. We have shown that these divergences are well-approximated by the series of nested subtractions given in Eq. (4.2.21). The proof of this matching, in covariant gauge, required us to construct a set of induced pinch surfaces, given by Eqs. (4.2.29) to (4.2.31). By comparing the action of the coordinate-space soft-collinear and hard-collinear approximations [32] to the web expansion, we also verified that the logarithm of the cusp is free of subdivergences. The construction of nested subtractions, including the treatment of overlapping subdivergences, applies not only to multieikonal amplitudes, but also to partonic amplitudes for fixed-angle scattering, as studied in coordinate space in Ref. [32].

Our discussion confirmed that for the cusp the only sources of divergences are the limits in which all lines approach the light cones or the origin together [33]. This is the content of Eq. (4.3.6), with a function f_W that is finite for finite values of variables τ and $\bar{\tau}$. For a conformal theory, this integrand is effectively constant. For QCD and related renormalizable theories, the running coupling produces nontrivial dependence on the variable $\tau\bar{\tau}$, which may be chosen as the renormalization scale.

In the general case, due to the non-trivial group structure of the webs the matching between UV subtraction terms, which factorize, and decompositions of the exponential of the webs no longer holds in the same fashion. For the large-N_c limit of gauge theory, however, the arguments go through, and each web becomes a sum of terms involving the two-dimensional integrals found in cusps. In this case, as for the cusp, a geometrical interpretation of the web function applies [33].

Chapter 5

Epilogue

In this thesis we aimed to provide a new, coordinate-space analysis applicable to scattering amplitudes for massless gauge theories. Well-known coordinate-space studies exist for theories of gravity in the context of QFT in curved space-time (for instance, Ref. [115]), however, gauge theories are much less studied in coordinate space.

The results of Chapter 2 hold not only for a specific set of massless gauge theories but are much more general. The results for vertex functions can be generalized for fixed-angle scattering at large angles, because there is no interference between incoming and outgoing jets at large angles [42,92,93]. For scattering at small angles, a different power counting for the jets is needed. Furthermore, our discussion can be extended to S-Matrix elements, defining the reduction from Green functions directly in coordinate space, and eventually to cut diagrams for infrared-safe cross-sections.

The result of the cancellation of subdivergences in webs, that is the confirmation that the only sources of divergences for the cusp are the limits in which all lines approach the light cones or the origin together, illustrates that webs behave like a unit almost like a single gluon, which can be interpreted as a "QCD string". The web integrand depends only on a single scale through the running of the coupling, which, in our surface interpretation, is related to the renormalization scale that is set according to where the interactions take place on the surface. This interpretation can be generalized to a new formalism interpolating between the weak and strong coupling limits of gauge theories in certain infrared-safe cross sections.

In QCD, of course, our explicit knowledge of the web function is limited to the first few terms in the perturbative series, which run out of predictive power as the invariant distance increases. The integral forms derived above, however, hold to all orders in perturbation theory, and may point to an interpolation between short and long distances.

The subtraction procedure, which we constructed in Chapter 4, extends the proof of multiplicative renormalizability for cusps linking massive Wilson lines [84] to the massless case where lightcone singularities are present. This additive regularization procedure for nonlocal ultraviolet divergences can also be generalized as 'infrared regularization' for cross sections, where our subtraction terms play the role of 'counterterms' for (nonlocal) divergences that are not removed by the standard renormalization procedures for quantum field theory. Using webs, we have given a rederivation of factorization for scattering amplitudes in massless QCD and related theories in Feynman gauge, complementing momentum-space analyses in physical gauges.

Reformulating ordinary quantum field theory in coordinate space can be useful in many ways, for instance, to find new relations with the advances in conformal field theory and string theory. Furthermore, coordinate-space perspectives enable us to understand the running of the coupling in real spacetime. The formalism developed for web diagrams can simplify the calculations at higher orders for improved theoretical precision, and also give perturbative insights to long-distance behaviour of the theory. Sharpening our knowledge from the theory would allow us to isolate the QCD background in elementary processes more precisely, and thus increase our ability to identify new physics. A better understanding of the perturbative regime of QCD could also reveal the structure of the fundamental theory that contains it.

Appendix A

Extention of the analysis of singularities

A.1 Massive lines

For completeness, we consider the extension of pinch analysis to massive lines in coordinate space. Massive lines must be explored separately because the massive propagator in coordinate space has a more complicated form, it can be written in $4-2\varepsilon$ dimensions by

$$\Delta_F(x\,;\,m) \;=\; \left(\frac{-i}{8\pi^2}\right)\int_0^\infty d\xi\,\left(\frac{2\pi i}{\xi}\right)^{\varepsilon}\exp\left[i\left(-\frac{x^2}{2}\xi-\frac{m^2}{2\xi}+i\epsilon\right)\right]\;. \quad \text{(A.1.1)}$$

Since the massive propagator does not have a simple denominator, we can not do a Feynman parametrization. However, using Eq. (2.2.1) we can combine the propagators of each line of an arbitrary Feynman diagram with massive lines,

$$\tilde{I}(\{x_i^\mu\}) = \prod_{\text{lines }j}\int_0^\infty d\xi_j \prod_{\text{vertices }k}\int d^D y_k\,\exp\Big[-i\tilde{D}(\xi_j,x_i,y_k)\Big]\times\tilde{F}(\xi_j,x_i,y_k)\;, \quad \text{(A.1.2)}$$

where ξ_j is now the parameter of the jth line with dimensions of mass square. The phase $\tilde{D}$ of the exponent is given directly from (A.1.1) by

$$\tilde{D}(\xi_j,x_i,y_k) \;=\; \sum_j \xi_j\frac{z_j^2}{2}+\frac{m_j^2}{2\xi_j}\;, \quad \text{(A.1.3)}$$

with z_j^μ a linear function of the external coordinates $\{x_i^\mu\}$ and the positions of (internal) vertices $\{y_k^\mu\}$ as before. The functions $\tilde{F}(\xi_j, x_i, y_k)$ include constants and the "numerators", which might come from derivatives of three-point vertices acting on the exponentials.

One can obtain the Landau conditions from the integral representation (A.1.2) for diagrams with massive lines by the method of stationary phase. The conditions of stationary phase with respect to the positions of internal vertices,

$$\frac{\partial}{\partial y_k^\mu}\,\tilde{D}(\xi_j, x_i, y_k) \;=\; \sum_{\text{lines } j \text{ at vertex } k} \eta_{jk}\,\xi_j\,z_j^\mu \;=\; 0\;, \tag{A.1.4}$$

where $\eta_{jk} = +1$ (-1) if the line j ends (begins) at vertex k, and is zero otherwise, give exactly the same result as Eq. (2.2.9) for the massless case because the masses of the lines do not depend on the positions of the internal vertices. The phase is stationary with respect to the ξ-parameters when

$$\frac{\partial}{\partial \xi_r}\,\tilde{D}(\xi_j, x_i, y_k) \;=\; z_r^2 \;-\; \frac{m_r^2}{\xi_r^2} \;=\; 0\;. \tag{A.1.5}$$

For massive lines, the stationary points are given by

$$\xi_r \;=\; \frac{m_r}{\sqrt{z_r^2}}\;, \qquad z_r^2 > 0\;. \tag{A.1.6}$$

If the mass of the line r is zero, Eq. (A.1.5) is only satisfied if its coordinates have a lightlike separation, irrespective of the value of ξ_r.

Repeating the same reasoning as in the massless case, we identify the product $\xi_r z_r^\mu$ with a momentum vector p_r^μ for line r, while this time ξ_r is determined by (A.1.6). The time-component of this momentum vector,

$$p_r^0 \;=\; m_r\,\frac{z_r^0}{\sqrt{(z_r^0)^2 - |\vec{z}_r|^2}} \;=\; \frac{m_r}{\sqrt{1-\beta_r^2}}\;, \tag{A.1.7}$$

equals the energy of a classical particle with mass m_r propagating with the speed of $\beta_r = |\vec{z}_r|/z_r^0$. Therefore, we can interprete the stationary phases in the integral representation (A.1.2), in the same way as pinch singularities explained in Sec. 2.2, as a physical process in space-time where classical particles propagate between vertices with their momenta conserved at each vertex.

A.2 Power counting for path-ordered exponentials

We shall lastly do the power counting for the vacuum expectation value of path ordered exponentials with constant lightlike velocities meeting at a cusp. Consider one Wilson line, which starts from the point $x_1^\mu = x_1\,\delta^{\mu-}$ in $\beta_1^\mu = \delta^{\mu-}$ direction, and meets the other line at the origin, which moves in $\beta_2^\mu = \delta^{\mu+}$ direction and ends at the point $x_2^\mu = x_2\,\delta^{\mu+}$. Formally, we consider the diagrams for the vacuum expectation value of the following operator,

$$\Gamma_{\beta_1,\beta_2}(x_1,x_2) = \left\langle 0 \left| T\left(\Phi_{\beta_2}(x_2,0)\,\Phi_{\beta_1}(0,x_1) \right) \right| 0 \right\rangle , \tag{A.2.1}$$

with constant-velocity ordered exponentials,

$$\Phi_{\beta_i}(x+\lambda\beta_i,x) = \mathcal{P}\exp\left(-ig\int_0^\lambda d\lambda'\beta_i\cdot A(x+\lambda'\beta_i) \right) . \tag{A.2.2}$$

As for the vertex function, there may be divergences when some vector and/or fermion lines get collinear to the eikonal lines forming two jets, which can interact softly at large distances and have a hard interaction at the cusp.

In analogy to Eq. (2.4.22) for the vertex function, the overall degree of divergence of such path ordered exponentials in coordinate space can be written with a bound from below,

$$\begin{aligned} \gamma^{\text{eik}} \quad \geq \quad & w^H + 4(V_3^H + V_4^H) - 2N_g^H - 3N_f^H - V_{3g}^H \\ & + \sum_{i=+,-} \Big[2(V_3^{J_{(i)}} + V_4^{J_{(i)}}) - N_g^{J_{(i)}} - 2N_f^{J_{(i)}} - V_{3g}^{J_{(i)}} \\ & \qquad + \frac{1}{2}(V_3^{J_{(i)}} - S_{(i)}^J - J_{(i)g}^H + w^{J_{(i)}}) \Big] , \end{aligned} \tag{A.2.3}$$

with w^H the total number of hard lines attached to the Wilson lines, and $w^{J(\pm)}$ the number of attachments of the jet in the $\pm$ direction to the Wilson line in the same direction. The lines that connect a jet to the Wilson line in the opposite direction are soft lines, and are counted together with the connections of the jet to the soft subdiagram by $S_{(i)}^J$.

In Eq. (A.2.3), we have added a term $+w^H$ for the integrations over the locations of the attachments of the hard subdiagram to the eikonals to the contributions from the hard part, because these connections have to move to the cusp in order that all components of these hard lines vanish. Furthermore, the derivatives at each three-gluon vertex will bring vectors that form

invariants in the numerator, which will be of the form either $(\beta_i \cdot z)$ or $(z \cdot z')$. The number of vectors β_i that can show up in the numerator is equal to the sum of the number of attachments to each Wilson line. The net effect from all three-gluon vertices in the hard subdiagram is given by the term $-V_{3g}^H$ as for the vertex function. In a jet, a three-gluon vertex z that is connected to the Wilson line in the same direction as the jet produces an invariant $(\beta_i \cdot z)$ linear in λ in the numerator, while one connected to the opposite Wilson line produces an invariant zeroth order in λ. Therefore, we add $w^J = w^{J_{(+)}} + w^{J_{(-)}}$ to the number of jet three-point vertices for the term for the minimum numerator suppressions in γ^{eik}, and subtract the connections of the jets to the opposite eikonals with those to the soft subdiagram.

The relations of the number of lines to the number of the vertices for the jets and the hard subdiagram are in this case slightly different than Eqs. (2.4.25) and (2.4.26) for the vertex function,

$$2N^H + J^H + S^H = w^H + 3V_3^H + 4V_4^H \ , \tag{A.2.4}$$

$$2N^J + S^J = w^J + J^H + 3V_3^J + 4V_4^J \ , \tag{A.2.5}$$

for the hard part and the jets, respectively. Similarly, the relation between the number of fermion lines and the fermion-gluon vertices in the hard part is given by

$$V_{3f}^H = N_f^H + \frac{1}{2}(S_f^H + J_f^H) \ , \tag{A.2.6}$$

while for the jets they are related by

$$V_{3f}^J = N_f^J + \frac{1}{2}(S_f^J - J_f^H) \ . \tag{A.2.7}$$

Note also that $J_f^H \geq 0$ in this case. Plugging these graphical identities for the subdiagrams into Eq. (A.2.3), we find

$$\gamma^{\text{eik}} \ \geq \ S_g^H + \frac{3}{2}S_f^H + \frac{1}{2}(S_f^J + J_f^H) \ . \tag{A.2.8}$$

Any direct connection between the hard and soft subdiagrams and fermion lines connecting any two subdiagrams suppress the integral as for the vertex function. The collinear singularities of path ordered exponentials with constant lightlike velocities are also at worst logarithmic in coordinate space [58].

Appendix B

Two-loop integrals of webs

B.1 The 3-scalar integral

To evaluate the the 3-scalar term in Eq. (3.3.16), we integrate over the position of the three-gluon vertex after combining the denominators by Feynman parametrization. Introducing the Feynman parameters α_1 and α_2, the 3-scalar contribution is given by

$$\begin{aligned} E_{3s} \;=\; -\;\mathcal{N}_{3g}(\varepsilon)\int_0^\infty d\lambda\, d\sigma \int d^{4-2\varepsilon}y\,\frac{\Gamma(3-3\varepsilon)}{\Gamma^3(1-\varepsilon)} \\ \times\int_0^1 d\alpha_1\int_0^{1-\alpha_1} d\alpha_2 \frac{(1-\alpha_1-\alpha_2)^{-\varepsilon}\alpha_1^{-\varepsilon}\alpha_2^{-\varepsilon}}{\left[-y^2+2\alpha_2(1-\alpha_1-\alpha_2)\lambda\sigma+i\epsilon\right]^{3-3\varepsilon}}\;, \end{aligned} \tag{B.1.1}$$

where $y \equiv x-\alpha_2\lambda\beta_1-(1-\alpha_1-\alpha_2)\sigma\beta_2$. The integral over y is straightforward after doing a clockwise Wick rotation,

$$\begin{aligned} E_{3s} \;=\; -\;\mathcal{N}_{3g}(\varepsilon)\left(\frac{-i\pi^{2-\varepsilon}}{2^{1-2\varepsilon}}\frac{\Gamma(1-2\varepsilon)}{\Gamma^3(1-\varepsilon)}\right)\int_0^\infty \frac{d\lambda\; d\sigma}{(\lambda\sigma)^{1-2\varepsilon}} \\ \times\int_0^1 d\alpha_1\int_0^{1-\alpha_1} d\alpha_2 (1-\alpha_1-\alpha_2)^{-1+\varepsilon}\alpha_1^{-\varepsilon}\alpha_2^{-1+\varepsilon}\;. \end{aligned} \tag{B.1.2}$$

The integrals over Feynman parameters α_1, α_2 now factor from the integrals over eikonal parameters λ, σ. After a change of variables $\eta \equiv \alpha_2/(1-\alpha_1)$, they can be integrated independently,

$$\int_0^1 d\alpha_1\,\alpha_1^{-\varepsilon}(1-\alpha_1)^{2\varepsilon-1}\int_0^1 d\eta\,\eta^{\varepsilon-1}(1-\eta)^{\varepsilon-1} \;=\; \frac{1}{\varepsilon^2}\Gamma(1-\varepsilon)\Gamma(1+\varepsilon)\;. \tag{B.1.3}$$

In Eq. (B.1.2), this gives the scaleless λ, σ integral times a constant with a double pole in ε, given in Eq. (3.3.17).

B.2 The end-point

We now return to the $\lambda_2 = \Lambda$ end-point contribution from the second term on the right-hand side of Eq. (3.3.14), which vanishes in the $\Lambda \to \infty$ limit for any fixed values of the vertex x^μ. If we integrate over x^μ first, however, we get a singular contribution, associated with the renormalization of a Wilson line of finite length. It cancels in the gauge-invariant polygons discussed in Sec. 3.4, and extensively in Refs. [43, 58]. After the x^μ integral, we have

$$E_{\rm end} = -\,\mathcal{N}_{3g}(\varepsilon)\left(\frac{-i\pi^{2-\varepsilon}}{2^{1-2\varepsilon}}\frac{\Gamma(1-2\varepsilon)}{\Gamma^3(1-\varepsilon)}\right)\int_0^\Sigma \frac{d\sigma}{\sigma^{1-2\varepsilon}}\int_0^\Lambda d\lambda \\ \times\int_0^1 d\alpha_1\int_0^{1-\alpha_1} d\alpha_2\,\alpha_1^{\varepsilon-1}(1-\alpha_1-\alpha_2)^{-\varepsilon}\alpha_2^{-\varepsilon}\left[\alpha_2\Lambda+(1-\alpha_1-\alpha_2)\lambda\right]^{-1+2\varepsilon}\,. \tag{B.2.1}$$

Changing variables to $\eta = \alpha_2/(1-\alpha_1)$, we find a form that is easy to evaluate,

$$\begin{aligned} E_{\rm end} &= -\,\mathcal{N}_{3g}(\varepsilon)\left(\frac{-i\pi^{2-\varepsilon}}{2^{1-2\varepsilon}}\frac{\Gamma(1-2\varepsilon)}{\Gamma^3(1-\varepsilon)}\right)\int_0^\Sigma \frac{d\sigma}{\sigma^{1-2\varepsilon}} \\ &\qquad\times\int_0^1 d\alpha_1\,\alpha_1^{\varepsilon-1}\int_0^1 d\eta\,(1-\eta)^{-\varepsilon}\eta^{-\varepsilon}\int_0^\Lambda d\lambda\,\left[\eta\Lambda+(1-\eta)\lambda\right]^{-1+2\varepsilon} \\ &= \left(\frac{\alpha_s}{\pi}\right)^2\frac{C_A\,C_F}{64\varepsilon^4}\left(2\pi\mu^2\Lambda\Sigma\right)^{2\varepsilon}\left[\Gamma(1-2\varepsilon)\Gamma(1-\varepsilon)\Gamma(1+\varepsilon)-\Gamma^2(1-\varepsilon)\right]\,. \end{aligned} \tag{B.2.2}$$

If we add this result to the expressions found by integrating the σ and λ integrals of E_{3s}, Eq. (3.3.17) and E_{pse}, Eq. (3.3.18), over the finite intervals of 0 to Σ and Λ, we recover the expression quoted for this diagram in Refs. [43,58].

Appendix C

Ward identity and soft-collinear approximation

The factorization of soft gluons from jets and of unphysical polarized collinear gluons from the hard subdiagram has been derived and used extensively in the literature in momentum space [31]. This procedure follows in much the same way in coordinate as in momentum space, and for illustration we give here a brief derivation of soft-collinear factorization for a single gluon coupled to the matrix element of a path-ordered exponential. The extension to multiple gluon connections has been discussed in momentum space, for example in [55] and recently in [102], and since these discussions rely only on the Ward identities, they hold in the same way in coordinate space.

C.1 Derivation of the Ward identity

We begin with a rederivation of the single-gluon Ward identity, which was originally given in Ref. [89]. Here, we will use the BRST invariance to rederive the Ward identity of interest. Consider the vacuum expectation value of the time-ordered product of the anti-ghost field b at a point y_0 with N gauge fields A^{μ_j} at points y_j where $j = 1, \ldots, N$

$$\langle 0|T[b(y_o)\, A^{\mu_N}(y_N) \cdots A^{\mu_1}(y_1)\,]|0\rangle = 0 \ . \tag{C.1.1}$$

The BRST-variation of this vacuum expectation value also vanishes. Therefore, varying each field in this expression according to the BRST rules we

obtain[1]

$$\langle 0|T[\partial\cdot A(y_0)A^{\mu_1}(y_1)\cdots A^{\mu_N}(y_N)\,]|0\rangle \;= \\ \langle 0|T\left(b(y_0)\sum_{j=1}^{N}A^{\mu_N}(y_N)\cdots D^{\mu_j}(y_j)c(y_j)\cdots A^{\mu_1}(y_1)\right)|0\rangle\ . \tag{C.1.2}$$

This is the basic Ward identity which we will employ in our rederivation of the single-gluon Ward identity for path-ordered exponentials. To apply the Ward identity to explicit calculations of the diagrams in a more direct way, we note the following relation for the matrix element on the left-hand side above

$$\langle 0|T[\partial\cdot A(y_0)A^{\mu_1}(y_1)\cdots A^{\mu_N}(y_N)\,]|0\rangle \;= \\ \int d^4y'\,\Delta(y_0-y')\,\langle 0|T\left[\partial^{\nu}\left(\frac{\partial\mathcal{L}_{\rm int}}{\partial A^{\nu}(y')}\right)A^{\mu_1}(y_1)\cdots A^{\mu_N}(y_N)\right]|0\rangle\ , \tag{C.1.3}$$

where $\Delta(y_0-y')$ is the scalar propagator and $\mathcal{L}_{\rm int}$ is the interaction Lagrangian. Particularly, we are interested in the BRST variation of

$$\Xi(y)\equiv\langle 0|T\left(\partial\cdot A(y)\,P\exp\left[ig\int_C d\lambda\,\beta(\lambda)\cdot A(\lambda\beta(\lambda))\right]\right)|0\rangle\ , \tag{C.1.4}$$

where the curve C denoting the path of integration is parametrized by λ and the velocity vector $\beta(\lambda)$. Expanding the exponential we write $\Xi(y)$ as

$$\Xi(y)=\sum_{N=0}^{\infty}(ig)^N\langle 0|T\Big(\partial\cdot A(y)\int_{\lambda_I}^{\lambda_F}d\lambda_N\,\beta(\lambda_N)\cdot A(\lambda_N\beta(\lambda_N)) \\ \times\int_{\lambda_I}^{\lambda_N}d\lambda_{N-1}\,\beta(\lambda_{N-1})\cdot A(\lambda_{N-1}\beta(\lambda_{N-1}))\times\cdots\Big)|0\rangle\ , \tag{C.1.5}$$

where we labeled the initial point of the path by λ_I and the endpoint by λ_F. In this form, it can be easily seen that using Eq. (C.1.2), $\Xi(y)$ is identically

[1] In Feynman gauge, the BRST transformation rule for the the anti-ghost field is $\delta_{BRST}b(x)=-(\partial\cdot A)(x)\Lambda$ while that of the gauge field is given by $\delta_{BRST}A^{\mu}(x)=D^{\mu}c(x)\Lambda$, where $D^{\mu}=\partial^{\mu}-ig[A^{\mu},c]$ denotes the covariant derivative.

equal to

$$\Xi(y) = \sum_{N=0}^{\infty} (ig)^N \langle 0|T\Bigg(b(y) \sum_{j=1}^{N} \prod_{k=j+1}^{N} \int_{\lambda_I}^{\lambda_{k+1}} d\lambda_k \, \beta(\lambda_k) \cdot A(\lambda_k \beta(\lambda_k)) \\ \times \int_{\lambda_I}^{\lambda_{j+1}} d\lambda_j \Big\{ \beta(\lambda_j) \cdot \partial c(\lambda_j \beta(\lambda_j)) - ig[\beta(\lambda_j) \cdot A(\lambda_j \beta(\lambda_j)), c(\lambda_j \beta(\lambda_j))] \Big\} \\ \times \prod_{i=1}^{j-1} \int_{\lambda_I}^{\lambda_{i+1}} d\lambda_i \, \beta(\lambda_i) \cdot A(\lambda_i \beta(\lambda_i)) \Bigg) |0\rangle \ . \tag{C.1.6}$$

Here, we labeled $\lambda_{N+1} \equiv \lambda_F$. For convenience, we separate $\Xi(y)$ into two parts where the first part includes the gradient terms while the latter includes the commutator terms

$$\Xi(y) = \Xi_I(y; \beta \cdot \partial c) + \Xi_{II}(y; [\beta \cdot A, c]) \ . \tag{C.1.7}$$

We would like to change the derivatives on the ghosts in $\beta \cdot \partial c$-terms to derivatives with respect to λ_j such that the integration over them becomes trivial. In order to do that we first note the relation

$$\frac{d}{d\lambda} c(\lambda \beta(\lambda) + x^\mu) = \left(\beta^\mu(\lambda) + \lambda \frac{\partial \beta^\mu(\lambda)}{\partial \lambda} \right) \frac{\partial c}{\partial x^\mu} \ . \tag{C.1.8}$$

From this relation we see that the two derivatives are equal only if β is constant, therefore from now on we will assume that $\beta(\lambda) = \beta$ and we have

$$\beta^\mu \frac{\partial c}{\partial x^\mu} = \beta \cdot \partial c = \frac{dc}{d\lambda} \ . \tag{C.1.9}$$

Before proceeding with integrations in Eq. (C.1.6), we shall introduce the notation below for our path-ordered exponentials

$$\Phi_\beta(\lambda_F, \lambda_I) \equiv P \exp\left(ig \int_{\lambda_I}^{\lambda_F} d\lambda \, \beta \cdot A(\lambda\beta) \right) \ . \tag{C.1.10}$$

We then note the following two identities

$$\Phi_\beta(\lambda_F, \lambda) = 1 + ig \int_{\lambda}^{\lambda_F} d\sigma \, \Phi_\beta(\lambda_F, \sigma) \times \beta \cdot A(\sigma\beta) \text{ for } \sigma > \lambda, \tag{C.1.11}$$

$$\Phi_\beta(\lambda, \lambda_I) = 1 + ig \int_{\lambda_I}^{\lambda} d\sigma' \, \beta \cdot A(\sigma'\beta) \times \Phi_\beta(\sigma', \lambda_I) \text{ for } \lambda > \sigma'. \tag{C.1.12}$$

Rewriting Eq. (C.1.6), the vacuum expectation value $\Xi(y)$ is now given by

$$\Xi(y) = \langle 0|T\Big(b(y)\int_{\lambda_I}^{\lambda_F} d\lambda\,\Phi_\beta(\lambda_F,\lambda) \times \big\{\beta\cdot\partial c(\lambda) - ig[\beta\cdot A(\lambda), c(\lambda)]\big\} \times \Phi_\beta(\lambda,\lambda_I)\Big)|0\rangle\ . \tag{C.1.13}$$

Employing Eq. (C.1.9) and Eqs.(C.1.11)–(C.1.12), the 'gradient' part of $\Xi(y)$ becomes

$$\Xi_I(y) = \langle 0|T\Big[b(y)\int_{\lambda_I}^{\lambda_F} d\lambda\left(1 + ig\int_{\lambda}^{\lambda_F} d\sigma\,\Phi_\beta(\lambda_F,\sigma)\times\beta\cdot A(\sigma\beta)\right) \times \frac{d}{d\lambda}c(\lambda\beta)\times\left(1 + ig\int_{\lambda_I}^{\lambda} d\sigma'\,\beta\cdot A(\sigma'\beta)\times\Phi_\beta(\sigma',\lambda_I)\right)\Big]|0\rangle\ . \tag{C.1.14}$$

Multiplying every term above and changing the order of λ-integrals with σ- and σ'-integrals in each term, and then doing the integrations over λ one finds

$$\begin{aligned}\Xi_I(y) = \langle 0|T\Big[b(y)\Big\{&\big(c(\lambda_F\beta) - c(\lambda_I\beta)\big)\\ &+ ig\int_{\lambda_I}^{\lambda_F} d\sigma\,\Phi_\beta(\lambda_F,\sigma)\times\beta\cdot A(\sigma\beta)\times\big(c(\sigma\beta) - c(\lambda_I\beta)\big)\\ &+ ig\int_{\lambda_I}^{\lambda_F} d\sigma'\,\big(c(\lambda_F\beta) - c(\sigma'\beta)\big)\times\beta\cdot A(\sigma'\beta)\times\Phi_\beta(\sigma',\lambda_I)\\ &+ (ig)^2\int_{\lambda_I}^{\lambda_F} d\sigma\int_{\lambda_I}^{\sigma} d\sigma'\,\Phi_\beta(\lambda_F,\sigma)\times\beta\cdot A(\sigma\beta)\\ &\quad\times\big(c(\sigma\beta) - c(\sigma'\beta)\big)\times\beta\cdot A(\sigma'\beta)\times\Phi_\beta(\sigma',\lambda_I)\Big\}\Big]|0\rangle\ .\end{aligned} \tag{C.1.15}$$

Notice that the first term in the first line above plus the first term in the third line gives

$$\begin{aligned}&c(\lambda_F\beta)\times\Big(1 + ig\int_{\lambda_I}^{\lambda_F} d\sigma'\,\beta\cdot A(\sigma'\beta)\times\Phi_\beta(\sigma',\lambda_I)\Big)\\ &= c(\lambda_F\beta)\times\Phi_\beta(\lambda_F,\lambda_I)\ .\end{aligned} \tag{C.1.16}$$

Similarly, the second term in the first line plus the second term in the second

line is equal to

$$- \Phi_\beta(\lambda_F, \lambda_I) \times c(\lambda_I \beta) \ . \tag{C.1.17}$$

On the other hand, integrating the first term of the fourth line over σ' and adding it to the first term of the second line we get

$$+ ig \int_{\lambda_I}^{\lambda_F} d\sigma \, \Phi_\beta(\lambda_F, \sigma) \times \beta \cdot A(\sigma\beta) \times c(\sigma\beta) \times \Phi_\beta(\sigma, \lambda_I) \ . \tag{C.1.18}$$

Lastly, we change the order of integrations over σ and σ' in the second term of the fourth line, and combine it with the second term of the third line as follows

$$\begin{aligned} - ig \Bigg(& 1 \times \int_{\lambda_I}^{\lambda_F} d\sigma' \, c(\sigma'\beta) \times \beta \cdot A(\sigma'\beta) \times \Phi_\beta(\sigma', \lambda_I) \\ & + \int_{\lambda_I}^{\lambda_F} d\sigma' \left[ig \int_{\sigma'}^{\lambda_F} d\sigma \, \Phi_\beta(\lambda_F, \sigma) \times \beta \cdot A(\sigma\beta) \right] \\ & \qquad \times c(\sigma'\beta) \times \beta \cdot A(\sigma'\beta) \times \Phi_\beta(\sigma', \lambda_I) \Bigg) \\ = & -ig \int_{\lambda_I}^{\lambda_F} d\sigma \, \Phi_\beta(\lambda_F, \sigma) \times c(\sigma\beta) \times \beta \cdot A(\sigma\beta) \times \Phi_\beta(\sigma, \lambda_I) \ , \end{aligned} \tag{C.1.19}$$

where the square-brackets in the second line gives $[\Phi_\beta(\lambda_F, \sigma') - 1]$ where -1 cancels with the first line, and we relabeled $\sigma' \to \sigma$ in the last line. Combining everything we find

$$\begin{aligned} \Xi_I(y) = \langle 0 | T \Big[b(y) \Big\{ & c(\lambda_F \beta) \times \Phi_\beta(\lambda_F, \lambda_I) - \Phi_\beta(\lambda_F, \lambda_I) \times c(\lambda_I \beta) \\ & + ig \int_{\lambda_I}^{\lambda_F} d\sigma \, \Phi_\beta(\lambda_F, \sigma) \times [\beta \cdot A(\sigma\beta), c(\sigma\beta)] \times \Phi_\beta(\sigma, \lambda_I) \Big\} \Big] | 0 \rangle \ . \end{aligned} \tag{C.1.20}$$

The second line above exactly cancels the 'commutator'-part $\Xi_{II}(y)$ of $\Xi(y)$ in Eq. (C.1.13), and the single-gluon Ward identity for path-ordered exponentials is given by

$$\begin{aligned} & \langle 0 | T \Big[\partial \cdot A(y) \times \Phi_\beta(\lambda_F, \lambda_I) \Big] | 0 \rangle = \\ & \qquad \langle 0 | T \Big[b(y) \Big\{ c(\lambda_F \beta) \times \Phi_\beta(\lambda_F, \lambda_I) - \Phi_\beta(\lambda_F, \lambda_I) \times c(\lambda_I \beta) \Big\} \Big] | 0 \rangle \ . \end{aligned} \tag{C.1.21}$$

We can use Eq. (C.1.3) for the left-hand side, and a similar relation for the antighost field on the right-hand side. Acting with $\Box_y$ on both sides, we will get delta functions from the propagators, which will bring the fields to the point y. Therefore, the single-gluon Ward identity can be rewritten as

$$\begin{aligned}\langle 0|T\Big[\partial^\nu\left(\frac{\partial\mathcal{L}_{\rm int}}{\partial A^\nu(y)}\right)\,\Phi_\beta(\lambda_F,\lambda_I)\Big]|0\rangle\;=\\ \langle 0|T\Big[\frac{\partial\mathcal{L}_{\rm int}}{\partial c(y)}\Big\{c(\lambda_F\beta)\,\Phi_\beta(\lambda_F,\lambda_I)-\Phi_\beta(\lambda_F,\lambda_I)\,c(\lambda_I\beta)\Big\}\Big]|0\rangle\;.\end{aligned}\tag{C.1.22}$$

C.2 Factorization of a single soft gluon from a jet

The soft-collinear approximation replaces jet-soft connections by 'scalar polarized' gluons as shown in Eqs. (2.5.15) and (4.2.37), which allows us to use the Ward identity (C.1.22) to a diagram with a single soft gluon attached to a jet as shown in Fig. C.1.

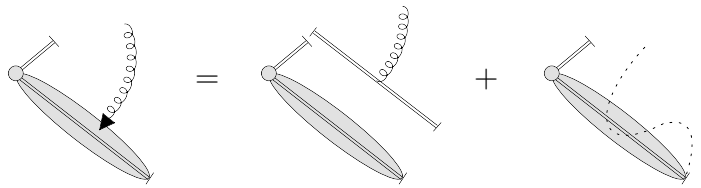

Figure C.1: Result of the Ward identity, a factorized single gluon. The difference between the original diagram and the web subtraction is given by a term with an interacting ghost attached to the end-point, which can be neglected by arguments given in Sections 3.3.3 and 3.3.4.

We get two terms, one for the contribution of a free ghost and another for the interactions of the ghost field with the jet. The first term, which has a free ghost field stuck at the end of the eikonal line, is equivalent to a soft gluon with its arrow acting on the eikonal, because the eikonal propagators are step-functions in coordinate space. It is, thus, simply a gluon attached to an eikonal in the direction of the jet. Note that the Ward identity is evaluated for fixed values of vertices internal to the jet, and as a result, we may systematically neglect endpoint contributions that vanish in the limit the endpoint goes to infinity, as in the second term on the right-hand side of the relation in Fig. C.1 for an interacting ghost [33]. The remainder is a factorized single gluon.

C.3 Soft-collinear approximation for two-loop web diagrams

We give a diagrammatic sketch of the factorization of subdivergences in two-loop web diagrams after the soft-collinear approximation.

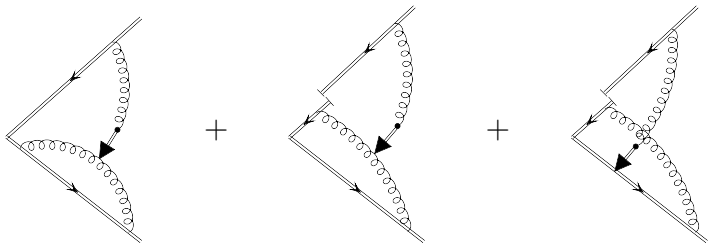

Figure C.2: Representation of the soft-collinear approximation with the two-loop web diagrams.

The 'broken' eikonal line in these figures indicates our use of a different vector $\bar{\beta}_2^\mu$ instead of β_1^μ for the hard-collinear approximation. The double line indicates integration over the dotted point up to the vertex x, which comes from integration by parts in the soft-collinear approximation. The color flow is the same through both eikonal pieces.

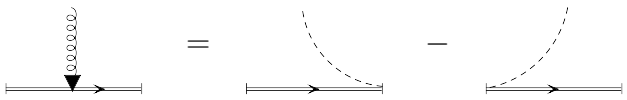

Figure C.3: Eikonal Ward identity.

We will make use of the two identities depicted in Figs. C.3 and C.4.

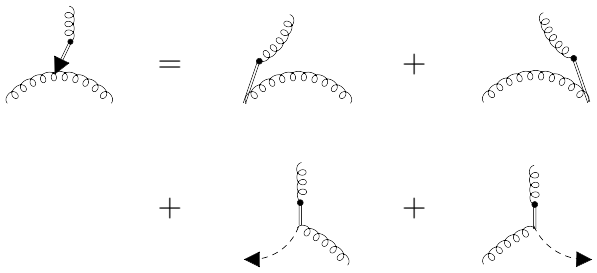

Figure C.4: Graphical represention of the Ward identity for a soft gluon at a three-gluon vertex.

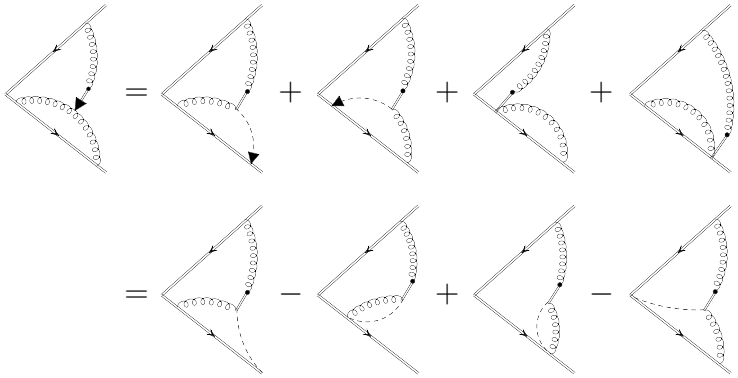

Figure C.5: Application of the Ward identity to the first two-loop web diagram in Fig. C.2.

The last two diagrams in the first line in Fig. C.5 vanish because $\beta_2^2 = 0$, while the second and the third in the second line vanish individually by the integral over the $\beta_2 \cdot x$ component.

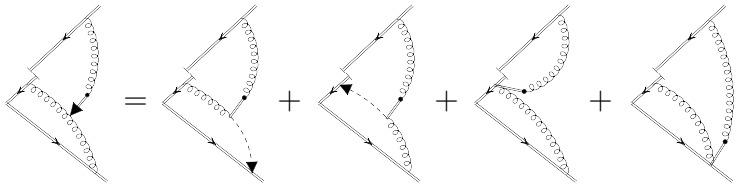

Figure C.6: Application of the Ward identity to the second diagram in Fig. C.2.

In Figure C.6, the third diagram vanishes as $\lim_{\bar{\beta}_2 \cdot x \to 0} (\bar{\beta}_2 \cdot x)^\varepsilon / \varepsilon$, while the last one combines with the non-zero piece of the cross-ladder diagram to give two factorized gluons as shown in Fig. C.10.

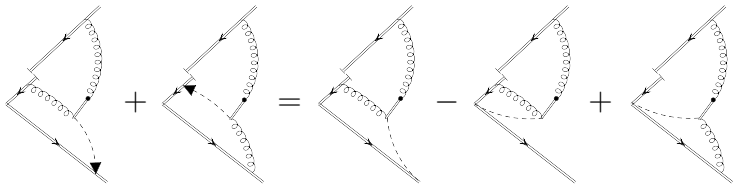

Figure C.7: The result of the eikonal Ward identity for the first two diagrams in Fig. C.6.

In Figure C.7, the second diagram on the right-hand side vanishes after the $\beta_2 \cdot x$ integral, while the last one exactly cancels the last in the second line

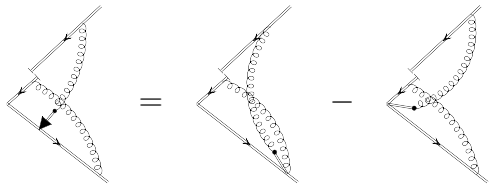

Figure C.8: Application of the eikonal Ward identity to the cross-ladder diagram.

of Fig. C.5. In Figure C.8 for the cross-ladder diagram, the second diagram on the right-hand side vanishes again as $\lim_{\bar{\beta}_2 \cdot x \to 0} (\bar{\beta}_2 \cdot x)^\varepsilon / \varepsilon$.

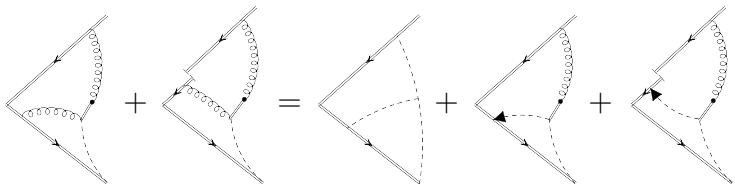

Figure C.9: Two left-over diagrams from Figs. C.5 and C.7.

The two left-over diagrams from Figs. C.5 and C.7 give an end-point term with three scalar propagators after integration by parts on the derivative from the ghost-gluon vertex. The last two diagrams cancel each other.

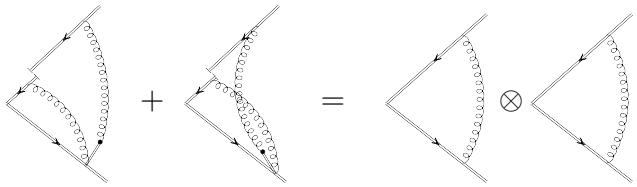

Figure C.10: Resulting factorization of two gluons.

The last diagram in Fig. C.6 plus the nonzero diagram from the cross-ladder diagram in Fig. C.8 give two factorized gluons.

Bibliography

[1] J.D. Bjorken and S.D. Drell, *Relativistic Quantum Fields* (McGraw Hill, New York, 1965).

[2] C. Itzykson and J.B. Zuber, *Quantum Field Theory* (McGraw Hill, New York, 1980).

[3] P. Ramond, *Field Theory* (Benjamin-Cummings, Reading, Mass., 1981).

[4] S. Weinberg, *Quantum Theory of Fields, Vol. 1* (Cambridge University Press, Cambridge, 1995).

[5] G. Sterman, *An Introduction to Quantum Field Theory* (Cambridge University Press, Cambridge, England, 1993).

[6] R. Brock *et al.* [CTEQ Collaboration], Rev. Mod. Phys. **67**, 157 (1995).

[7] G. F. Sterman, In *Boulder 1995, QCD and beyond* 327-406 [hep-ph/9606312].

[8] C. N. Yang and R. L. Mills, Phys. Rev. **96**, 191 (1954).

[9] E. D. Bloom, D. H. Coward, H. C. DeStaebler, J. Drees, G. Miller, L. W. Mo, R. E. Taylor and M. Breidenbach *et al.*, Phys. Rev. Lett. **23**, 930 (1969);
M. Breidenbach, J. I. Friedman, H. W. Kendall, E. D. Bloom, D. H. Coward, H. C. DeStaebler, J. Drees and L. W. Mo *et al.*, Phys. Rev. Lett. **23**, 935 (1969).

[10] J. I. Friedman and H. W. Kendall, Ann. Rev. Nucl. Part. Sci. **22**, 203 (1972).

[11] R. P. Feynman, Phys. Rev. Lett. **23**, 1415 (1969).

[12] J. D. Bjorken and E. A. Paschos, Phys. Rev. **185**, 1975 (1969).

[13] M. Gell-Mann, Phys. Lett. **8**, 214 (1964).

[14] G. Zweig, CERN-TH-401.

[15] J. J. J. Kokkedee, "The Quark Model", Benjamin, New York, (1969).

[16] M. Y. Han and Y. Nambu, Phys. Rev. **139**, B1006 (1965).

[17] O. W. Greenberg, Phys. Rev. Lett. **13**, 598 (1964).

[18] C. G. Callan, Jr. and D. J. Gross, Phys. Rev. Lett. **22**, 156 (1969).

[19] M. Veltman, Phys. Rev. Lett. **17**, 553 (1966).

[20] J. S. Bell, Nuovo Cimento A **50**, 129 (1967).

[21] L. D. Faddeev and V. N. Popov, Phys. Lett. B **25**, 29 (1967).

[22] G. 't Hooft, Nucl. Phys. B **33**, 173 (1971); **35**, 167 (1971).

[23] G. 't Hooft and M. J. G. Veltman, Nucl. Phys. B **44**, 189 (1972).

[24] H. Fritzsch, M. Gell-Mann and H. Leutwyler, Phys. Lett. B **47**, 365 (1973);
D. J. Gross and F. Wilczek, Phys. Rev. D **8**, 3633 (1973);
S. Weinberg, Phys. Rev. Lett. **31**, 494 (1973).

[25] H. D. Politzer, Phys. Rev. Lett. **30**, 1346 (1973);
D. J. Gross and F. Wilczek, Phys. Rev. Lett. **30**, 1343 (1973).

[26] K. G. Wilson, Phys. Rev. **179**, 1499 (1969).

[27] K. G. Wilson and J. B. Kogut, Phys. Rept. **12**, 75 (1974).

[28] C. G. Callan, Jr., Phys. Rev. D **2**, 1541 (1970).

[29] K. Symanzik, Commun. Math. Phys. **18**, 227 (1970).

[30] P. W. Higgs, Phys. Lett. **12**, 132 (1964);
P. W. Higgs, Phys. Rev. Lett. **13**, 508 (1964);
F. Englert and R. Brout, Phys. Rev. Lett. **13**, 321 (1964);
P. W. Higgs, Phys. Rev. **145**, 1156 (1966);
G. S. Guralnik, C. R. Hagen and T. W. B. Kibble, Phys. Rev. Lett. **13**, 585 (1964).

[31] J. C. Collins, D. E. Soper and G. Sterman, in "Factorization of Hard Processes in QCD", A.H. Mueller, ed., Adv. Ser. Direct. High Energy Phys. **5**, 1 (1988) [arXiv:hep-ph/0409313].

[32] O. Erdoğan, Phys. Rev. D **89**, 085016 (2014) [arXiv:1312.0058 [hep-th]].

[33] O. Erdoğan and G. Sterman, arXiv:1112.4564 [hep-th].

[34] O. Erdoğan and G. Sterman, in preparation.

[35] R. J. Eden, P. V. Landshoff, D. I. Olive, J. C. Polkinghorne, *The Analytic S-Matrix* (Cambridge University Press, Cambridge, England, 1966).

[36] L. J. Dixon, L. Magnea and G. F. Sterman, JHEP **0808**, 022 (2008) [arXiv:0805.3515 [hep-ph]].

[37] Z. Bern, L. J. Dixon, D. C. Dunbar and D. A. Kosower, Nucl. Phys. B **425**, 217 (1994) [hep-ph/9403226].

[38] R. Britto, F. Cachazo, B. Feng and E. Witten, Phys. Rev. Lett. **94**, 181602 (2005) [hep-th/0501052].

[39] L. J. Dixon, J. Phys. A **44**, 454001 (2011) [arXiv:1105.0771 [hep-th]].

[40] R. Britto, J. Phys. A **44**, 454006 (2011) [arXiv:1012.4493 [hep-th]].

[41] G. P. Korchemsky and G. Marchesini, Nucl. Phys. B **406**, 225 (1993) [hep-ph/9210281].

[42] S. M. Aybat, L. J. Dixon and G. F. Sterman, Phys. Rev. D **74**, 074004 (2006) [hep-ph/0607309].

[43] J. M. Drummond, G. P. Korchemsky and E. Sokatchev, Nucl. Phys. B **795**, 385 (2008) [arXiv:0707.0243 [hep-th]].

[44] J. M. Drummond, J. Henn, G. P. Korchemsky and E. Sokatchev, Nucl. Phys. B **795**, 52 (2008) [arXiv:0709.2368 [hep-th]].

[45] L. D. Landau, Nucl. Phys. **13**, 181 (1959).

[46] S. Coleman and R. E. Norton, Nuovo Cim. **38**, 438 (1965).

[47] G. Sterman, Phys. Rev. D **17**, 2773 (1978).

[48] G. Date, Ph.D. thesis, SUNY, Stony Brook, 1982 (Report No. UMI-83-07385).

[49] R. C. Hwa and V. L. Teplitz, *Homology and Feynman Integrals* (W. A. Benjamin, Inc., New York, 1966).

[50] J. Hadamard, Acta Math. **22**, 55 (1899).

[51] F. Cachazo, arXiv:0803.1988 [hep-th].

[52] J. S. Ball and T. -W. Chiu, Phys. Rev. D **22**, 2542 (1980).

[53] J. Collins, *Foundations of Perturbative QCD* (Cambridge University Press, Cambridge, England, 2011).

[54] G. T. Bodwin, Phys. Rev. D **31**, 2616 (1985) [Erratum-ibid. D **34**, 3932 (1986)].

[55] J. C. Collins, D. E. Soper and G. Sterman, Nucl. Phys. B **261**, 104 (1985); **308**, 833 (1988).

[56] G. 't Hooft and M. J. G. Veltman, Nucl. Phys. B **50**, 318 (1972).

[57] G. P. Korchemsky, A. V. Radyushkin, Nucl. Phys. **B283**, 342-364 (1987).

[58] I. A. Korchemskaya, G. P. Korchemsky, Phys. Lett. **B287**, 169-175 (1992).

[59] I. Bialynicki-Birula, Bull. Acad. Polon. Sci. **11**, 135 (1963);
S. Mandelstam, Phys. Rev. **175**, 1580 (1968).

[60] C. N. Yang, Phys. Rev. Lett. **33**, 445 (1974);
A. M. Polyakov, Phys. Lett. B **72**, 477 (1978);
L. Susskind, Phys. Rev. D **20**, 2610 (1979).

[61] K. G. Wilson, Phys. Rev. D **10**, 2445 (1974).

[62] G. P. Korchemsky, G. Marchesini, Phys. Lett. **B313**, 433-440 (1993).

[63] G. P. Korchemsky and G. F. Sterman, Nucl. Phys. B **437**, 415 (1995) [hep-ph/9411211].

[64] A. V. Belitsky, Phys. Lett. B **442**, 307 (1998) [hep-ph/9808389].

[65] R. Kelley, M. D. Schwartz, R. M. Schabinger and H. X. Zhu, Phys. Rev. D **84**, 045022 (2011) [arXiv:1105.3676 [hep-ph]].

[66] E. Laenen, G. F. Sterman and W. Vogelsang, Phys. Rev. D **63**, 114018 (2001) [hep-ph/0010080].

[67] I. O. Cherednikov, T. Mertens, P. Taels and F. F. Van der Veken, Int. J. Mod. Phys. Conf. Ser. **25**, 1460006 (2014) [arXiv:1308.3116 [hep-ph]].

[68] L. F. Alday and J. M. Maldacena, JHEP **0706**, 064 (2007) [arXiv:0705.0303 [hep-th]];
L. F. Alday and J. Maldacena, JHEP **0711**, 068 (2007) [arXiv:0710.1060 [hep-th]].

[69] L. F. Alday and R. Roiban, Phys. Rept. **468**, 153 (2008) [arXiv:0807.1889 [hep-th]].

[70] Y. -T. Chien, M. D. Schwartz, D. Simmons-Duffin and I. W. Stewart, Phys. Rev. D **85**, 045010 (2012) [arXiv:1109.6010 [hep-th]].

[71] B. Basso, A. Sever and P. Vieira, Phys. Rev. Lett. **111**, 091602 (2013) [arXiv:1303.1396 [hep-th]].

[72] G. 't Hooft, Nucl. Phys. B **72**, 461 (1974).

[73] N. Kidonakis, G. Oderda and G. F. Sterman, Nucl. Phys. B **531**, 365 (1998) [hep-ph/9803241].

[74] C. W. Bauer, D. Pirjol and I. W. Stewart, Phys. Rev. D **65**, 054022 (2002) [hep-ph/0109045].

[75] A. Mitov, G. F. Sterman and I. Sung, Phys. Rev. D **79**, 094015 (2009) [arXiv:0903.3241 [hep-ph]].

[76] M. Beneke, P. Falgari and C. Schwinn, Nucl. Phys. B **842**, 414 (2011) [arXiv:1007.5414 [hep-ph]].

[77] A. Ferroglia, M. Neubert, B. D. Pecjak and L. L. Yang, JHEP **0911**, 062 (2009) [arXiv:0908.3676 [hep-ph]].

[78] N. Kidonakis, Phys. Rev. D **82**, 114030 (2010) [arXiv:1009.4935 [hep-ph]].

[79] E. Gardi, E. Laenen, G. Stavenga and C. D. White, JHEP **1011**, 155 (2010) [arXiv:1008.0098 [hep-ph]].

[80] R. Kelley and M. D. Schwartz, Phys. Rev. D **83**, 045022 (2011) [arXiv:1008.2759 [hep-ph]].

[81] T. T. Jouttenus, I. W. Stewart, F. J. Tackmann and W. J. Waalewijn, Phys. Rev. D **83**, 114030 (2011) [arXiv:1102.4344 [hep-ph]].

[82] E. Gardi, J. M. Smillie and C. D. White, JHEP **1306**, 088 (2013) [arXiv:1304.7040 [hep-ph]].

[83] E. Gardi, arXiv:1401.0139 [hep-ph].

[84] R. A. Brandt, F. Neri and M. -a. Sato, Phys. Rev. D **24**, 879 (1981). arXiv:1302.6765 [hep-th].

[85] I. A. Korchemskaya and G. P. Korchemsky, Nucl. Phys. B **437**, 127 (1995) [hep-ph/9409446].

[86] G. F. Sterman, AIP Conf. Proc. **74**, 22 (1981).

[87] J. G. M. Gatheral, Phys. Lett. B **133**, 90 (1983).

[88] J. Frenkel and J. C. Taylor, Nucl. Phys. B **246**, 231 (1984).

[89] V. S. Dotsenko and S. N. Vergeles, Nucl. Phys. B **169**, 527 (1980).

[90] C. F. Berger, arXiv:hep-ph/0305076;
C. F. Berger, Phys. Rev. D **66**, 116002 (2002) [arXiv:hep-ph/0209107].

[91] L. Magnea and G. Sterman, Phys. Rev. D **42**, 4222 (1990).

[92] S. Catani, Phys. Lett. B **427**, 161 (1998) [hep-ph/9802439].

[93] G. Sterman and M. E. Tejeda-Yeomans, Phys. Lett. B **552**, 48 (2003) [arXiv:hep-ph/0210130].

[94] Z. Bern, L. J. Dixon and V. A. Smirnov, Phys. Rev. D **72**, 085001 (2005) [arXiv:hep-th/0505205].

[95] M. Kruczenski, JHEP **0212**, 024 (2002) [hep-th/0210115].

[96] G. 't Hooft and M. J. G. Veltman, NATO Adv. Study Inst. Ser. B Phys. **4**, 177 (1974).

[97] A. Mitov, G. Sterman, I. Sung, Phys. Rev. **D82**, 096010 (2010). [arXiv:1008.0099 [hep-ph]].

[98] N. A. Sveshnikov and F. V. Tkachov, Phys. Lett. B **382**, 403 (1996) [hep-ph/9512370];
G. P. Korchemsky, G. Oderda and G. F. Sterman, hep-ph/9708346;
C. W. Bauer, S. P. Fleming, C. Lee and G. F. Sterman, Phys. Rev. D **78**, 034027 (2008) [arXiv:0801.4569 [hep-ph]].

[99] A. V. Belitsky, S. Hohenegger, G. P. Korchemsky, E. Sokatchev and A. Zhiboedov, arXiv:1309.0769 [hep-th];
A. V. Belitsky, S. Hohenegger, G. P. Korchemsky, E. Sokatchev and A. Zhiboedov, arXiv:1309.1424 [hep-th].

[100] H. Elvang, Y. -t. Huang and C. Peng, JHEP **1109**, 031 (2011) [arXiv:1102.4843 [hep-th]].

[101] A. Sen, Phys. Rev. D **28**, 860 (1983).

[102] I. Feige and M. D. Schwartz, arXiv:1403.6472 [hep-ph].

[103] C. T. Sachrajda, Phys. Lett. B **73**, 185 (1978);
S. B. Libby and G. F. Sterman, Phys. Rev. D **18**, 3252 (1978);
G. C. Nayak, J. -W. Qiu and G. F. Sterman, Phys. Rev. D **72**, 114012 (2005) [hep-ph/0509021].

[104] W. Zimmermann, Commun. Math. Phys. **15**, 208 (1969) [Lect. Notes Phys. **558**, 217 (2000)].

[105] C. W. Bauer, S. Fleming and M. E. Luke, Phys. Rev. D **63**, 014006 (2000) [hep-ph/0005275].

[106] J. C. Collins and D. E. Soper, Nucl. Phys. B **193**, 381 (1981) [Erratum-ibid. B **213**, 545 (1983)] [Nucl. Phys. B **213**, 545 (1983)].

[107] V. A. Smirnov, Phys. Lett. B **465**, 226 (1999) [hep-ph/9907471];
V. A. Smirnov, hep-ph/0101152.

[108] J. M. F. Labastida and G. F. Sterman, Nucl. Phys. B **254**, 425 (1985).

[109] J. C. Collins and T. C. Rogers, Phys. Rev. D **78**, 054012 (2008) [arXiv:0805.1752 [hep-ph]].

[110] E. Gardi, J. M. Smillie and C. D. White, JHEP **1109**, 114 (2011) [arXiv:1108.1357 [hep-ph]].

[111] E. Laenen, L. Magnea, G. Stavenga and C. D. White, JHEP **1101**, 141 (2011) [arXiv:1010.1860 [hep-ph]].

[112] S. Plätzer, Eur. Phys. J. C **74**, 2907 (2014) [arXiv:1312.2448 [hep-ph]].

[113] S. M. Aybat, L. J. Dixon and G. F. Sterman, Phys. Rev. Lett. **97**, 072001 (2006) [hep-ph/0606254].

[114] C. Lee and G. F. Sterman, Phys. Rev. D **75**, 014022 (2007) [hep-ph/0611061].

[115] B. S. DeWitt, Phys. Rept. **19**, 295 (1975).